


Summer 2018

Internal composition, structure, and hydrological significance of rock glaciers in the Eastern Cascades, Washington

Adam Riffle
adam.riffle@cwu.edu

Follow this and additional works at: <https://digitalcommons.cwu.edu/etd>

 Part of the [Climate Commons](#), [Geology Commons](#), [Geomorphology Commons](#), [Glaciology Commons](#), and the [Water Resource Management Commons](#)

Recommended Citation

Riffle, Adam, "Internal composition, structure, and hydrological significance of rock glaciers in the Eastern Cascades, Washington" (2018). *All Master's Theses*. 1010.
<https://digitalcommons.cwu.edu/etd/1010>

This Thesis is brought to you for free and open access by the Master's Theses at ScholarWorks@CWU. It has been accepted for inclusion in All Master's Theses by an authorized administrator of ScholarWorks@CWU. For more information, please contact pingfu@cwu.edu.

INTERNAL COMPOSITION, STRUCTURE, AND HYDROLOGICAL
SIGNIFICANCE OF ROCK GLACIERS IN THE EASTERN
CASCADES, WASHINGTON

A Thesis

Presented To

The Graduate Faculty

Central Washington University

In Partial Fulfillment

of the Requirements for the Degree

Master of Science

Cultural and Environmental Resource Management

by

Adam J. Riffle

August 2018

CENTRAL WASHINGTON UNIVERSITY

Graduate Studies

We hereby approve the thesis of

Adam J. Riffle

Candidate for the degree of Master of Science

APPROVED FOR THE GRADUATE FACULTY

Dr. Karl Lillquist, Committee Chair

Dr. Lisa Ely

Dr. Steven Hackenberger

Dean of Graduate Studies

ABSTRACT

INTERNAL COMPOSITION, STRUCTURE, AND HYDROLOGICAL SIGNIFICANCE OF ROCK GLACIERS IN THE EASTERN CASCADES, WASHINGTON

by

Adam J. Riffle

August 2018

Low summer river base flow places a strain on natural and economic resources of the Eastern Cascades. A major contributor to stream flow in this region is snow pack which has declined over the past few decades because of a warming climate. In addition, glacial runoff, which contributes significantly to base flow in summer dry periods, will diminish from glacial recession. However, rock glaciers, because their internal ice (i.e., permafrost) is insulated by an outer debris layer, react slowly to climate change, thus acting as sinks for ice and liquid water storage in mountain environments.

This study utilized ground penetrating radar (GPR) to investigate the internal structure, composition, and hydrological significance of a sample of nine Eastern Cascade rock glaciers. Analysis reveals that active layer thickness for all active rock glaciers are similar with an average of 3.4 meters (m). In addition, linear reflectors deeper in the profiles indicate bedrock and accurately depict the overall rock glacier depth. Other internal stratigraphic features show thrust planes throughout different sections of the profile which are closely tied to slope angle. Further, GPR shows the presence of massive

(i.e., solid) or interstitial internal permafrost indicating glaciogenic or talus origins.

Through measurements of rock glacier base depth and the active layer, this study was able to improve on previous research for estimating the total volume of ice-rich permafrost in these features. Results show a 64 percent over-estimation of permafrost-rich layer thickness using methods from previous studies. These show that previous studies over-estimate the hydrological significance of rock glaciers in comparison to ice glaciers. Results indicate a ratio of volume of rock glacier to ice glacier ice-water equivalence of 1:46 in the Eastern Cascades. In turn, results indicate Eastern Cascade rock glaciers rank similarly in terms of hydrological significance to other mountain ranges around the globe. While rock glaciers in this region will continue to contribute to base flow, they will not totally compensate for the inevitable loss of ice glaciers. This research provides insight for water management for the Eastern Cascades experiencing shifting water resources due to a warming climate.

ACKNOWLEDGEMENTS

This study would not have been possible if it were not for the help and guidance of many people. First, I would like to thank my thesis committee. Thank you to my advisor and chair of my committee Dr. Karl Lillquist for his support and guidance throughout this entire project. Your high expectations pushed me to succeed and your voice of reason helped guide me through not just my thesis, but the entire graduate program. In addition, thank you to Dr. Steven Hackenberger, one of my committee members, for helping me learn how to use the ground penetrating radar and always providing words of encouragement. Also thanks to Dr. Lisa Ely, my other committee member, for also helping me with the ground penetrating radar and letting me haul it around the backcountry.

I would also like to thank my many funding sources: the Mazamas Graduate Student Grant, the Evolving Earth Foundation Student Grant, and Central Washington University's Graduate Student Summer Research Fellowship. These funding sources allowed me to gain all the equipment, gas, and supplies needed to fully invest myself in this project. Along with that, thank you to Monica Bruya in the Geography Department at CWU for helping coordinate funding sources and purchase supplies.

In addition, I would like to thank all the folks at Sensors & Software Inc. who helped me with GPR surveying and data processing. Also, thank you to Dr. Christophe Kinnard at Université du Québec à Trois-Rivières who helped with GPR interpretations.

Also, a special thanks to my mom, Deedee, and brother, Toby, for their unconditional support. And thank you to all of my friends for their support and for

providing much needed procrastination. I would not be a sane human if it were not for you keeping me fun and positive.

None of this would have been possible if it had not been for my field crew, Team RG: Angus Brookes, Adam Taylor, Daniel Mongovin, Noah Driver, and Logan Jones as well as Ellie Meyers, Sarah Newcomb, Melanie Swick, and Carina LeFave. Thank you for schlepping all the gear through the rugged off-trail backcountry of the Cascades. Thank you mostly for keeping spirits up and making field work fun and exhilarating—“them Goat Rawks are sick!”

TABLE OF CONTENTS

Chapter	Page
I INTRODUCTION	1
Problem	1
Purpose.....	2
Significance.....	3
II LITERATURE REVIEW	5
Permafrost	5
Rock Glaciers.....	5
Rock Glacier Spatial Distribution.....	6
Rock Glacier Movement and Activity	8
Rock Glacier Morphology	11
Rock Glacier Genesis.....	12
Rock Glacier Ages	13
Internal Composition and Structure	14
The Mountain Hydrologic Cycle	23
Snowpack as a Water Source	23
Glaciers as Water Sources	23
Rock Glaciers as Water Sources	25
III STUDY AREA	28
Geology and Geomorphology.....	29
Pre-Historic Glaciation	29
Present Glaciation	31
Climate.....	32
Hydrology	34
Vegetation	34
Land Use	35
Study Area Sites.....	36
Study Area 1: Northeastern Cascades.....	38
Study Area 2: Southeastern Cascades.....	43
IV METHODS	46
Rock Glacier Sampling.....	46
Field Data Collection	47
Internal Structure and Composition	47
Topography	50
Data Analysis and Processing.....	51
Ice-Water Equivalence.....	54

TABLE OF CONTENTS (CONTINUED)

Chapter	Page
	Management Implications.....56
V	RESULTS AND DISCUSSION57
	Rock Glacier Composition and Structure57
	Varden Creek 157
	Varden Creek 264
	Bridge Creek 170
	North Creek 172
	West Fork Buttermilk Creek 381
	West Fork Buttermilk Creek 485
	East Fork Buttermilk Creek 289
	Tronsen Creek 197
	Spruce Creek 5106
	Bear Creek 1106
	Bear Creek 3111
	Composition and Structure Synthesis116
	Comparing Lillquist and Weidenaar’s Inventory120
	Vegetation Implications122
	Water Content122
	Rock Glacier Study Sites122
	Glacier Inventory125
	Rock Glacier Inventory125
	Water Content Synthesis126
VI	MANAGEMENT IMPLICATIONS AND FURTHER RESEARCH.....130
	Management Implications130
	Future Research and Improvements130
	REFERENCES133
	APPENDIXES144
	Appendix A—Eastern Cascades Active Rock Glaciers.....144
	Appendix B—Eastern Cascades Inactive Rock Glaciers.....146
	Appendix C—Eastern Cascades Ice Glaciers150

LIST OF TABLES

Table		Page
1	Radar Velocities for Known Material.....	20
2	Eastern Cascade Rock Glacier Study Sites.....	36
3	Rock Glacier Sample Distribution.....	47
4	GPR Summary Table for Select Eastern Cascade Rock Glaciers.....	58
5	Ice-Water Equivalence of Eight Individual Rock Glaciers.....	123
6	Total Ice-Water Equivalence: Brenning Compared to GPR.....	124
7	Ice-Water Equivalence of Eastern Cascade Rock Glaciers and Ice Glaciers.....	127
8	Results from Previous Studies Compared to Results from GPR	127

LIST OF FIGURES

Figure		Page
1	Rock glacier morphology.....	11
2	Illustration of GPR transmitter (Tx) and receiver (Rx) positions, and direction of EM waves.....	19
3	GPR cross section of two road tunnels	19
4	Eastern Cascades.....	28
5	A) Snoqualmie Pass (1910-2002) and B) Lake Cle Elum (1908-1977) climographs.....	34
6	Eastern Cascades study sites.....	37
7	Northeastern Cascades study sites inset map 1	39
8	Rainy Pass, WA climograph (1989-2017).....	39
9	Northeastern Cascades study sites inset map 2.....	41
10	Stockdill Ranch, WA climograph (1909-1963).....	41
11	Northeastern Cascades study sites inset map 3.....	42
12	Blewett Pass, WA climograph (1989-2017).....	42
13	Southeastern Cascades study sites inset map 4.....	44
14	Pigtail Peak, WA climograph	44
15	The pulseEKKO PRO System used in this study	49
16	The pulseEKKO PRO in use on WFBC3 rock glacier	49
17	Example of hyperbola fitting from EKKO_Project 5.....	52
18	Example of hyperbola fitting	52
19	Google Earth image of VC1	59
20	Protalus rampart at head of VC1.....	60

LIST OF FIGURES (CONTINUED)

Figure		Page
21	Migrated and topographically corrected longitudinal GPR Profile of VC1a	62
22	Migrated and topographically corrected transverse GPR Profile of VC1b	63
23	Google Earth image of VC2	65
24	Migrated and topographically corrected longitudinal GPR Profile of VC2a	67
25	Migrated and topographically corrected transverse GPR Profile of VC2b	68
26	Water over Permafrost on VC2	69
27	Google Earth image of BrC1	71
28	Google Earth image of NC1	73
29	Ground photographs of NC1.....	74
30	Migrated and topographically corrected longitudinal GPR Profile of NC1a	76
31	Migrated and topographically corrected transverse GPR Profile of NC1b.....	77
32	Migrated and topographically corrected transverse GPR Profile of NC1c	78
33	Migrated and topographically corrected longitudinal GPR Profile of NC1d.....	79
34	Google Earth image of WFBC3.....	82
35	Migrated and topographically corrected longitudinal GPR Profile of WFBC3	83
36	Google Earth image of WFBC4.....	86

LIST OF FIGURES (CONTINUED)

Figure		Page
37	Migrated and topographically corrected longitudinal GPR Profile of WFBC4	88
38	Google Earth image of EFBC2	90
39	Permafrost found beneath surface of EFBC2	91
40	Toe of eastern lobe of EFBC2	93
41	Migrated and topographically corrected top transverse GPR Profile of EFBC2a	94
42	<i>Figure 42.</i> Migrated and topographically corrected longitudinal GPR Profile of EFBC2b	95
43	Migrated and topographically corrected bottom transverse GPR Profile of EFBC2c	96
44	Google Earth image of TC1	98
45	Migrated and topographically corrected lower longitudinal GPR Profile of lower TC1a	100
46	Migrated and topographically corrected upper longitudinal GPR Profile of upper TC1a	101
47	Migrated and topographically corrected transverse GPR Profile of TC1b	102
48	Migrated and topographically corrected transverse GPR Profile of TC1c	103
49	Migrated and topographically corrected transverse GPR Profile of TC1d	104
50	Migrated and topographically corrected transverse GPR Profile of TC1e	104
51	Google Earth image of BC1	107

LIST OF FIGURES (CONTINUED)

Figure		Page
52	Migrated and topographically corrected longitudinal GPR Profile of BC1a	109
53	Migrated and topographically corrected transverse GPR Profile of BC1b	110
54	Google Earth image of BC3.....	112
55	Migrated and topographically corrected transverse GPR Profile of BC3a	113
56	Migrated and topographically corrected longitudinal GPR Profile of BC3b	114

CHAPTER I

INTRODUCTION

Problem

Summer streamflow is essential to the Eastern Cascades region of Washington State for economic and natural resources, such as the agricultural industry and spawning salmon populations (Pelto, 1993). This area naturally experiences summer drought. Seasonal snowmelt, a significant streamflow contributor, helps alleviate the impacts of drought on streamflow until the snow resource is mostly exhausted by late summer (Sinclair and Pitz, 1999; Siler et al., 2013). Glacial meltwater becomes a major contributor to Eastern Cascades streamflow during these late summer months and supplies more, percentage-wise, to base flow in warmer, dryer years (Pelto, 2011a). However, a period of increased air temperatures over the past few decades, which will likely continue through the 21st century, will eventually lead to diminishing snow pack, glaciers, and glacial meltwater further stressing the mountain runoff system (Granshaw and Fountain, 2006; Pelto, 2011a, 2011b; Treser, 2011; IPCC, 2013).

Active and inactive rock glaciers are landforms of continental settings that are similar in size and morphology to ice glaciers. They consist of internal ice (i.e., permafrost) insulated by an outer, rocky debris layer, known as the active layer, which allows them to react slowly to climate change (Haeberli et al., 1993; Arenson et al., 2002; Degenhardt, 2009). Runoff from the seasonal melt of the active layer as well as permafrost contained in these features may be an important contributor to the mountain hydrologic cycle (Croce and Milana, 2002). However, few studies have quantified water storage capacity of rock glaciers, none of which focus on the Eastern Cascades (Azocar

and Brenning, 2010; Perucca and Angillieri, 2011; Rangecroft et al., 2015; Jones et al., 2018). Previous studies elsewhere take a qualitative approach with a lack of quantitative field data to support their findings (Arenson and Jakob, 2010; Duguay et al., 2015).

A recent inventory compiled over 147 rock glaciers in Washington's Eastern Cascades, of which the internal structure and potential water content is currently unknown (Lillquist and Weidenaar, in preparation). In addition, a limited number of studies have been conducted on rock glaciers in the Eastern Cascades but none have dealt directly with internal structure, composition, and potential water storage capacity (Goshorn-Maroney, 2012; Weidenaar, 2013; Fegel et al., 2016).

Purpose

The purpose of this study was to determine the internal composition, structure, and hydrological significance of a sample of active and inactive rock glaciers in Washington's Eastern Cascades. Specifically, this study: 1) investigated the internal composition and structure of 9 selected Eastern Cascade rock glaciers using ground penetrating radar (GPR); 2) analyzed stratigraphy and identified the distribution of subsurface material including permafrost-rich layers and liquid water; 3) measured depth to rock glacier bases and thickness of active layers; 4) differentiated between glaciogenic (massive ice) and talus (interstitial ice) origins; 5) estimated potential water content of all active and inactive rock glaciers and ice glaciers in Washington's Eastern Cascades; and 6) made this information available for water managers in the state to help with water policy decisions.

Significance

Rock glacier runoff in the Eastern Cascades contributes to river base flow, which is a vital resource that shapes not only the adjacent agricultural industry, a significant economic resource, but also natural resources such as salmon populations (Pelto, 1993; Moore et al., 2009). This region is significant because it makes up a large portion of the middle Columbia River Watershed, a vital hydrologic resource of the Pacific Northwest (Siler et al., 2013). Determining internal structure and potential water content of these features fills a void in the current research and provides a more complete picture of water sources in the Eastern Cascades. This research helps determine the presence of ice within inactive rock glaciers, determining whether they are significant stores of water. Rock glacier contribution to the mountain hydrologic cycle is often overlooked and is not incorporated into future climate predictions in a warming world (Millar and Westfall, 2008). This research will help policy makers and local administrators make informed decisions on water supplies in the drainages of the Eastern Cascades and neighboring lowland communities. Determining the internal composition, structure, and potential water storage capacity of these features provides useful insight into the mountain hydrologic cycle for this region, which is experiencing shifting water resources due to a changing climate.

In addition, little is known about the composition and structure of rock glaciers (Duguay et al., 2015). A field survey of such a large sample of rock glaciers has not been conducted before; this research provides new information on potential water equivalency of this resource on a local scale, further contributing to the larger body of knowledge of rock glaciers. As a result, this investigation provides valuable information on the internal

composition and structure of rock glaciers that can be used to gain a better understanding of ice content which can help determine talus or glacial origin. Inner stratigraphy also reveals features that are tied to the movement of these structures.

Further, investigations on the internal structure and water content of rock glaciers have not been done before in a marine-influenced mountain range such as the Eastern Cascades. This is significant because it provides a more accurate representation of the distribution of permafrost in this region. These data can be added to the global research on permafrost and periglacial environments which will help illustrate internal composition and structure of rock glaciers globally, and also can contribute to understanding worldwide trends of alpine permafrost distribution (IPA, 2015).

CHAPTER II
LITERATURE REVIEW

Permafrost

To discuss rock glaciers it is important to first define and outline permafrost. Permafrost can be defined as perennially frozen ground that has been in a frozen state for at least two years (Harris et al., 1988). Permafrost exists anywhere temperatures are sufficiently cold to support it. The majority of Earth's permafrost is found in high latitudes but it can also be found at high altitudes (i.e., alpine environments). Permafrost can be: continuous, which covers an entire region; discontinuous, which covers a portion of a region; or sporadic, which occurs in isolated areas. Alpine permafrost is often discontinuous, especially in mid-latitude settings, because sufficiently cold temperatures can only be found at high elevations limiting its distribution. In addition, permafrost distribution favors the cold and dry conditions of continental settings. Typically, marine alpine climates receive large amounts of snow which insulates the ground hindering it from freezing permanently (Harris et al., 2009). If cold conditions persist, snow often metamorphoses into ice causing the formation of ice glaciers (Mathews, 1955). However, Sattler et al. (2016) used the distribution of rock glaciers to model permafrost distribution in the maritime Southern Alps of New Zealand and found that permafrost persists at lower elevations than that of more continental settings. They attribute this, in part, to lower summer temperatures caused by oceanic influence.

Rock Glaciers

Rock glaciers are often used as an indicator of permafrost distribution in alpine settings. Rock glaciers, a form of permafrost creep, are masses of unconsolidated rock

debris with interstitial or solid ice cores (i.e., permafrost) that exhibit downslope movement and are common in mountain systems around the globe (Wahrhaftig and Cox, 1959; Haeberli, 1985; Barsch, 1996). These features were first observed in the late 1800s, and in-depth research into their existence only began about 60 years ago (Duguay et al., 2015). Because this is a relatively new field, gaps still exist in our understanding of rock glaciers, such as the internal distribution and characteristics of permafrost. However, rock glacier distribution, form, movement, and origin, which have all been extensively studied, can provide indications to permafrost content and its role in the mountain hydrologic cycle.

Rock Glacier Spatial Distribution

Rock glaciers exist in mountain ranges all over the world, from the European Alps to the Himalayas of Asia, to the Rockies, Sierra Nevada, Olympics and Cascade Mountains of North America (White, 1971; Barsch, 1996; Owen and England, 1998; Millar and Westfall, 2008; Welter, 1987; Weidenaar, 2013). Like other permafrost features, rock glaciers form best in cold, dry climates. Temperature in these locations is typically below -2°C mean annual air temperature (MAAT) (but can be as high as 2°C MAAT). Such low temperatures are found at either high latitudes and/or high altitudes. Precipitation in these climates is typically less than 2,500 millimeters (mm) per year which is driven by orographic influences or continentality (Haeberli, 1985; Barsch, 1996). Such climates characterize continental alpine settings (Haeberli, 1985).

Historically, rock glaciers were not thought to be common in maritime mountain ranges. This is due to the fact that high amounts of precipitation found in these ranges leads to the development of ice glaciers (Mathews, 1955; Haeberli, 1985). However, rain

shadows created by mountain divides allow for a continental climate on the leeward side of the range (Brazier et al., 1998; Siler et al., 2013; Sattler et al., 2016). Sattler et al. (2016) showed rock glaciers are common on the dryer eastern, or leeward, side of the Main Divide in the maritime Southern Alps of New Zealand. In the same way, rock glaciers are common on the leeward slopes of the Sierra Nevada (Millar and Westfall, 2008). Charbonneau (2012) attributed the occurrence of 187 rock glaciers in the British Columbia Coast Mountains, another maritime range, to this same rain shadow affect. Rock glacier formation is even evident in extreme examples like the Olympic Mountains of Washington where the windward side receives enough precipitation to be considered rainforest yet rock glaciers are found on the drier, leeward side of the range (Welter, 1987). Similarly, within the maritime Cascades, Weidenaar (2013) revealed that due to a dramatic decrease in precipitation on the leeward side of the Cascade Crest rock glaciers are common there as well.

Very little research has been conducted on rock glaciers in the Cascade Mountains. Only three comprehensive studies directly focus on rock glaciers in the Cascades (Goshorn-Maroney, 2012; Weidenaar, 2013; Fegel et al., 2016). Until recently, the study of these features in the Cascades has been limited mainly to their identification in a small portion of the range. Prior to Weidenaar (2013), only 29 rock glaciers had been recorded in the Eastern Cascades (Thompson, 1962; Hopkins, 1966; Merrill, 1966; Libby, 1968; Long, 1975; Tabor et al., 1982; Beckey, 2000; Scurlock, 2005; Goshorn-Maroney, 2012). Weidenaar's (2013) inventory of rock glaciers provides a detailed list of 103 active, inactive, and relict rock glaciers in the Eastern Cascades. An update of this inventory by Lillquist and Weidenaar (in preparation) expands the total count of rock

glaciers in the Eastern Cascades to 147. In this new inventory, 33 active and 97 inactive rock glaciers are identified. These rock glaciers increase in density at higher latitudes and are found on predominantly north-facing slopes.

Rock Glacier Movement and Activity

Rock glaciers are categorized by different states of activity and morphology based on their movement. It is important first to outline the factors behind the creep processes that cause these significant landforms to move. Three basic factors are needed for rock glacier development: presence of permafrost, sufficient rock supply, and topographic relief (Haeberli, 1985; Barsch, 1996). Internal ice and topographic relief allow rock glaciers to creep downhill. Their movement is not only dependent on internal ice but also on a sufficient escarpment (often a cirque headwall) to provide rockfall (Barsch, 1996; Humlum, 2000). Ideally, such an escarpment consists of harder igneous and metamorphic rock which is prone to fracturing into medium to large blocks as opposed to smaller fragments which have more potential to be removed by fluvial processes (Wahrhaftig and Cox, 1959; Barsch, 1996). Some suggest that rockfall that feeds rock glaciers is more a discontinuous supply of massive slope failures than a constant supply of small rockfalls (Degenhardt, 2009). However, an equilibrium needs to exist between headwall height, talus production, slope angle and flow velocity for rock glacier formation and survival (Burger et al., 1999). Further, it is estimated that rock glaciers in certain ranges can account for 20-60 percent of total debris transport (Giarndino and Vitek, 1988; Barsch, 1996).

The creep processes involved are tied to shear strength and shear stress of the inner material where thickness, grain size, type of ice crystals, and ice density all play a

role in the rheology of the rock glaciers (Barsch, 1996). Further, different types of movement include ice-core creep (i.e., glaciogenic), interstitial ice creep (i.e., talus), and/or basal shear and pore pressures which could apply to both glaciogenic and talus rock glaciers (Giardino and Vick, 1987). Basal shear is based on evidence of an unfrozen saturated layer beneath the permafrost-rich core (Giardino and Vick, 1987).

The surface of rock glaciers is pronounced in the form of pressure ridges and furrows that are expressions of plastic flow (Barsch, 1996). Pressure ridges typically run transverse to the structure while furrows parallel flow. Pressure ridges are mainly found in locations of compressional stresses and decelerating flow where slope angle decreases. Furrows, on the other hand, are often observed in areas of extensional stresses where there may be an acceleration in flow. They are also observed on the sides of rock glaciers where they are the result of the lateral flanks having a slower velocity so that material builds up on the side while the body advances at a quicker rate (Barsch, 1996).

Rock glacier activity is classified as active, inactive, and relict (Barsch, 1996). Rock glaciers that contain interstitial ice and appear inflated, exhibit a downslope movement of 0.1-2.0 meters (m) per year on average, and are typically non-vegetated, are referred to as *active* (Barsch, 1996). In addition to movement and little vegetation, active rock glaciers are characterized by oversteepened fronts that often exceed the angle of repose of 35° (Wahrhaftig and Cox, 1959; Barsch, 1996). Krainer and Mostler (2006) found the velocity of multiple active rock glaciers in the Austrian Alps to be up to 3 m per year. Goshorn-Maroney (2012) measured the flow of an active rock glacier in the Eastern Cascades with a ground-based terrestrial laser scanner (LiDAR) and

found it had a downslope movement of up to 10 cm per year. This rate is considered slow for rock glacier movement (Burger, 1996).

Rock glaciers that contain internal ice and retain an inflated appearance, are partially covered in vegetation, but no longer exhibit movement are *inactive* (Wahrhaftig and Cox, 1959; Barsch, 1996). Barsch (1996) offers two versions of inactive rock glaciers. *Climatically inactive* rock glaciers are halted due to the melting of the interstitial ice. The second form, known as *dynamic inactive*, occurs when a rock glacier flows too far from its talus slope from which it is fed, or stopped by an obstacle such as an uphill slope (Barsch, 1996). Weidenaar (2013) showed this is the case for the Mount Stuart rock glacier which has been inactive since the mid-1600s even though it is located where $MAAT < 0^{\circ}C$. As a result, it is dynamically inactive because it crept away from its talus supply.

Relict rock glaciers are devoid of ice, often heavily vegetated, and stationary. These features exhibit a deflated appearance that is flat or concave in cross section because their once ice-rich, internal structure has melted (Barsch, 1996). Relict rock glaciers are often located at lower elevations than active and even inactive rock glaciers. This elevation difference is an indicator of past, colder climate regimes (Kerschner, 1978; Weidenaar, 2013). These features also display what is to become of inactive and active rock glaciers with increasingly warming climates.

Active, inactive and relict rock glaciers have all been identified in the Eastern Cascades (Lillquist and Weidenaar, in preparation). The majority of rock glaciers (>65 percent) in this region are inactive. Active rock glaciers make up approximately 22 percent of the population while relict rock glaciers comprise <12 percent.

Rock Glacier Morphology

Rock glacier morphology, depicted in Figure 1, may be: *lobate*, in which width is greater than the length; *tongue-shaped*, where length exceeds width; and *complex*, which exhibit traits of the two previous types in addition to different lobe ages, split lobes, multiple sources of rocks or multiple overlapping rock glaciers (Barsch, 1996). These forms are a result of rock glacier flow, underlying and adjacent topography, and rock source (Burger et al., 1999).

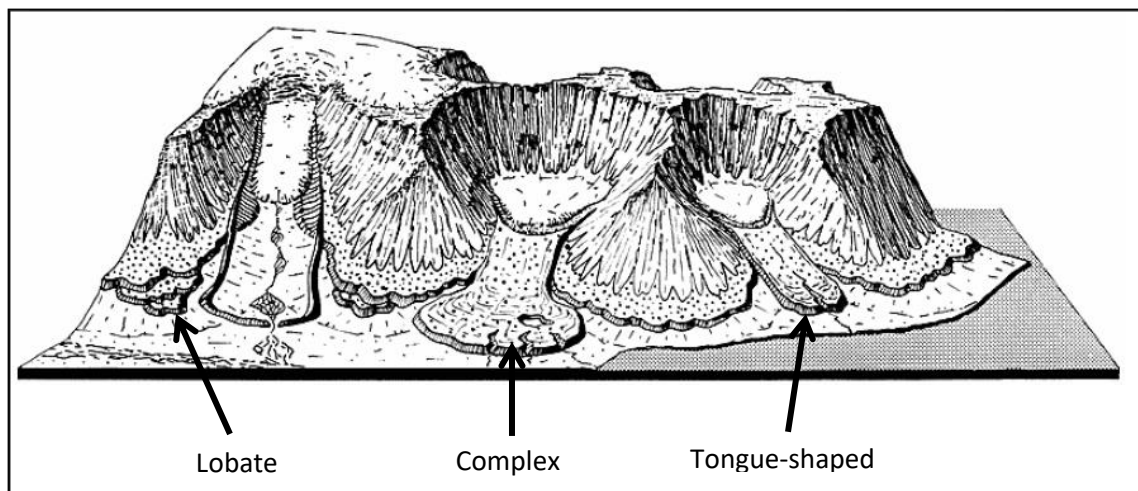


Figure 1. Rock glacier morphology. Adapted from Humlum (1982).

Topography is a characteristic that plays an important role in morphology. Haeberli (1985) notes that permafrost creep is common on slopes from 5° to 30° but steeper slopes inhibit talus accumulation thereby making it more difficult for rock glacier formation. Many lobate rock glaciers form on valley sides from coalescing talus cones (Degenhardt, 2009). Conversely, tongue-shaped rock glaciers get their supply of rock fall from cirque headwalls and creep outward which often result in tongue-shaped rock glaciers (Degenhardt, 2009). However, the overall factor that dictates morphology is

topography where creep processes cause the landform to follow the path of least resistance (i.e., downslope).

All forms of rock glacier morphology have been identified in the Eastern Cascades (Lillquist and Weidenaar, in preparation). There, tongue shaped rock glaciers are the most common features making up more than half of the total rock glacier population.

Rock Glacier Genesis

Another distinguishing characteristic of rock glaciers is their genesis, of which two origins exist. A *talus-derived* origin involves a permafrost core of interstitial ice (i.e., ice mixed with silt, sand, gravel, and boulders) topped by the active layer. Ice in such rock glaciers is thought to form from groundwater or surface water, like snowmelt, seeping into talus and freezing. Upon freezing, the now cohesive mass of ice and rock begins to creep downslope through deformation processes within the internal structure (Haeberli, 1985; Barsch, 1996).

A *glaciogenic* origin has a massive ice core (i.e., solid ice) overlain by a debris layer. These are thought to form from solid glacial ice being covered by repeated major rockfall events (Potter, 1972; Stieg et al., 1998). It also has been proposed that snowpack that is covered and compressed by repeated major rockfall events is a possible origin for some rock glaciers that contain massive ice (Burger et al., 1999). In addition, it is possible for a rock glacier to form from an end moraine and contain massive ice (Burger et al., 1999). This classification has long been debated within the literature where Barsch (1996) argues that a massive ice core is glacial ice and therefore not permafrost. However, in this paper, glaciogenic is an origin for rock glaciers.

Close to 90 percent of the rock glaciers in the Eastern Cascades are talus rock glaciers (Lillquist and Weidenaar, in preparation). Interestingly, all of the glaciogenic rock glaciers are classified as active. In addition, rock glaciers that formed from end moraines often result in lobate morphology in the Eastern Cascades (Lillquist and Weidenaar, in preparation).

Rock Glacier Ages

Dating rock glaciers provides information on activity and may also provide valuable information on past climate conditions. Many methods are used to date rock glacier formation including dendrochronology, weathering rinds, lichenometry, and weathering pits (Barsch, 1996). Another dating mechanism is observing ages of glacial advance and recession. This is helpful with rock glaciers that form directly from ice glacier end moraines. In addition, studies have utilized ice glacier data to help build climate models to identify periods that favor rock glacier development. Some now relict rock glaciers date back to the late Pleistocene. Active rock glaciers generally date back to the Little Ice Age (LIA) (1450-1850 AD) but some have been shown to be several thousand years old dating to the mid-Holocene (Steinman et al., 2012).

In the Eastern Cascades Weidenaar (2013) used dendrochronology, weathering rinds, and lichenometry field methods to date eight rock glaciers. All of the rock glaciers he surveyed were either inactive or relict and he broke them into two groups based on when they became inactive. Five of the eight became inactive at the end of the LIA due to changes in climate. The other three rock glaciers became inactive toward the beginning-middle of the LIA and fall into Barsch's dynamic inactive category where they possibly crept too far from rockfall sources or a decline in rockfall production occurred. In

addition, weathering rind thickness data from the rock glaciers on Table Mountain at the boundary between the Northeast and Southeast Cascades indicate ages of >300 ka (300,000). These extreme ages are suspicious but their location in non-glaciated terrain helps support this (Weidenaar, 2013).

Rock Glacier Internal Composition and Structure

Rock Glacier Active Layer

All permafrost features (including rock glaciers) have an active layer which is the portion of the upper permafrost that seasonally melts and refreezes (Barsch, 1996). Depending on the thickness of the permafrost and the temperatures during the summer melt season the active layer can vary from 0.5 to 7.0 m in thickness on active rock glaciers (Barsch, 1996; Haeberli et al., 2006). The active layer varies in different rock glacier types and locations. Active layer thickness on inactive rock glaciers can reach 10 m (Barsch, 1996).

Studies of the active layer can reveal much about rock glacier temperature regimes. Active layers are determined by local temperature regimes where increased variation between summer highs and winter lows increase their thickness. Along with this, active layers tend to increase in thickness in a warming climate (Barsch, 1996). Of course, rock glaciers favor shaded alpine regions such as north-facing slopes (in the northern hemisphere) so active layers can only reveal temperature regimes for these microclimates (Haeberli et al., 2006). Often the active layer is thickest near the toe of the rock glacier which is often more exposed to insolation and at lower elevations than the head (Barsch, 1996; Haeberli et al., 2006). The active layer tends to be thicker with the presence of finer grained surface material because blocky surface material favors Balch

cooling where the larger voids at the surface allow more cold, dense air to penetrate instead of insulate (Barsch, 1996). However, in parts of the high Andes where climate conditions support continuous permafrost, the insulating blocky surface layer is not needed to maintain internal permafrost so rock glaciers can persist in this area where weathering produces finer grained talus (Janke et al., 2015).

In addition, Goshorn-Maroney (2012) showed that temperatures in the active layer of two active rock glaciers in the North Cascades were above -2°C MAAT based on one year of data. This is thought to be above the temperature threshold for rock glacier occurrence. Similar to Goshorn-Maroney's (2012) findings, Sattler et al.'s (2016) used rock glacier occurrence to model permafrost distribution in the Alps of New Zealand, another maritime mountain range. Their model suggests that permafrost can occur in areas of up 2°C with the mean rock glacier initiation line altitude at 1°C .

Identifying Rock Glacier Internal Composition and Structure

Identifying the internal composition and structure of rock glaciers is difficult given the thick, outer coating of hard, rocky debris inherent to rock glaciers. A range of methods are utilized to investigate the internal structure of rock glaciers (Maurer and Hauk, 2007). These techniques can be separated into two categories: direct and indirect methods. Both approaches have shown to provide useful information on internal structure (Maurer and Hauk, 2007; Degenhardt, 2009; Monnier and Kinnard, 2015).

Direct Methods—Coring and Excavating. The most direct method to observe internal structure is through borehole drilling or excavation (Duguay et al., 2015). This method uses special drill bits, designed to prevent the borehole from overheating due to the drilling process, to drill down through the various layers and remove cylindrical

samples (Monnier and Kinnard, 2013). These samples, if well preserved, can be analyzed to show the different layers of the substructure. The remaining hole can also be utilized to measure temperature at depth and movement of the structure as a whole (Maurer and Hauk, 2007).

Borehole samples from the active rock glacier Murtel in the Swiss Alps show movement processes, depth, and composition of the different layers (Haeberli et al., 1998). Arenson et al. (2002) used boreholes to investigate kinematics of the Murtel rock glacier. Their study found that, although the overall structure moved at a very slow rate, the various inner layers moved at different rates resulting in varied surface morphology. In addition, it was observed that the upper part of the rock glacier mantle moved faster than the lower portion (Arenson et al., 2002). Another important use of boreholes is identifying ice content. Two boreholes drilled into a rock glacier in Switzerland revealed it to have 30 to 80 percent ice content by volume and, based on deformation measurements, to be active (Hoelzle et al., 1998).

Potter (1972) excavated pits and used ice exposures on the Galena Creek rock glacier in Wyoming to show that it consisted of solid ice indicating that it was of glacial, rather than talus, origin. He also found that the active layer was much thicker near the toe of the rock glacier (Potter, 1972). Steig et al. (1998) drilled boreholes into the same rock glacier and extracted solid ice samples. They then found similarities between movements in the ice core layers of this rock glacier to movements found in ice glaciers, implying that this rock glacier has a glaciogenic origin (Steig et al., 1998).

Although boreholes can provide precise visual evidence on internal structure, this method only offers insight into one distinct location on the rock glacier. In addition,

drilling boreholes can be extremely costly and time consuming as well as requiring much gear and equipment (Maurer and Hauk, 2007). Due to these factors, coring and excavating are unsuited for rock glaciers in remote locations without easy road access and are unreasonable for surveys focusing on several rock glaciers (Croce and Milana, 2002; Maurer and Hauk, 2007).

Indirect Methods—Geophysical. When analyzing numerous rock glaciers, it is more practical to use geophysical methods which use tools and instruments to indirectly measure and model the internal structure (Maurer and Hauk, 2007). The methods include diffusive electromagnetic techniques, geoelectrics, seismics and ground penetrating radar (GPR). The various geophysical imaging approaches can produce accurate depictions of internal layers compared to what is found in borehole samples (Maurer and Hauk, 2007).

Electromagnetic techniques measure electrical conductivity of a structure and, based on electric transmission rates, can provide information on different materials present in a substructure. Similarly, seismic methods use seismographs to record impact transmission rates through a structure, which can provide data on changes within materials present (Croce and Milana, 2002). Often researchers use previously drilled boreholes in rock glaciers to compare results of these indirect methods (Maurer and Hauk, 2007; Monnier and Kinnard, 2013). However, this is becoming unnecessary as it has continually been proven that geophysical methods produce accurate data (Maurer and Hauk, 2007; Monnier and Kinnard, 2013).

Ground Penetrating Radar (GPR). Ground penetrating radar (GPR) technology uses the velocity of radar waves transmitted into a substructure and received by a receiver to model internal composition (Annan, 2003; Monnier and Kinnard, 2013, 2015). This is

accomplished by utilizing the different electromagnetic (EM) fields present in subsurface material by recording the time it takes for EM waves to penetrate and bounce off a given material (Figure 2) (Annan, 2003; Degenhardt, 2009). Different materials present different and distinct EM wave velocities that are portrayed as hyperbola in the data (Figure 3). In addition, different subsurface layers can be depicted as linear reflectors in the data that often occur at the interface between two different materials like the rock glacier base and bedrock (Krainer et al., 2010). GPR has a wide range of applications from locating buried utility lines to archeological uses such as identifying buried grave sites, and has proven to be a very useful tool in the field of geology and glaciology as well (Annan, 2003).

Attenuation, or reduction in signal amplitude, is inherent when using GPR over non-uniform material. As EM waves are transmitted into the material some sort of signal loss is characteristic due to energy dissipation within the substrate (Annan, 2003). Different frequency antennas provide a range of resolutions and depth penetration ranging from 1 MHz to 1000 MHz (Annan, 2003). Lower frequency antennas are able to penetrate deeper into the subsurface. However, some degree of resolution is sacrificed with lower frequencies so that higher frequencies give a better depiction of the subsurface but are not able to penetrate as deep. For rock glaciers, it is common to use frequencies ranging from 25 MHz to 500 MHz depending on the goal of the study at hand (Maurer and Hauk, 2007; Monnier and Kinnard, 2013).

Within this range, Monnier and Kinnard (2013) used two 50 MHz antennas to conduct five constant-offset (CO) profiles of a rock glacier in the Chilean Andes which involved manually triggering recordings, or traces, at a set interval along a transect. They

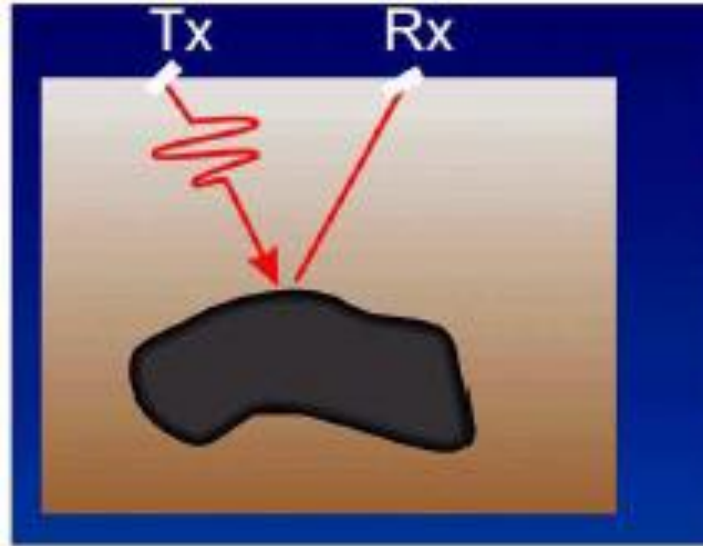


Figure 2. Illustration of GPR transmitter (Tx) and receiver (Rx) positions, and direction of EM waves. Adapted from Annan (2003).

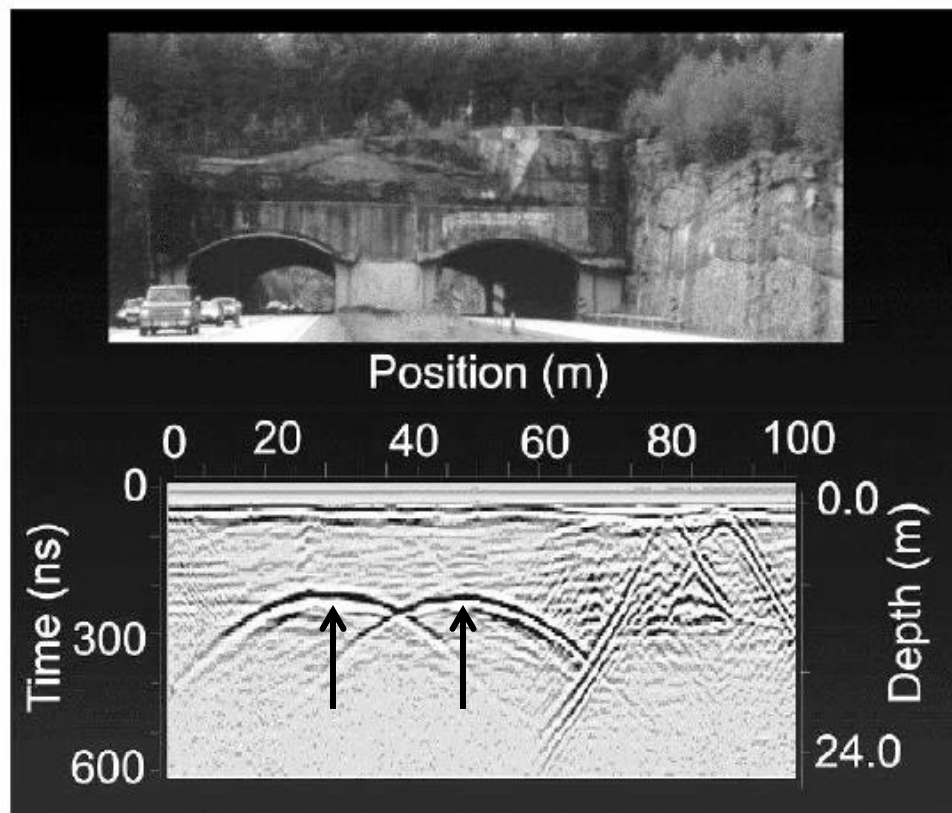


Figure 3. GPR cross section of two road tunnels obtained with a 50 MHz antenna. Notice the pronounced reflectors caused by the roof of the tunnels. Adapted from Annan (2003).

determined that it was inactive based on above freezing temperatures observed at depth in boreholes and multiple water signatures present in the GPR profile, indicating a melting state. They also were able to show that the internal structure was a heterogeneous mix of material thus was talus in origin (Monnier and Kinnard, 2013).

GPR can efficiently model internal layers of rock glaciers along a transect by distinguishing between different materials using known EM transmission velocities of ice, water, and rock debris, shown in Table 1 (Maurer and Hauck, 2007; Monnier and Kinnard, 2013, 2015). Once the internal structure is discovered, it can provide information on activity, morphology, and genesis as discussed above, and can also provide information on its role in the mountain hydrologic cycle.

Table 1. Radar Velocities for Known Material. Adapted from Annan (2003).

	m/ns ⁻¹
Water	0.033
Saturated Material	0.060-0.10
Rock	0.10-0.150
Ice	0.160
Air	0.300

GPR is most effective for identifying bedrock depth (Maurer and Hauck, 2007; Leopold et al., 2011). However, some rock glaciers do not sit directly on bedrock. For example, Isaksen et al. (2000) found that, on the Hiorthfjellet rock glacier in Svalbard, the GPR profile did not pick up a far reflector, or base/bedrock reflector. This was explained by the fact that the rock glacier had likely overridden a series of talus cones that had formed previous to its current extent, thus extending the depth to bedrock past detectable levels. They used a 50 MHz antenna which was able to penetrate to depths of just over 20 m. In addition, Hausmann et al. (2007) found a continuous linear reflector at

a depth of 30 m with indications of material below a rock glacier in Austria. With the help of seismic refraction, further penetration was achieved to find bedrock below this linear reflective layer which indicated that the reflector was a boundary between ice-saturated material and dry till underneath.

Another key section GPR can depict is the active layer. Just as it identifies the bedrock as a far reflector, GPR can pick up a near reflector which has been interpreted as the highest extent of the active layer (Farbrot et al., 2005; Leopold et al., 2011; Monnier and Kinnard 2013, 2015). Identifying the active layer is important for depicting temperature regimes. This near reflector boundary also gives strong evidence of the presence of ice below by indicating a change in stratigraphy or state of moisture (Monnier and Kinnard, 2015).

GPR can reveal much in real time but even more information can be deduced once it is digitally processed. Combined with topographic data, GPR can be a powerful tool to depict internal flow and stratigraphy (Degenhardt, 2009). This involves collecting accurate topographic data along a profile so that it can be topographically-corrected once in the software. GPR can be useful for identifying shear zones where shear stress causes inner deformation of the rock glacier (Degenhardt, 2009). This is closely tied to flow characteristics which dictate different morphologies. These shear zones are interpreted as thrust planes and are depicted as curved reflectors in the data (Maurer and Hauck, 2007; Fukui et al., 2008; Monnier et al., 2008, 2011). Linear reflectors in talus rock glaciers represent layers of higher ice content that were formed from snow cover getting buried and compacted by rockfall (Isaksen et al., 2000). Oppositely, in glaciogenic rock glaciers which have a massive ice core these linear reflectors represent ice-poor sediment layers

within the massive ice (Monnier et al., 2011; Guglielmin et al., 2018). In addition, areas dense with diffracting points near the surface of glaciogenic rock glaciers could be crevasses filled by rockfall (Guglielmin et al., 2018). Reflectors that are curved, concave, and upward or downward-dipping represent compressional stresses (Monnier et al., 2008, 2011). Stacked and surface parallel reflectors show areas of extensional forces (Hausmann et al., 2012). Undulating reflectors are a result of pressure ridges and toplapping reflectors are possible areas where a maximum compression threshold is breached (Monnier et al., 2008).

Many researchers present and analyze results based on topographically-corrected and digitally-processed GPR profiles. In order to conduct such processing techniques an average velocity of the entire medium must be determined in order to calculate accurate depth measurements. Raw or unmigrated GPR data can be used to estimate average velocity of internal material based on synthetic hyperbolae fitting (Monnier et al., 2008, 2011; Degenhardt, 2009; Krainer et al., 2010; Florentine et al., 2014). This method involves matching a synthetic hyperbola to hyperbolas depicted in the unmigrated data. Monnier and Kinnard (2015) used this technique to estimate quantities of ice, rock, and saturated debris in a rock glacier in the Chilean Andes. They collected a longitudinal transect that extended over 2 kilometers (km) down the center of the rock glacier. They were able to estimate percentages of material by comparing average velocity rates identified through hyperbolae fitting to amount of diffracting points, or material that reflects the GPR signal, in 25 m sections of the transect. They showed that the Las Liebres rock glacier average 66% ice content with a higher percentage near the head and a lower percentage near the toe (Monnier and Kinnard, 2015). However, diffraction

points can be a combination of reflection and diffraction instances, and the overall data can be highly influenced by external noise (Guglielmin et al., 2018). Further, this method can be extremely subjective as hyperbola fitting is prone to user error.

The Mountain Hydrologic System

Snowpack as a Water Source

Snowpack in high elevation mountain ranges acts as a natural reservoir for water. During the winter season snow accumulates on mountain slopes. As seasons shift and temperature increases, the snowpack gradually melts contributing to streamflow. Depending on the amount of snow received in a given year the snowpack can provide meltwater well into spring and even early summer months. However, Stoelinga et al. (2010) found that Cascade snowpack decreased by 23 percent since the 1930s. They showed that this is partly due to shifts in circulation patterns. In addition, they found the dates of maximum snowpack and 90 percent meltout have moved five days earlier in the season. These shifts suggest that earlier meltout would have a negative effect on baseflow in late summer months after this resource is depleted. Additionally, their future projections using climate modeling attribute the notable decrease in snowpack to anthropogenic climate warming (Stoelinga et al., 2010).

Glaciers as Water Sources

Glaciers also contribute significantly to streamflow in mountain environments. Glaciers seasonally ablate (i.e., waste away) and accumulate (through the addition of snow). The relationship between these seasonal processes is referred to as the mass balance. The mass balance of a glacier can either be: in equilibrium, where its rate of accumulation is equal to its rate of ablation; positive, where its rate of accumulation

exceeds its rate of ablation (ice loss); or negative, where ablation exceeds accumulation (Pelto, 1993). Whether a glacier has a positive or negative mass balance it still contributes to streamflow during the melt season. North Cascade glaciers currently have negative mass balances due to a warming climate (Pelto, 2011a). Due to less surface area for insolation to melt, decreased late summer stream flows have been observed on rivers stemming from glaciated basins in the Cascades (Pelto, 2011a). According to Post et al. (1971) meltwater from North Cascades glaciers contributed about 800 million cubic meters (m^3) annually to streamflow in 1971 but has since declined (Pelto, 2011a). In addition, higher mass losses from glaciers can generate higher peak flows and larger diurnal variations in streamflow (Moore et al., 2009). On a shorter time scale, this means a larger contribution of meltwater during the late summer dry period but it also means this resource is due to deplete faster. When this resource does deplete, extreme stress will be put on the mountain hydrologic cycle.

A way of measuring glacial change is to estimate glacial volume change over time. Estimating glacier volume can provide a better insight on total ice quantity and water equivalence. Estimating volume of a glacier has traditionally been accomplished by area-volume scaling equations. These equations are formed from a sample of glaciers where field measurements of glacial depth are attained from geophysical methods such as radio echo soundings. These models can then be applied to estimate volume of entire populations of glaciers with measured surface areas. Granshaw and Fountain (2006) compared three different area-volume scaling techniques with known depths from field measurements of five North Cascade Glaciers. They then used the best fit model to apply to the entire population of glaciers within the park to two different datasets, one from

1958 and one from 1998, to determine glacial volume change over time. During this period, they estimated these glaciers lost approximately 0.8 km³ of ice which they equate to about 6 percent of late summer streamflow (Granshaw and Fountain, 2006).

Rock Glaciers as Water Sources

Many researchers have analyzed the role of rock glaciers in the mountain hydrologic cycle (Haeberli, 1985; Barsch, 1996; Krainer and Mostler, 2002; Krainer et al., 2007; Kellerer-Pirklbauer et al., 2013; Geiger et al., 2014). Geiger et al. (2014) compared discharge rates in two adjacent basins, one containing rock glaciers and one without. They found that discharge rates from the rock glacier basin were steadier year round than discharge rates from basins lacking rock glaciers. They also found that peak stormflow was delayed, higher, and contained more surface runoff after a precipitation event in rock glacier basins. In addition, they found that discharge rates from the basin containing rock glaciers gradually declined throughout the summer, compared to the non-rock glacier basin, emphasizing the insulating capabilities of the outer debris layer (Geiger et al., 2014).

Rock Glacier Water Storage Capacity

Few studies of rock glacier water storage capacity have been conducted and those completed are currently restricted to portions of the Andes Mountains and the Nepalese Himalaya. These studies span the Chilean Andes (Azocar and Brenning, 2010), Bolivian Andes (Rangecroft et al., 2015), and Argentinean Andes (Perucca and Angillieri, 2011) as well as a more recent study of the Nepalese Himalaya (Jones et al., 2018). This research established rock glaciers as significant water stores for areas of depleting or shifting water resources (Azocar and Brenning, 2010; Perucca and Angillieri, 2011;

Rangecroft et al., 2015). Each study created, or used an existing inventory of rock glaciers that were compiled from various combinations of aerial and satellite imagery, including Google Earth (Azocar and Brenning, 2010; Perucca and Angillieri, 2011; Rangecroft et al., 2015; Jones et al., 2018). They used the inventories to calculate overall surface areas of all rock glaciers. From there, estimates of average ice content and thicknesses of the ice-rich layers were combined with surface areas and used to calculate total water equivalence of rock glaciers in the study area.

Although these techniques seem sufficient for assessing water equivalency of rock glaciers, Arenson and Jakob (2010) criticized the validity of the data. In addition, Duguay et al. (2015) analyzed the amount of research available on rock glaciers and glaciers throughout the past century, specifically looking at articles focused on the hydrology of rock glaciers. They argued that in order for results to be accurate the study needs to be conducted through a quantitative approach with emphasis on field data to support the results, and that the above techniques were essentially qualitative. The reliance on estimations of ice content and permafrost depths without field research to substantiate claims is their main area of concern. Duguay et al. (2015) only actually discuss Azocar and Brenning's (2010) research along with a handful of other studies. However, Perucca and Angillieri (2011), Rangecroft et al. (2015), and Jones et al. (2018) all used the same techniques as Azocar and Brenning (2010). In addition, Duguay et al. (2015) points out the lack of emphasis on the complexity of the rock glacier hydrologic cycle. These other studies directly compare rock glacier hydrology to ice glacier hydrology. Rock glacier ice consists of permafrost which has been permanently frozen for multiple centuries or longer whereas glacier ice is typically younger due to the process of mass exchange

(Arenson and Jakob, 2010). In turn, glaciers are highly affected by short term climate fluctuations whereas rock glaciers react over longer periods of time (Duguay et al., 2015). These two features, while similar, act differently in the mountain system and need to be treated as such when assessing hydrological significance (Arenson and Jacob, 2010; Duguay et al., 2015).

All four of the water equivalency studies use Brenning's (2005) methods to calculate estimations of water equivalence. Brenning (2005) developed his own empirical formula for the thickness of the ice-rich rock glacier permafrost. He states that the formula is derived from field measurements, but does not elaborate on these measurements.

Due to these shortcomings, Duguay et al. (2015) emphasize the gap in hydrological research of rock glaciers. These estimations will be used as a reference for comparison of original field measures produced in this study. No previous studies have used geophysical field techniques to survey a large amount of rock glaciers in a single mountain range to assess internal composition, structure, and potential ice-water equivalency.

CHAPTER III
STUDY AREA

The area of focus for this research is the Eastern Cascades of Washington (Figure 4). This area is defined as the mountainous region that begins at the Cascade Crest, which is a physical boundary that divides the Cascade Range into eastern and western portions, and spans east to the Okanogan, Columbia, and Yakima Rivers. The region runs from the Washington-Oregon border north to the Washington-Canadian border, which spans over 3° of Latitude from 45.5° N to 49° N. Specific study sites fall within parts of Okanogan, Chelan, and Yakima counties.

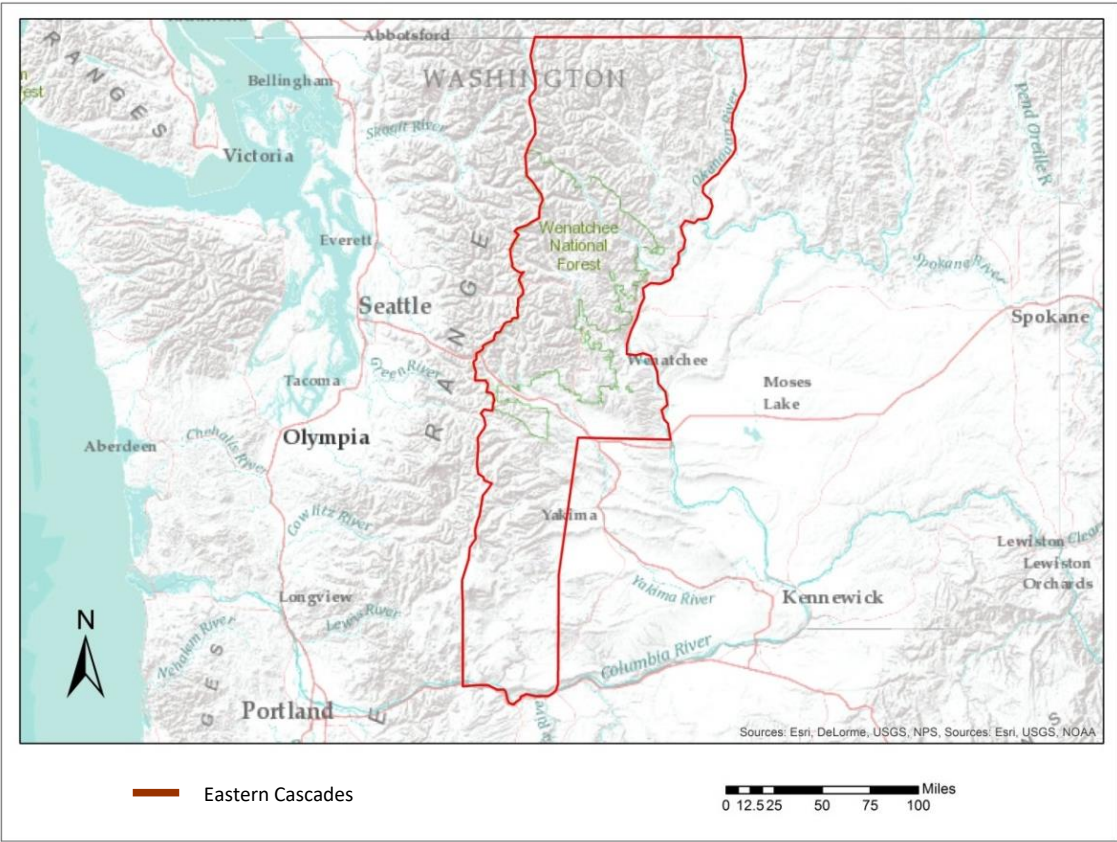


Figure 4. Eastern Cascades.

Geology and Geomorphology

The Cascade Range is a volcanic mountain chain that spans from Lassen Peak in northern California north through Oregon and Washington and into southern British Columbia, Canada (Beckey, 2000). Its peaks range in elevation from a few hundred meters (m) to above 4,000 m (Beckey, 2000). The Eastern Cascades includes the Sawtooth, Wenatchee Ranges, and Goat Rocks, each of which possess rock glaciers (Weidenaar, 2013). The highest peaks in the range are mostly active stratovolcanoes that lie west of the Cascade Crest and outside the study area. The exception is Mount Adams which sits on the crest. The area includes the two highest non-volcanic peaks east of the crest—Bonanza Peak at 2,899 m and Mount Stuart at 2,870 m. Much of this terrain is characterized by steep slopes with sharp, jagged ridgelines and peaks (Beckey, 2000).

The Cascade Range has a complex geologic makeup with predominantly volcanic rock mixed with sedimentary rock and granitic intrusions (Tabor et al., 1989). In addition, areas like the Wenatchee Range are rich in serpentinite, which is an ultramafic rock formed from oceanic floor material (Price et al., 2013). Hard rocks such as andesite, basalt, and granite are instrumental for forming talus that is key for many rock glaciers (Barsch, 1996).

Pre-Historic Glaciation

Glaciation is a major geomorphic process that once dominated the Cascade Range and is responsible for much of its current form. The last extensive glaciation occurred during the Pleistocene Epoch which spanned from about 2.6 million years to 11,700 years ago. During this time period, cirque and valley glaciers shaped Cascade Range landscapes (Porter, 1976). The last glacial maximum in the Cascades occurred during the

Fraser glaciation of the Pleistocene Epoch (Porter, 1977). During this period Porter (1977) estimates the glaciation threshold to be about 900 m lower than currently observed. Pollen records indicate that July average temperatures in this area were, on average, 4.5°C cooler during the Pleistocene than those at present (Heusser, 1972).

Moving into the Holocene, which began shortly after the Fraser glaciation ended 11,700 years ago, alpine glaciers experienced a period of rapid recession as a result of climate warming. Throughout this time, glaciers experienced fluctuations in size with multiple advances that then culminated in the largest glacial advancement of the Holocene during the LIA (Menouos et al., 2009). This was a period of glacial advance in the Cascades that lasted from approximately the mid-15th century to the mid-to-late 19th century (Steinman et al., 2012). During this time the Cascades experienced a slightly cooler climate regime with MAAT being 1.0-1.5°C cooler than present (Pelto and Hedlund, 2001).

Cirques are predominantly north-northeast facing in the Cascades because this orientation receives the least amount of direct solar radiation (Porter, 1977). In addition, west winds load leeward slopes encouraging glacial growth (Evans, 1977). Mitchell and Montgomery (2006) suggest that the main control of peak elevation in the Cascades is glaciation. This is due to rapid erosion caused by cirque glaciers in the range leaving behind over-steepened slopes. They show a correlation between average Quaternary Equilibrium Line Altitudes (ELA), cirque floor altitudes, and peak elevations. Most importantly, they identify the significant role of glaciation to the over-steepened slopes seen at higher elevations in the range. They, in turn, state that glacial erosion has played a more significant role in shaping the range than fluvial erosion processes (Mitchell and

Montgomery, 2006). These glaciers eroded U-shaped troughs and formed an extensive number of deep cirques. As a result of this glaciation and upon recession of these masses, the Cascades are now subject to over-steepened valley slopes and cirque headwall escarpments (Mitchell and Montgomery, 2006).

The stress related to glacial loading and unloading has likely enhanced mass wasting after deglaciation. Glacial debuitressing, or unloading, during times of glacial recession and deglaciation can provide a “stress release” factor that may cause the underlying structure to react through mass wasting processes (Cossart et al., 2008). This over-steepening forms abrupt fall faces (Ritter et al., 2011). In addition, frost wedging, through the process of freeze-thaw, works with the steep terrain and jointing created by unloading, to degrade the landscape. The rockfall and resulting talus is essential for rock glacier formation (Burger et al., 1999).

Present Glaciation

Since the end of the LIA in the late 1800s, glaciers began to retreat on a world-wide scale. This retreat has generally continued through present with the ~1940-1970 period as the only exception when a period of cold and wet weather tied to Pacific Decadal Oscillation (PDO) led to a positive mass balance in many glaciers (Moore et al., 2009). Since the 1980s, most glaciers have been in negative mass balance.

Washington State includes over half of the total glacier surface area in the U.S. south of Alaska (Post et al., 1971). A 1971 inventory of North Cascade glaciers found 756 glaciers $>0.1 \text{ km}^2$ (Post et al., 1971). Surprisingly, many small cirque glaciers seem to persist without losing much mass and some have even advanced (O’Neal et al., 2015). On the other hand, larger glaciers like the South Cascade Glacier, which was designated

as a benchmark glacier and has been closely observed since the 1960s, has seen greater mass balance loss than many of the small cirque glaciers in recent decades (Fountain et al., 2009).

Average glaciation thresholds rise from 1,800 m on the western side of the range to 2,600 m at the full eastern extent of glaciation. This is due to the Cascade Crest impeding precipitation from moving east. However, mountain passes play an important role in terms of spatial variations for glacial extent. These passes allow moist air to penetrate further inland, allowing for glaciation further into the Eastern Cascades (Porter, 1977).

Climate

The climate of the Eastern Cascades relates directly to its position east of the Cascade Crest (Mass, 2008). The crest is a drainage divide for the range where precipitation falling east of the divide flows into the Columbia River, and precipitation falling on the western flanks flows to the Puget Sound and the Pacific Ocean. The Cascade Range sits perpendicular to the prevailing westerly winds. As such, the range acts as a barrier for wind and, in turn, weather systems. As westerly winds move inland, air masses and associated storm systems are forced up and over the range due to orographic uplift, which causes precipitation (Mass, 2008). This results in the windward (i.e., western) side of the mountains receiving the majority of the precipitation while the leeward, or eastern, side receives substantially less.

Overall temperature patterns in the Cascades are largely controlled by topography, marine influence, proximity to the Cascade Crest, and cloud cover (Mass, 2008). Due to the environmental lapse rate, temperatures decrease by approximately 1°C

for every 100 m gain in elevation (Price et al., 2013). Water also plays a role as MAAT is typically warmer closer to the Puget Sound (Mass, 2008). Similarly, cloud cover provides insulation for temperatures at night and reflects insolation during the day. This causes less variability in highs and lows as seen on the cloudier, western side of the crest (Mass, 2008). As a result, temperatures are more extreme moving east from the Cascade Crest.

Annual precipitation totals drastically decrease moving eastward from the crest. Snoqualmie Pass receives significantly more annual precipitation (2,540 mm) than does Lake Cle Elum (889 mm), which is located only about 24 km to the east (Figure 5) (WRCC, 2017). In addition, the majority of this precipitation in both regions is received as snowfall. The range has a precipitation pattern of wet winters and dry summers. The heaviest amount of precipitation falls from November through January, and because of the mountain environment, this often falls as snow (Mass, 2008). However, since this range is dominated by a maritime climate, it is common in winter to receive a mix of rain and snow or just rain, even at higher elevations. The driest season occurs during summer months from June through August. These seasonal precipitation patterns are largely due to shifts in the jet stream. In the winter, the Aleutian Low shifts south and helps facilitate the formation of storms in the Pacific causing the wet season to occur. In the summer, the Hawaiian High migrates north pushing the low pressure system away and hindering storm development thus causing dry conditions (Mass, 2008).

Overall, long-term climate data is lacking for most of the high Cascades. Weather stations are typically situated near major roadways in mountain passes. Snow Telemetry (SNOTEL) sites, maintained by the National Resources Conservation Service (NRCS), provide climate data for more remote locations throughout the range. However, most of

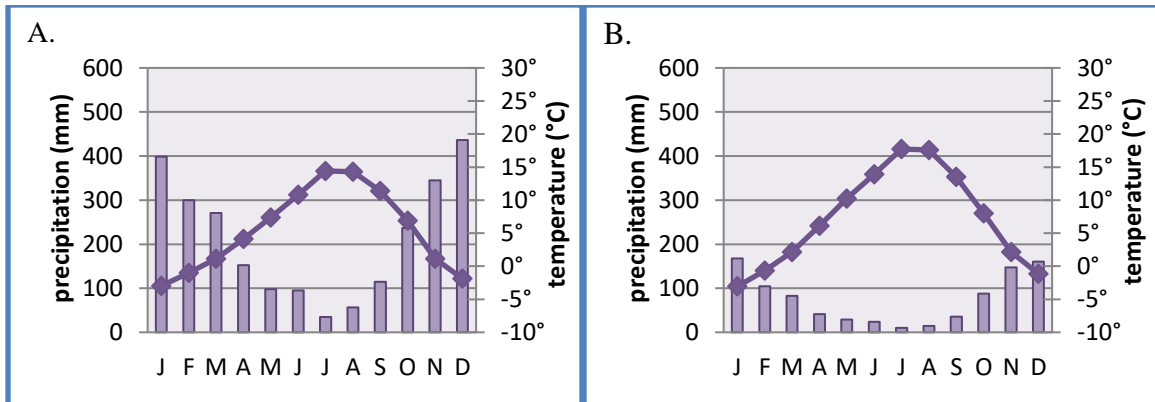


Figure 5. A) Snoqualmie Pass (1910-2002) and B) Lake Cle Elum (1908-1977) climographs. Data courtesy of Western Regional Climate Center (WRCC).

these sites do not provide full 30 year climate normal data because they were installed less than 30 years ago. In addition, these sites may sit at high elevations but none are located above timberline. As a result high elevation climate data representative of most rock glacier sites is not available.

Hydrology

The study area comprises a large portion of the middle Columbia River Basin. This region includes six major watersheds that are tributaries to the Columbia—the Yakima, Wenatchee, Entiat, Chelan, Methow, and Okanogan River watersheds. All of these rivers, with their associated tributaries, have their headwaters in the Eastern Cascades in basins containing rock glaciers.

Vegetation

Active and inactive rock glaciers in the Eastern Cascades are located near or above timberline. Timberline is a biological region that denotes the extent of forest in either high mountain environments, polar regions, or edges of grasslands (Arno, 1984). In the timberline regions of the Cascades, the depth and duration of snowpack plays a large

role in dictating tree and plant growth as well as solar radiation (Canaday and Fonda, 1974). Sites east of the Cascade Crest experience greater temperature extremes and less precipitation due to the reduced influence of the maritime climate. This causes the elevation of timberline to increase eastward (Arno, 1984). At Snoqualmie Pass, forest line, which is the highest extent of continuous forest, sits at about 1,500 m but 50 km east it increases to around 1,900 m (Arno, 1984). Forest line is also affected by latitude (i.e., temperature) so that by Hart's Pass, which sits on the crest over 150 km north on Snoqualmie Pass, timberline can be found at 1,830 m. Moving east from there, the Okanogan Highland rain-shadow zone in the North Cascades has a timberline elevation above 2,100 m (Arno, 1984).

The most common tree type found developing adjacent to, and on, rock glaciers in the Northeastern Cascades is the alpine larch. Larch (*Larix occidentalis*) trees are deciduous conifers. This species commonly grows on north-facing aspects, near glaciers, and on talus slopes (Arno, 1984). Other timberline tree species in Washington's Northeastern Cascades include subalpine fir (*Abies lasiocarpa*), white-bark pine (*Pinus albicaulis*), and Engelmann spruce (*Picea engelmannii*) (Arno, 1984). In Washington's Southeastern Cascades timberline tree species include mountain hemlock (*Tsuga mertensiana*), white-bark pine (*Pinus albicaulis*), and lodgepole pine (*Pinus contorta*).

Land Use

All of the study sites are located on Okanogan-Wenatchee National Forest lands. Six of the nine rock glaciers surveyed fall within wilderness areas managed by the U.S. Forest Service.

Study Area Sites

The overall study area encompasses the Eastern Cascades but specific field study sites are broken up into two different regions: the Northeastern Cascades and the Southeastern Cascades (Figure 6). Seven rock glaciers and one moraine were surveyed in the Northeastern Cascades and three rock glaciers were surveyed in the Southeastern Cascades. Table 2 provides a summary of all rock glacier study sites.

Table 2. Eastern Cascade rock glacier study sites.

Rock Glaciers	Latitude	Longitude	Distance from Crest (km)	Head Elevation (m)
VC1	48.55336	-120.554	10.5	2,083
VC2	48.55147	-120.559	10.4	2,135
BrC1	48.4934	-120.742	15.3	1,885
NC1	48.48472	-120.575	35.1	2,075
WFBC3	48.25301	-120.417	42.3	2,265
WFBC4	48.24925	-120.404	43	2,275
EFBC2	48.2231	-120.351	45.5	2,338
TC1	47.31146	-120.562	66	1,662
SC5	46.56469	-121.191	17	2,027
BC1	46.5307	-121.325	9.4	1,901
BC3	46.52486	-121.327	9.8	2,007

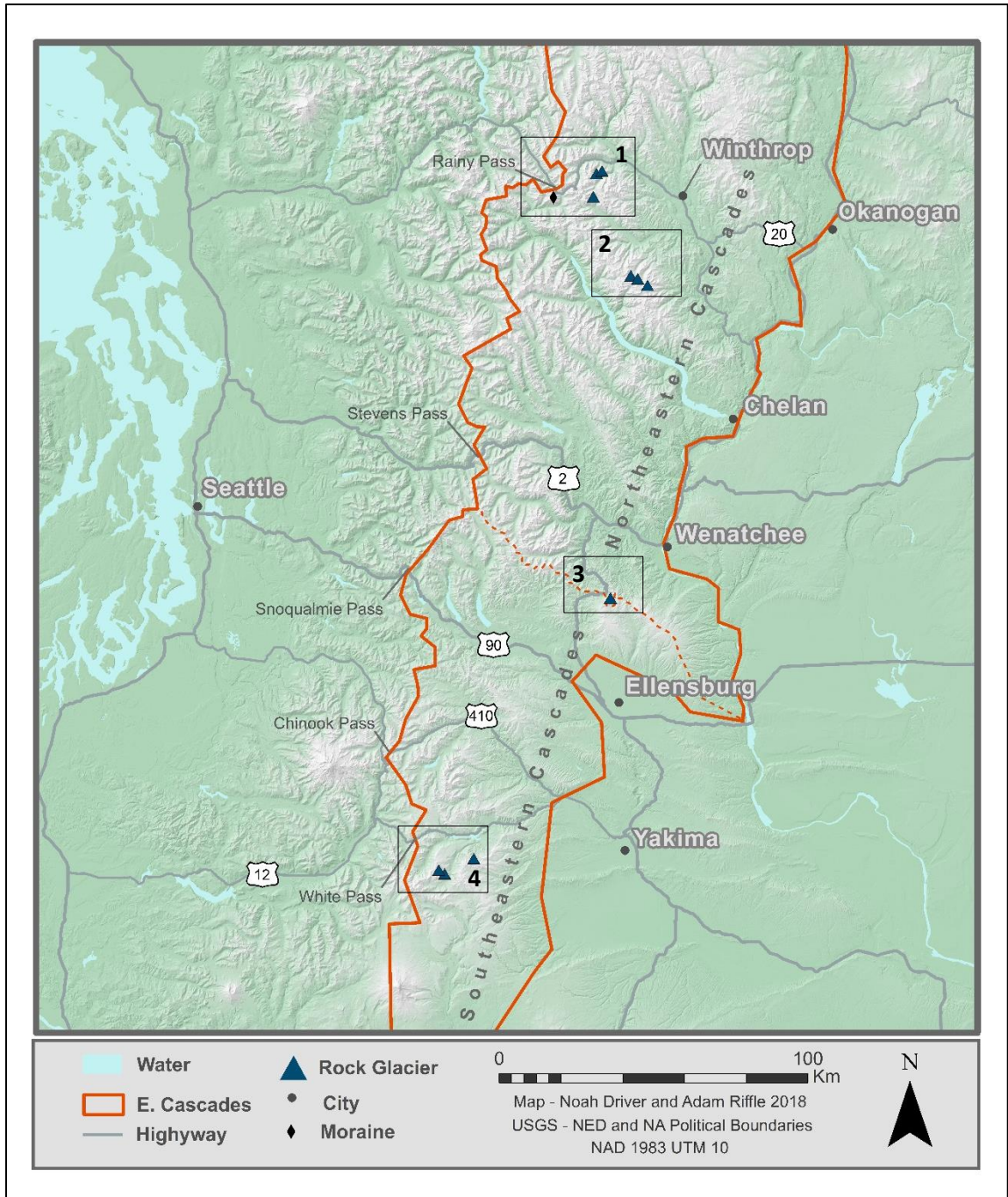


Figure 6. Eastern Cascades study sites. Numbers indicate subsequent inset maps.

Study Area 1: Northeastern Cascades

The Northeastern Cascades contain seven individual rock glaciers assessed in this study: Varden Creek 1 (VC1), Varden Creek 2 (VC2), North Creek 1 (NC1), West Fork Buttermilk Creek 3 (WFBC3), West Fork Buttermilk Creek 4 (WFBC4), East Fork Buttermilk Creek 2 (EFBC2), and Tronsen Creek 1 (TC1) and one moraine: Bridge Creek 1 (BrC1). As their names imply, each of these features sits at the head of the drainage they are named after. All study sites fall within the Okanogan-Wenatchee National Forest. Four of them are located in the Lake Chelan-Sawtooth Wilderness which include NC1, WFBC3, WFBC4, and EFBC2. In addition, all seven of the rock glaciers are located within the timberline zone. Six of these rock glaciers, including WFBC3, WFBC4, EFBC2, VC1, VC2, and TC1 have larch trees present on their surface.

The two northern-most surveyed rock glaciers are VC1 and VC2 (Figure 7). Both of these feed from Varden Creek into Early Winters Creek which then empties into the Methow River. BrC1 is located less than 3 km south of Rainy Pass. This drainage actually turns west and empties into the Stehekin River which flows into Lake Chelan and then into the Chelan River and on to the Columbia River. North Creek feeds into the Twisp River which runs into the Methow and finally into the Columbia River.

The three northern-most rock glaciers in this study area are situated closer to the Cascade Crest than any of the other four surveyed rock glaciers in the North Cascades. As a result, this area experiences increased amounts of precipitation (Figure 8). Average annual precipitation at Rainy Pass totals 1,452 mm while MAAT is 2.2°C (NRCS, 2018). The weather station is situated at an elevation of 1,490 m. Important to note is that the NRCS SNOTEL data only represents a 28 year average with some years missing from the

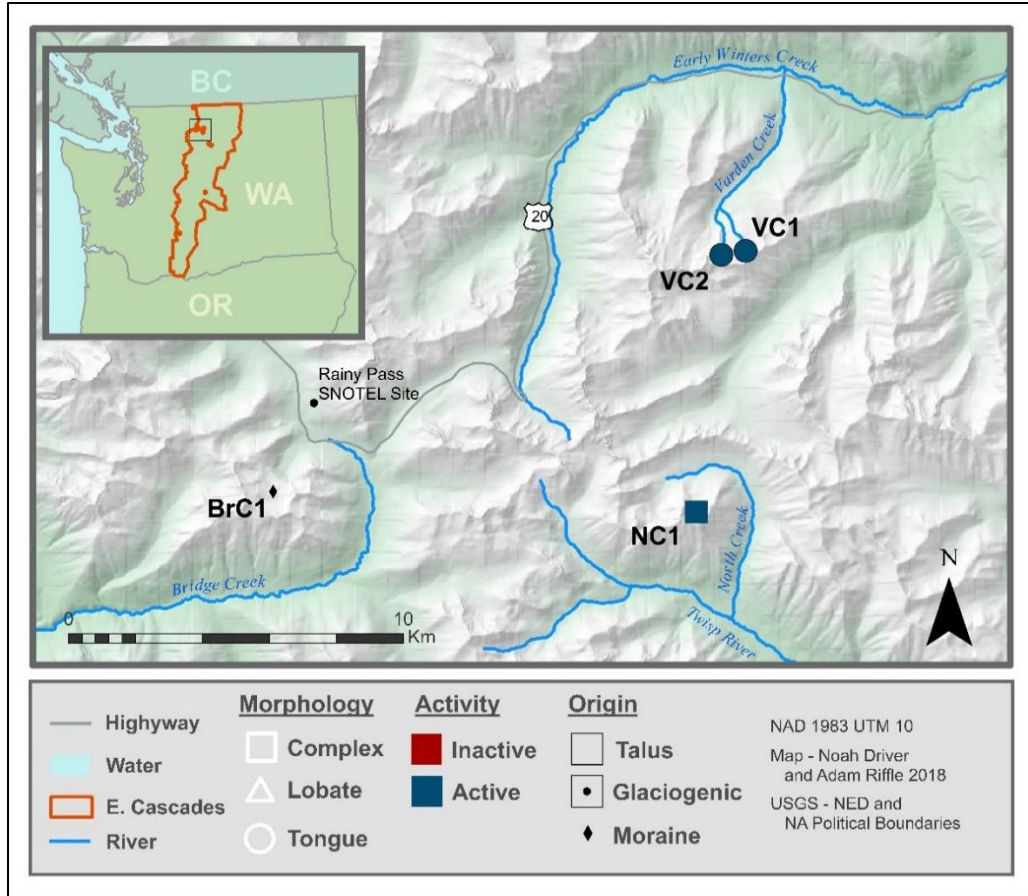


Figure 7. Northeastern Cascades study sites inset map 1.

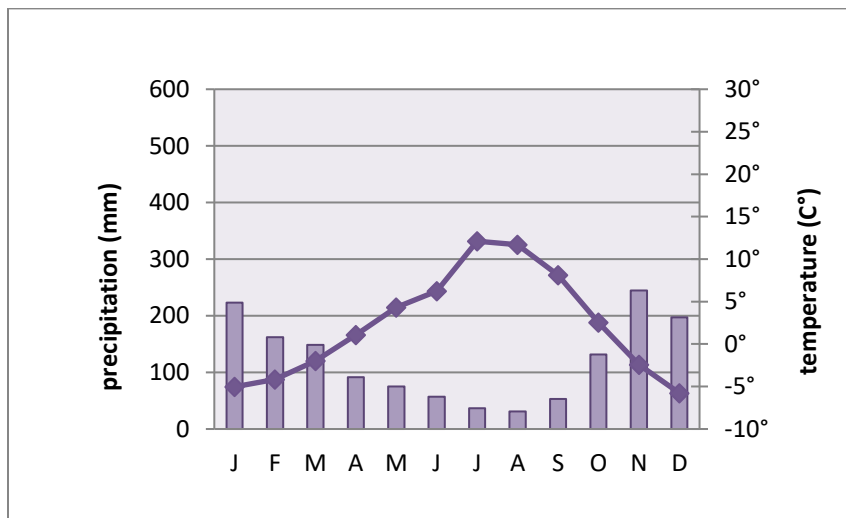


Figure 8. Rainy Pass, WA climograph (1989-2017). Data courtesy of Natural Resources Conservation Service (NRCS) Snow Telemetry (SNOTEL) Rainy Pass site.

data set. However, these sites are in closer proximity and higher in elevation than WRCC sites in the vicinity, and therefore provide a better representation of climate norms at their respective study sites. All three of these rock glaciers sit above 2,000 m but below 2,133 m.

Moving south, the next three rock glaciers are WFBC3, WFBC4, and EFBC2 (Figure 9). The closest weather station to these rock glaciers is Stockdill Ranch, WA (48°22'N, 120°20'W) which is located about 15 km north of the three Buttermilk Creek rock glaciers in the Twisp River valley (Figure 10). Average annual precipitation at this site is 438 mm and MAAT is 5.5°C (WRCC, 2018). This weather station sits at an elevation of 670 m which is substantially lower than these three rock glaciers which are all above 2,200 m. This implies that MAAT is much lower at the rock glacier sites. In addition, all of these rock glaciers are located above forest line and within the timberline zone.

Only one study site, TC1, is located in the southern portion of the Northeastern Cascades (Figure 11). This rock glacier is located at an elevation of 1,662 m. Tronsen Creek flows from above Blewett Pass down to Peshastin Creek which runs into the Wenatchee River and finally empties into the Columbia River. This site is in the Wenatchee National Forest and is located on the edge of Table Mountain. This location is unique because it is one of two study sites that fall outside the limit of glaciation in the Cascades.

The nearest weather station to Tronsen Creek is the Blewett Pass SNOTEL site (47°21'N, 120°40'12"W) that is located at an elevation of 1,292 m. Average precipitation at Blewett Pass is 889 mm and the MAAT is 5.71°C (Figure 12) (NRCS, 2018). Like the rest of the Cascades, the wet season here is during the winter with over half of the annual

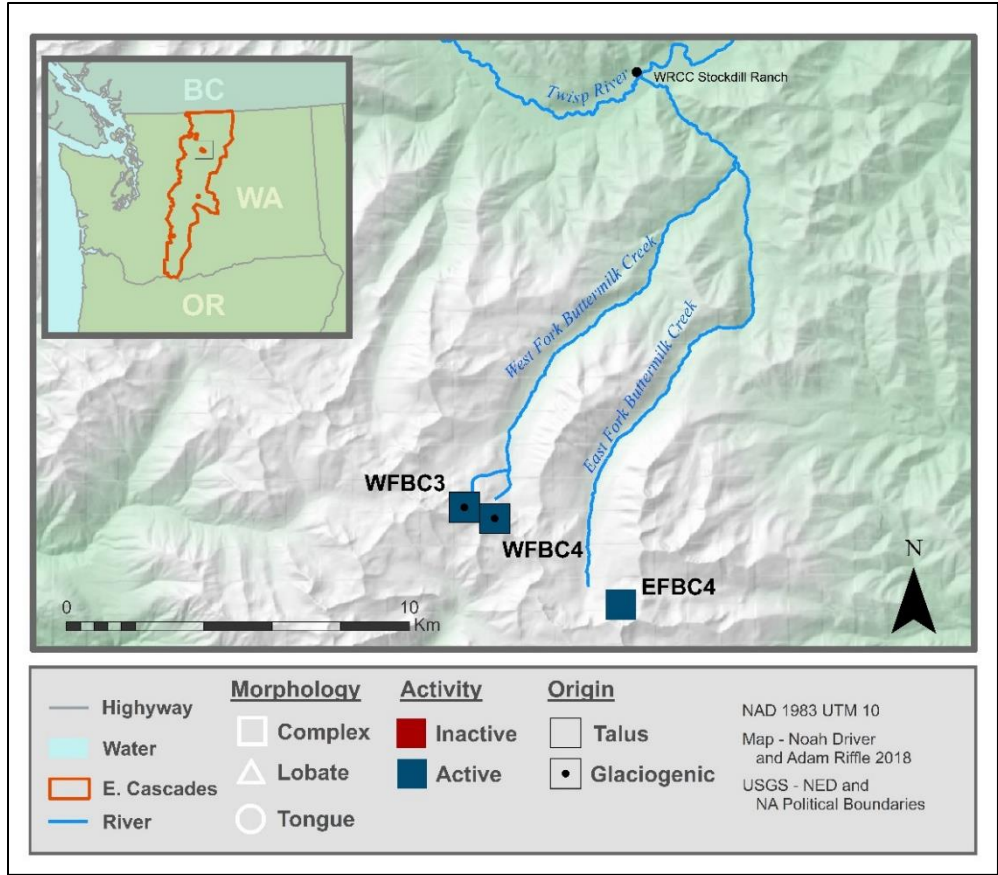


Figure 9. Northeastern Cascades study sites inset map 2.

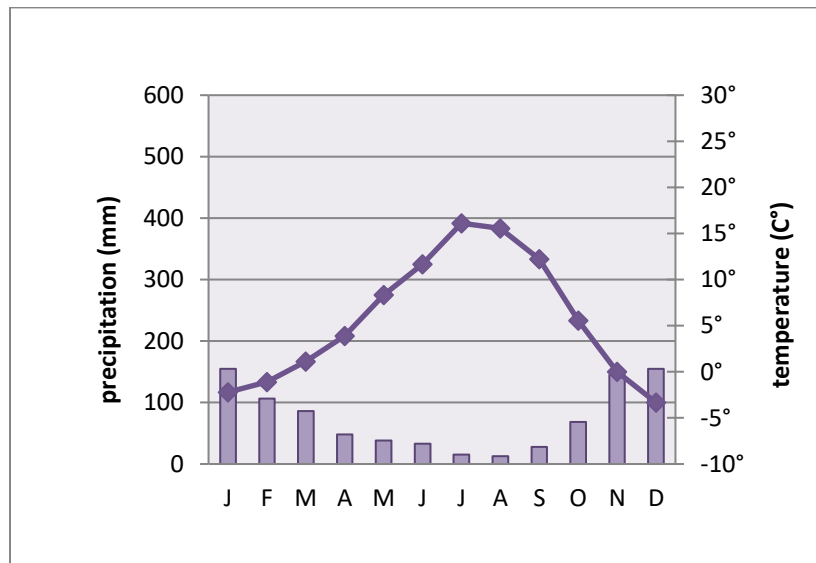


Figure 10. Stockdill Ranch, WA climograph (1909-1963). Data courtesy of WRCC.

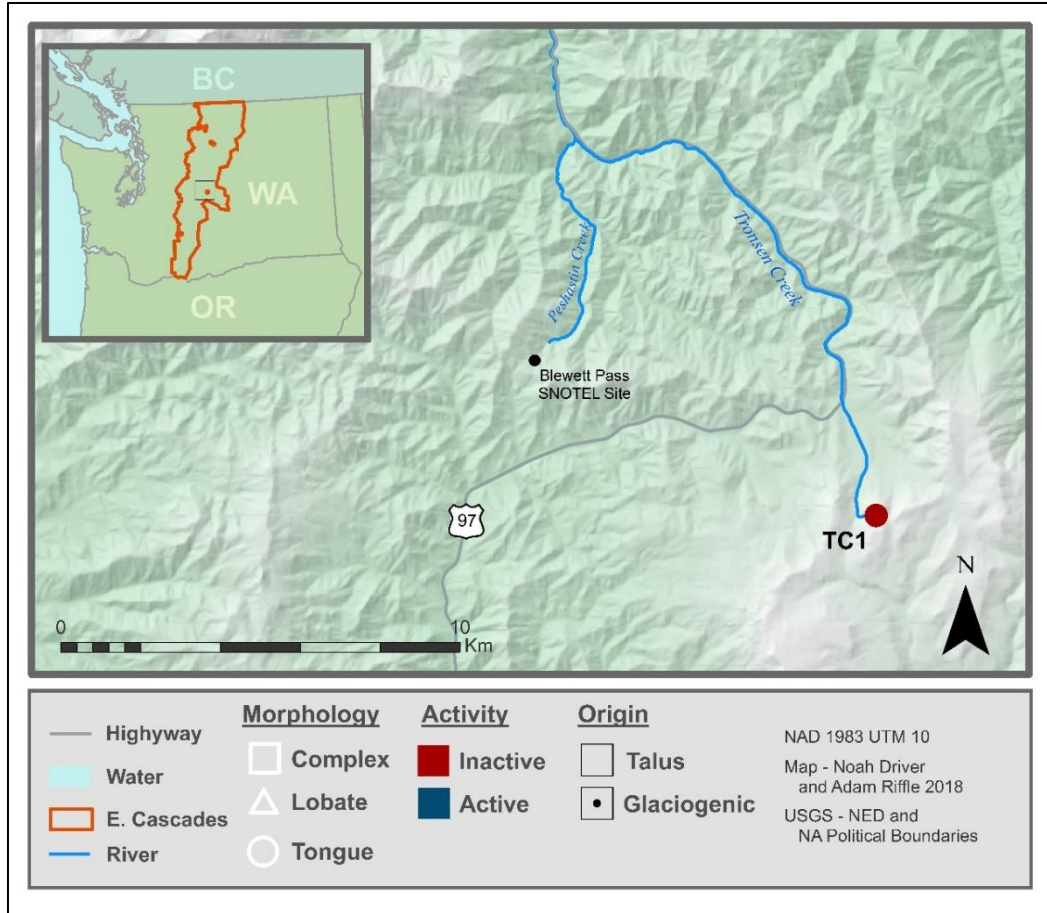


Figure 11. Northeastern Cascades study sites inset map 3.

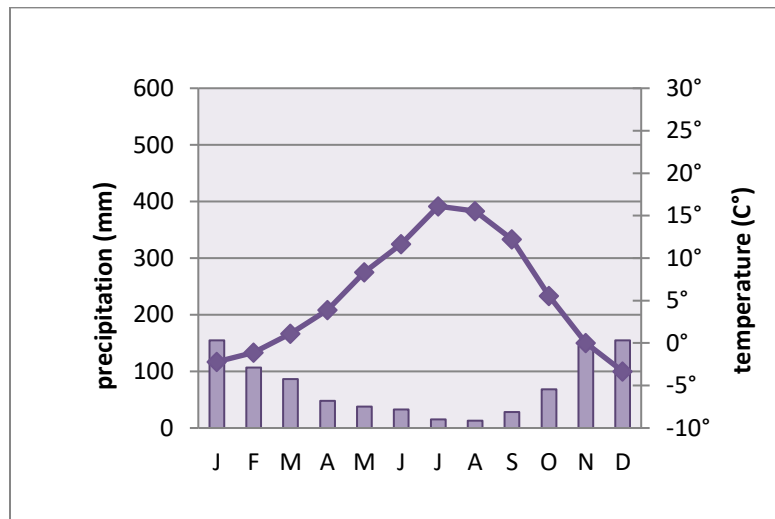


Figure 12. Blewett Pass, WA climograph (1989-2017). Data courtesy of NRCS SNOTEL Blewett Pass site.

precipitation falling from November through January at 470 mm. During these months average temperatures stay below freezing; however, the average temperature rises above freezing at 1°C. This warmer temperature at such a high elevation helps explain the inactive classification on the Tronsen Creek rock glacier.

Study Area 2: Southeastern Cascades

This study area is located within Washington's Southeastern Cascades and has a very different geologic and climatic makeup than the North Cascades (Figure 13). This area is dominated by andesite and basalt. Bear Creek 1 (BC1) and Bear Creek 3 (BR3) are located on the edge of the Goat Rocks Wilderness. Both of these two rock glaciers consist of andesite (Lillquist and Weidenaar, in preparation). Spruce Creek 5 (SC5) is not located in the Wilderness Area but sits just inside the Wenatchee National Forest which borders Washington Department of Natural Resources (DNR) land less than 0.5 km to the south. Spruce Creek consists of basalt. Both Bear Creek and Spruce Creek flow into the South Fork Tieton River which then merges with the Naches River. Subsequently, the Naches joins the Yakima River which flows into the Columbia River.

The closest permanent weather station is a SNOTEL site located at Pigtail Peak (46°37'12"N, 121°22'48"W) approximately 10 km to the northwest. Total annual precipitation is 2,050 mm and MAAT is 2.6°C (Figure 14) (NRCS, 2018). This location sits almost directly on the Cascade Crest which could help explain its high annual precipitation. The rock glaciers in the study area are approximately 10 km (Bear Creek 1 and 3) and 20 km (Spruce Creek) east of the crest. A sharp decrease in annual precipitation rates is likely, even at these distances. This site is situated at a higher elevation of 1,768 m; however, all three of the rock glaciers in this study area are above

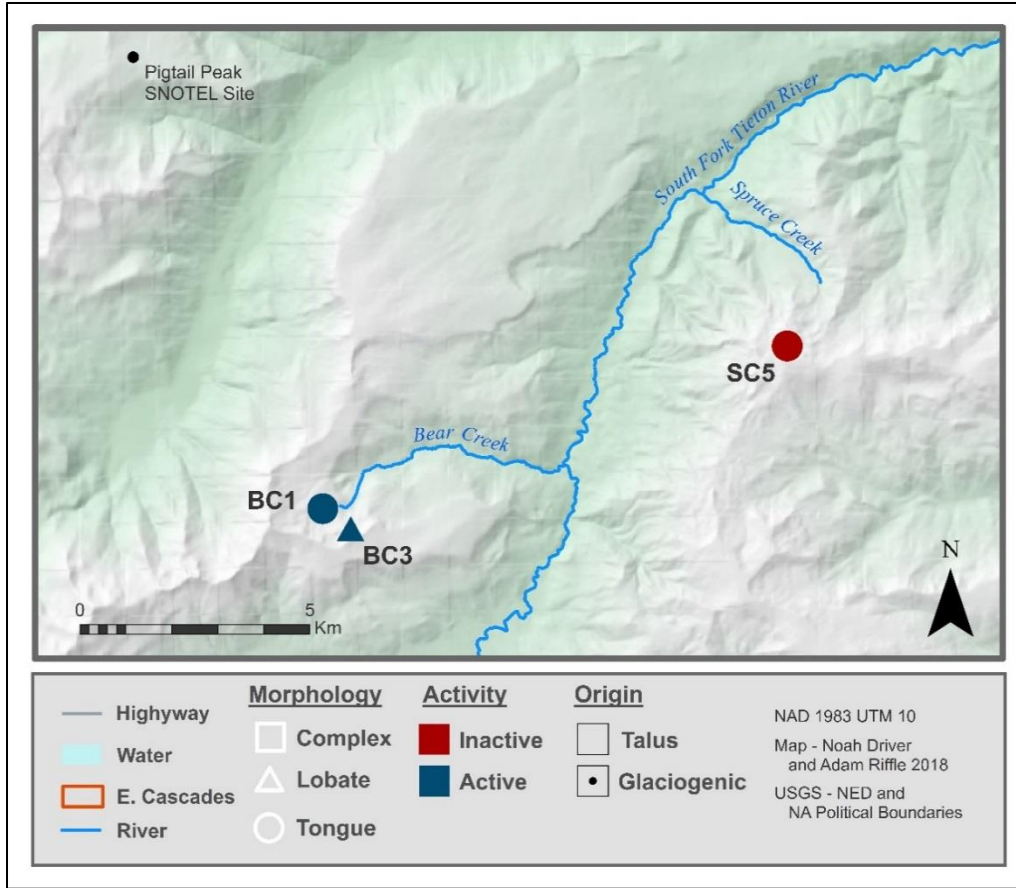


Figure 13. Southeastern Cascades study sites inset map 4.

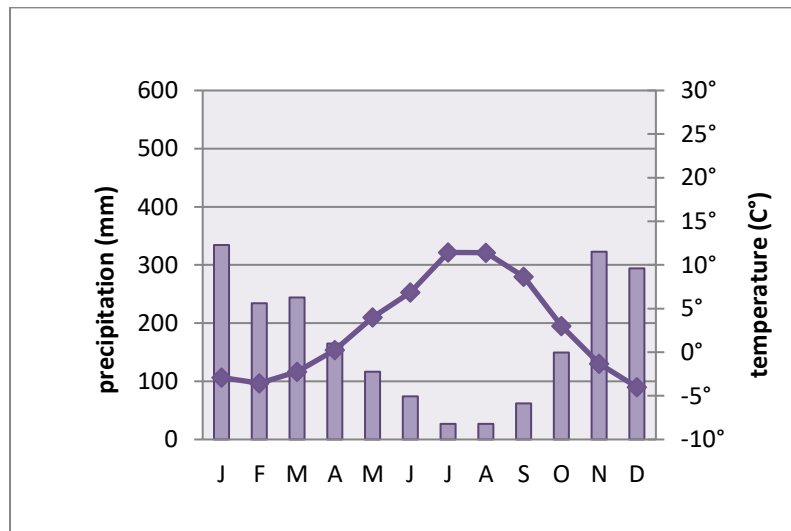


Figure 14. Pigtail Peak, WA climograph. Data courtesy of NRCS SNOTEL Pigtail Peak site (1989-2017).

1,900 m so MAAT at rock glacier sites are likely lower than that recorded for this station.

It is interesting that precipitation rates at Rainy Pass are over 500 mm less than Pigtail

Peak given that both of these stations sit almost directly on the Cascade Crest.

CHAPTER IV

METHODS

The internal structure of active and inactive rock glaciers in the Eastern Cascades was assessed by geophysical methods. At present, Lillquist and Weidenaar (in preparation) have identified 33 active, 97 inactive, and 17 relict rock glaciers. This study only focused on the active and inactive rock glaciers, as the relict features do not contain any ice, are no longer moving, and are of less geomorphological and hydrological importance.

Rock Glacier Sampling

To represent all the forms present across the population, rock glaciers from different ages, origins, and morphologies were surveyed. Because these categories overlap, active and inactive rock glaciers were sampled with lobate, tongue, and complex morphogenic types. In addition, no inactive-glaciogenic rock glaciers are found in the Eastern Cascades, but a large number of inactive-talus types do exist. This method was chosen to attempt to cover the range of variability across the population.

Sample rock glaciers were chosen based on distribution of rock glaciers and ease of backcountry access. Large wildfires during the summer 2017 field season precluded surveying any rock glaciers north of WA 20 and any in the Alpine Lakes Wilderness region. Originally 11 sample rock glaciers were chosen for field surveying, however, two rock glaciers were removed from the list after field investigations (Table 3). The first, Bridge Creek 1 (BrC1), was found to be a series of overlapping end moraines that emulated pressure ridges in satellite imagery. The second, Spruce Creek 5 (SC5), was

Table 3. Rock glacier sample distribution.

Rock Glacier Morphology				
	Lobate	Tongue-shaped	Complex	Total
Active-Glaciogenic	-	-	1	1
Active-Talus	-	2	3	5
Inactive-Talus	1	3	-	4
Moraine	1	-	-	1
Total	2	5	4	11

removed from the list due to inadequate GPR data. Therefore, ultimately nine rock glaciers were the focus of this study which encompasses approximately 7 percent of the population of active and inactive rock glaciers in the Eastern Cascades.

Field Data Collection

Each rock glacier was visited during the summer of 2017 with five field assistants. Data was collected over a total of eight multi-day backpacking trips and multiple single day trips located in the Lake Chelan-Sawtooth Wilderness, Goat Rocks Wilderness, and the Okanogan-Wenatchee National Forest. At least two full field days were spent at every rock glacier with the exception of BC1 which was surveyed in one day.

Backcountry navigation was primarily accomplished through map and compass techniques. Topographic maps combined with printouts of satellite imagery depicting trails and approximate backcountry routes were used for this. In addition, handheld GPS units were employed in this study.

Internal Structure and Composition

GPR surveys were conducted to investigate the internal composition and structure of nine rock glaciers. These features were analyzed using the portable pulseEKKO PRO (Sensors & Software Inc.) GPR system owned by the CWU Geological Sciences and

Anthropology departments (Figure 15). Low frequency (50 MHz) unshielded antennas were used to accurately capture the substructure (Isaksen et al., 2000; Farbrot et al., 2005; Leopold et al., 2011; Monnier and Kinnard, 2013, 2015). This system was mounted in bistatic mode and rock glaciers were surveyed by conducting constant-offset (CO) profiles with antennas oriented perpendicular to the profile direction (Monnier and Kinnard, 2013, 2015).

To record CO profiles, graduated 100 m measuring tapes were first laid onto the surface of the rock glacier. CO profiles were recorded along the measuring tape with a recording interval, or step size, of 50 cm and 2 m antenna separation with two 50 MHz unshielded antennas oriented perpendicular to profile direction (Figure 16) (Maurer and Hauck, 2007; Leopold et al., 2011; Monnier and Kinnard, 2015). Due to the rough, rocky surface of the rock glaciers each trace, or recording, was logged by lifting both antennas into position every half meter. Once graduated tapes were laid out and depending on surface material and morphology, a 100 m transect took anywhere from a 0.5 to 1.5 hours to complete.

An 800 nanosecond (ns) time window and a 400 volt (v) transmitter were used to generate a powerful signal to capture as much depth as possible. The transmitter and the receiver each require two 1.5 kilogram (kg) 12V “brick” batteries and the DVL and GPS each require a 2.5 kg 12V “belt” battery. At least eight brick batteries and three belt batteries were carried in on each backcountry trip. In addition, a Dewow filter was applied during sampling to help eliminate system background noise (Annan, 2003; Monnier and Kinnard, 2015). Each trace was the result of 16 stacks to enhance the signal-

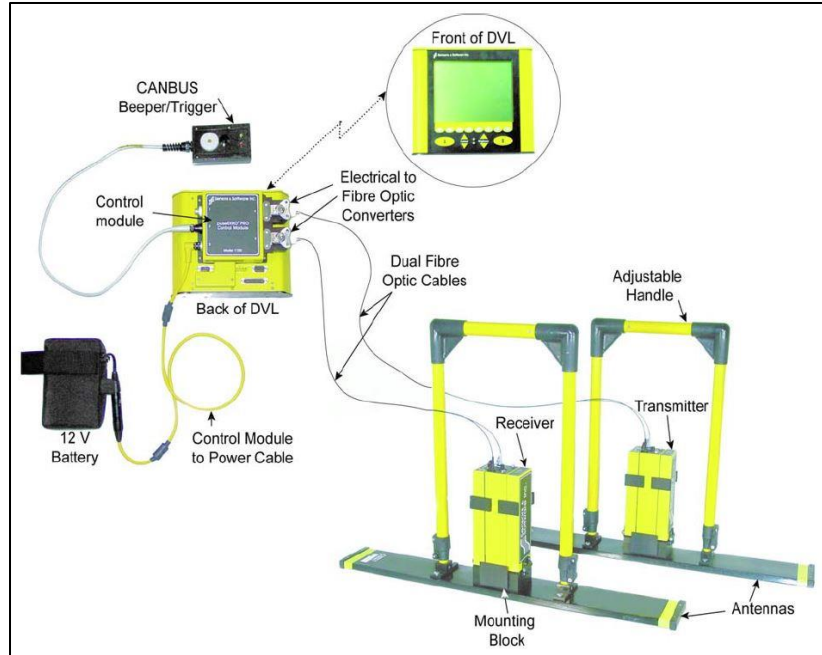


Figure 15. The pulseEKKO PRO System used in this study. Figure adapted from Sensors & Software Inc. (2012).



Figure 16. The pulseEKKO PRO in use on WFBC3 rock glacier. Photo taken by Noah Driver, 2017.

-to-noise ratio (Leopold et al., 2011; Monnier and Kinnard, 2015). This means that for each trace the GPR took 16 traces and stacked, or averaged, them together.

GPR measurements were recorded along one longitudinal transect at each rock glacier and most were surveyed with additional transverse transects (Monnier and Kinnard, 2013, 2015). The longitudinal transect ran down the center of each rock glacier from the head to the terminus, or toe. In addition, transverse transects were recorded approximately perpendicular to the longitudinal transect across the width of the rock glacier. Where multiple transverse transects were recorded, transects were surveyed near the head of the rock glacier and near the toe.

Topography

Surveying was completed along the GPR profiles to get accurate topographic data for GPR profile analysis. A laser rangefinder (LRF) was used to collect topographic data in the field. A LRF uses a laser to measure vertical, horizontal, and standard distance as well as slope angle and orientation to a given point. The LRF used in this study was a TruPulse 360R which is owned by the CWU Geological Sciences Department. Accuracy for distance measurements are within ± 30 cm, for inclination $\pm 0.25^\circ$ and for azimuth $\pm 1^\circ$ (Laser Technology, Inc., 2017). Since these instruments are small and lightweight they are ideal for backcountry travel. Surveying was completed by recording measurements from the LRF user to a given point (usually a field assistant) along a transect. In addition, several other transects apart from GPR transects were surveyed on all rock glaciers to better depict overall topography. Limited time in the field prevented detailed topographic surveying of each rock glacier.

Field data were manually recorded in field notebooks at the time of collection and later transferred into Microsoft Excel spreadsheets where the data could then be easily organized and analyzed. In addition, GPS points were recorded for every LRF entry. These points were utilized during data processing to provide spatial reference for the LRF data. A handheld Garmin eTrex 10 owned by the CWU Geography Department was used to record waypoints during LRF surveying. Waypoints were averaged for the beginning and end points along a given transect to provide more accurate spatial data.

Data Analysis and Processing

GPR data were analyzed using EKKO_Project 5 software (Sensors & Software Inc.) in CWU Geography Department's GIS Lab. First, trace editing was performed on GPR profiles which involves the manually removal of any blank traces or traces that were recorded twice. Profiles were then analyzed in an unfiltered and unmigrated form. This allowed specific diffracting objects to be analyzed more closely using hyperbola two-way traveltime measurements (Figure 17). An inventory of diffracting points was used to establish an average velocity for each rock glacier (Figure 18). This method is commonly referred to as hyperbola fitting and results in an average velocity measurement for the entire profile (Monnier et al., 2011; Florentine et al., 2014). Accurate average velocity measurements are important for obtaining precise depth measurements so hyperbola fitting was completed carefully to obtain the best results.

Once average velocities were calculated, time-to-depth conversions were made and accurate depth measurements could be obtained. Near and far reflectors were apparent in most profiles and were outlined on each profile where visible. Depth measurements from these outlines were then recorded for further analysis. The near

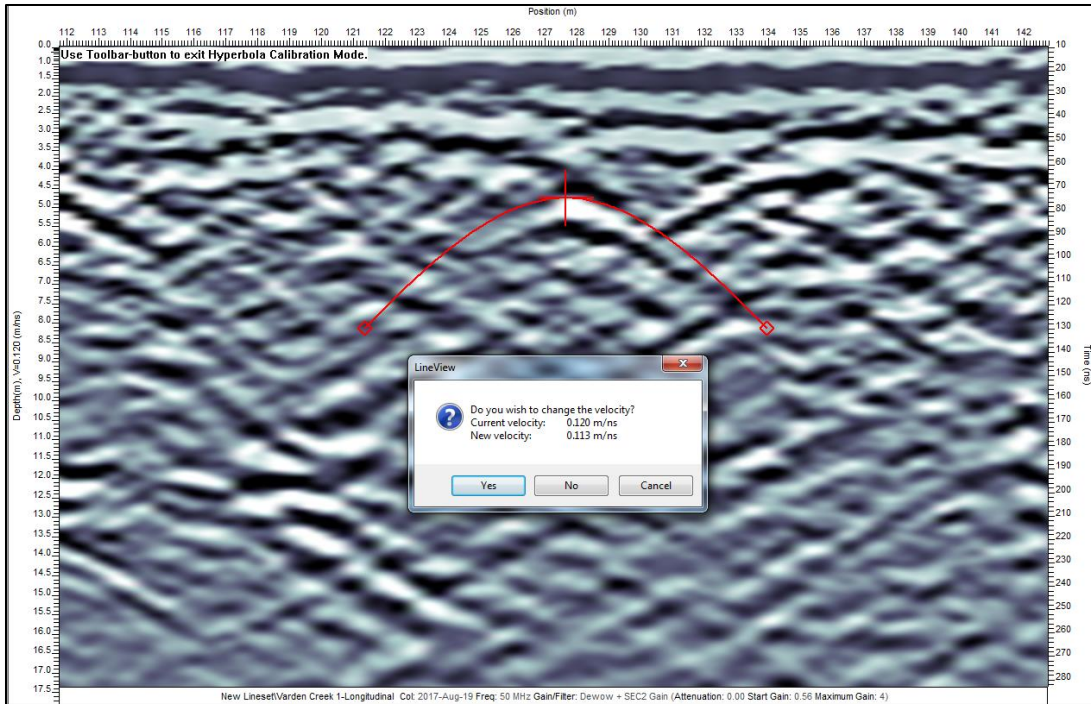


Figure 17. Example of hyperbola fitting from EKKO_Project 5 (Sensors & Software, 2012).

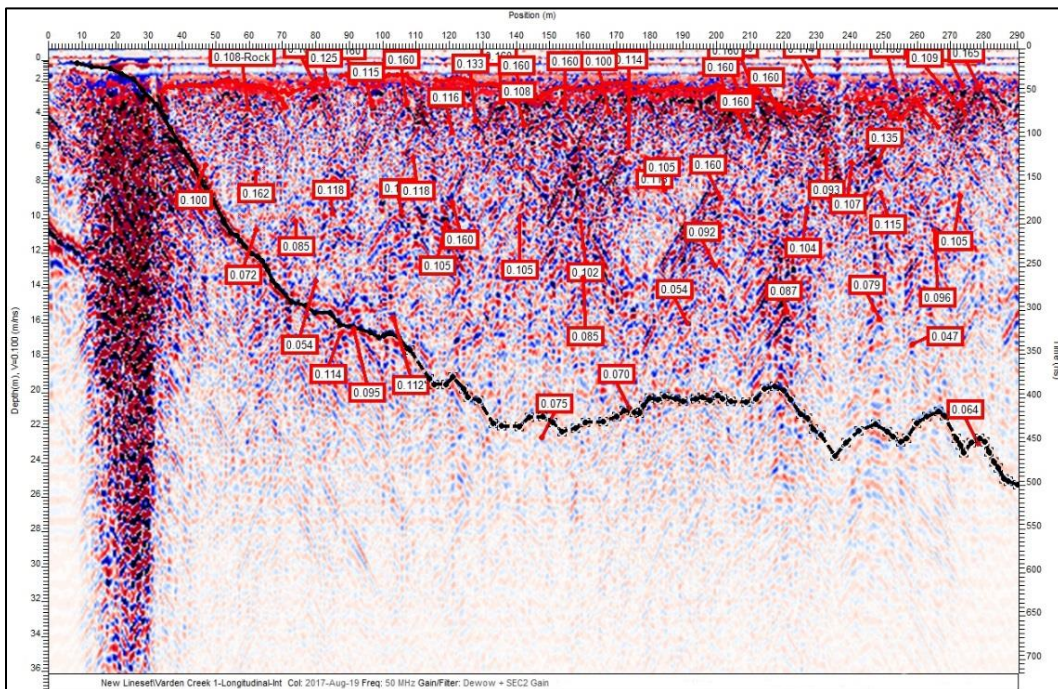


Figure 18. Example of hyperbola fitting and near (red line) and far reflector (black line) traces from EKKO_Project 5 (Sensors & Software, 2012).

reflector was interpreted as the base of the active layer and the far reflector was interpreted as the base of the rock glacier (Krainer et al., 2010; Monnier and Kinnard, 2015). Average depth to rock glacier base along with average depth to the active layer were calculated for each rock glacier.

To get a more geographically accurate representation of each rock glacier the profiles were topographically corrected which allowed for an expanded view of the data. To depict topographic relief, LRF data was imported into EKKO_Project. This view of the data helps to more accurately portray stratigraphic features.

Other processing techniques were utilized to portray the data in a more realistic stratigraphic format. These included migration which collapses hyperbolas back into points to provide a more realistic view of the substrate (Sensors & Software Inc., 2017). This is performed according to the average velocity obtained from hyperbola fitting along each profile (Monnier and Kinnard, 2013; Florentine et al., 2014). EKKO_Project migration uses a 2D FFT Stolt migration (Sensors & Software Inc., 2017). A bandpass filter was applied to some of the profiles to remove any extra noise from the data (Krainer et al., 2010; Florentine et al., 2014). This filter could be used to remove high or low frequency noise around a set velocity which is often the average velocity. Spherical and exponential compensation (SEC) gain was used which attempts to more accurately portray the variation in amplitude across the structure. Finally, background subtraction was applied to each of the profiles to remove noise (Leopold et al., 2011; Florentine et al., 2014).

Ice-Water Equivalence

Multiple datasets and methods were utilized to determine ice-water equivalence of glaciers and rock glaciers in the Eastern Cascades. The most important step in this process is calculating individual volumes for each feature. Multiple area-volume scaling methods were used to attain this information.

Areal measurements of these features was needed in order to calculate volume. First, Lillquist and Weidenaar's (in preparation) inventory was used for the areas for all active and inactive rock glaciers in the Eastern Cascades. Areal measurements in this inventory were calculated in square meters (m²) using Google Earth.

Second, no dataset exists of individual glacier area that encompasses all of the Cascades and, more specifically, the Eastern Cascades of Washington. These data were compiled from several previous studies on various Washington glaciers. First, measurements of North Cascade glaciers from Carisio (2012) were collected which includes all glaciers north of Snoqualmie Pass. Next, areal measurements of the glaciers of the Goat Rocks were collected from Heard (2012). Finally, areal measurements of glaciers on Mount Adams from Sitts et al. (2010) accounted for the southernmost glaciers in the Eastern Cascades. Each of these studies has areal measurements of glaciers down to the hundredth of a kilometer. Next these data were mapped in ArcMap 10.6 in the CWU Geography Department's GIS Lab and the Eastern Cascades glaciers were clipped out based on the Cascade Crest boundary.

Glacial volume and area have been proven to have a close correlation. Previous studies have used this relationship to devise empirical formulas to calculate volume of a glacier based on its surface area (Driedger and Kennard, 1986; Chen and Ohmura, 1990;

Bahr et al., 1997). Granshaw and Fountain (2006) compared known volumes of five North Cascade glaciers to results from three different area-volume scaling equations to determine the most appropriate for North Cascade glaciers. They found that the method by Bahr et al. (1997) provided the least error. This method requires data on individual glacier width, slope, side drag, and mass balance in addition to surface area.

Unfortunately, the data available on glaciers in the Eastern Cascades does not include all this information. Thus, the area-volume scaling method developed by Chen and Ohmura (1990) was used to determine ice volumes of Eastern Cascade glaciers (Equation 1).

Chen and Ohmura (1990) assign uncertainty intervals to <5 percent for this method.

$$28.5 \times (\text{area [km}^2\text{)})^{0.357} \quad (1)$$

Depth measurements were taken from GPR profiles at the study sites. This was accomplished by first calculating depth measurements of the base of the active layer and the depth to the rock glacier base in EKKO_project. Next, depth measurements were averaged to get a mean base depth and a mean active layer thickness. Average active layer thickness was then subtracted from average base depths to get the average thickness of the permafrost rich layer. This provides a more accurate depiction of the overall ice volume for these rock glaciers than estimation techniques.

For the population of rock glaciers, the empirical formula developed by Brenning (2005) was used to calculate average permafrost thickness (Equation 2). Next, a comparison among surveyed rock glaciers was completed between the results of GPR measurements of permafrost depth and permafrost depth according to Brenning's (2005) empirical formula. This comparison was then used to determine an average difference. The average difference was then subtracted from depth values for each rock glacier in the

population to provide a more accurate representation of average permafrost thickness.

$$50 \times (\text{area [km}^2\text{)})^{0.2} \quad (2)$$

For both the study sites and the overall rock glacier population average permafrost thickness was multiplied by total surface area to get individual volumes in km³ for each rock glacier. However, ice content in active rock glaciers varies from 30-80 percent by volume and can be as low as 30 percent in inactive rock glaciers (Barsch, 1996; Haeberli et al., 1998; Hoelzle et al., 1998; Burger et al., 1999; Arenson et al., 2002; Monnier and Kinnard 2013, 2015). Because ice content varies significantly, an average ice content of 50 percent was used for ice volume calculations on active rock glaciers. Also, it is assumed that inactive rock glaciers in the Cascades have a lower ice content than active rock glaciers. As a result, an ice content of 40 percent was used to calculate total ice volume of inactive rock glaciers. These ice contents were then applied to the volumes calculated for each rock glacier to get true rock glacier permafrost content.

Finally, permafrost and ice values for rock glaciers and ice glaciers were converted to a water equivalency. For both rock glaciers and glaciers Paterson's (1994) value for glacial ice density of 0.917 g/cm³ was used to calculate water equivalence. This was then converted into acre-feet (AF) to better portray results for local water managers.

Management Implications

Findings are compiled in this document and made available to the public through Dr. Karl Lillquist's web page as well as the online thesis archive of the Central Washington University library. Specific water quantity results will be of interest to water managers in the state while more detailed stratigraphic information will contribute to the worldwide knowledge base of rock glaciers.

CHAPTER V

RESULTS AND DISCUSSION

Results from GPR analysis and field surveying, summarized in Table 4, reveal information on the internal composition, structure, and hydrological significance of Eastern Cascade rock glaciers. Specifically, GPR analysis depicts internal stratigraphy including the active layer, base depth, and internal composition. In addition, GPR data are used to estimate the thickness of the ice-rich permafrost layer. This is then compared to rock glacier volume estimating techniques from previous research to improve accuracy. This is used to calculate total ice content and water equivalency of the entire Eastern Cascade rock glacier population. Finally, water equivalency of rock glaciers is compared to that of ice glaciers in the Eastern Cascades to determine hydrological significance.

Rock Glacier Composition and Structure

Varden Creek 1

Varden Creek 1 (VC1) is an active, talus, tongue-shaped rock glacier located in the Northeastern Cascades within the Methow River watershed (Table 4). It flows north from an east-west oriented ridgeline (Figure 19). This rock glacier is 386 m in length and 162 m wide. VC1 consists of granite that has a distinct oxidized appearance indicating a weathered state (Stoffel and McGroder, 1990). Surface material varied in size but was approximately 2 m in diameter on average.

Several streams were observed flowing from the toe of VC1. In addition, water was observed flowing near the top of the rock glacier toward the head. Like most of the rock glaciers observed in the North Cascades, larch trees were present on VC1. Larches

Table 4. GPR Summary table for select Eastern Cascade rock glaciers. BrC1 and SC5 are omitted from the table because BrC1 was found to be a moraine and SC5 due to poor quality data. Dashes indicate an attribute that was not observed. Activity, origin, and morphology from Lillquist and Weidenaar (in preparation).

Rock Glaciers	Activity	Origin	Morphology	Active Layer Avg. Depth (m)	Base Layer Avg. Depth (m)	Base Layer	Permafrost	Water Presence	Date Surveyed
VC1	Active	Talus	Tongue	3.4	21.9	Bedrock	Interstitial	active layer + stream	8/19/2017
VC2	Active	Talus	Tongue	3.4	15.1	Bedrock	Interstitial	active layer + stream	8/18/2017
NC1	Active	Talus	Complex	3.6	26.6	Colluvium	Interstitial	-	8/28/2017
WFBC3	Active	Glaciogenic	Complex	3.1	35.5	Bedrock	Massive	stream	7/31/2017
WFBC4	Active	Glaciogenic	Complex	3.0	21.1	Bedrock	Massive	stream	8/2/2017
EFBC2	Active	Talus	Complex	3.1	16.1	Bedrock	Interstitial	active layer + stream	8/4/2017
TC1	Inactive	Talus	Tongue	5.5	19.5	Bedrock	Interstitial	stream	5/20/2017 9/30/2017
BC1	Active	Talus	Tongue	2.4	25.6	Bedrock	Interstitial	-	9/14/2017
BC3	Active	Talus	Lobate	-	-	Colluvium	Interstitial	-	9/13/2017

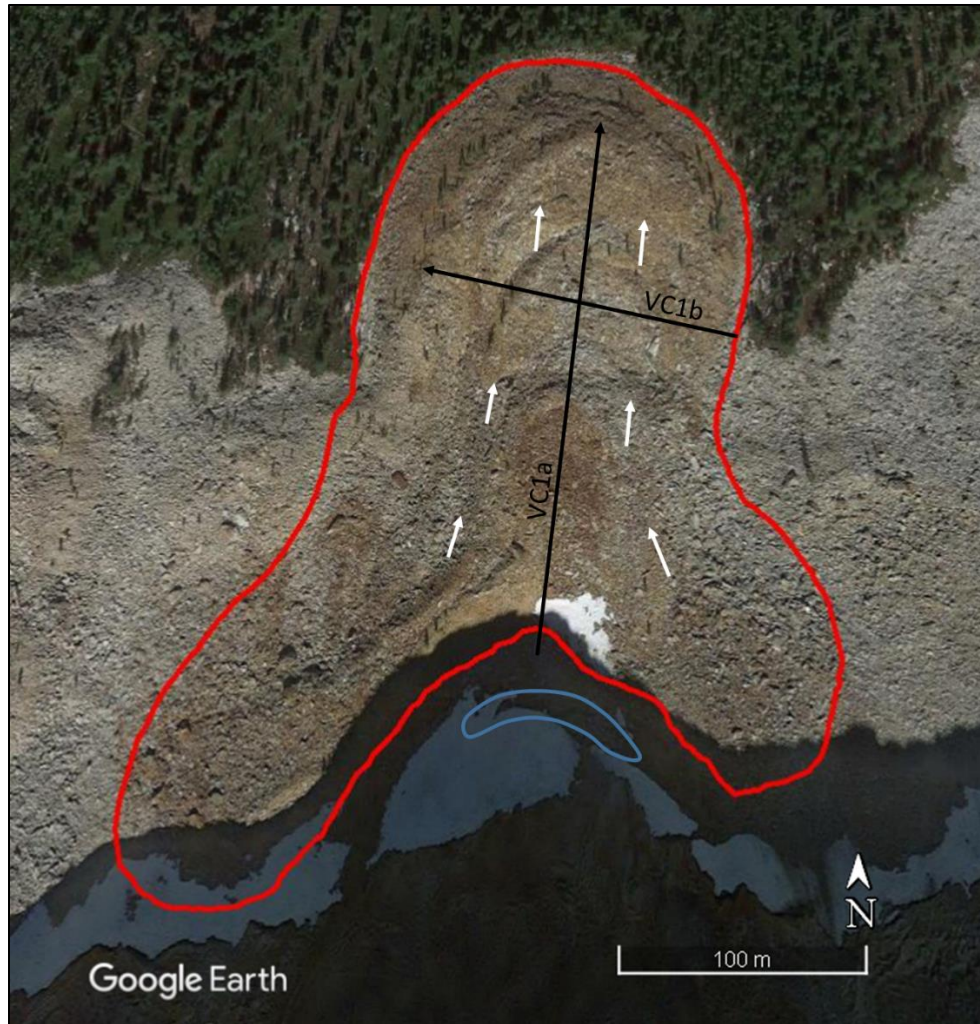


Figure 19. Google Earth image of VC1. Black lines depict location and direction of GPR profiles, white arrows indicate direction of flow of the rock glacier, red line indicates rock glacier boundary, and blue line outlines protalus rampart. Note snowfields above protalus rampart and larch trees, shown by their shadows, near the toe.

were observed atop the toe and, interestingly, linearly dispersed along the top of one pressure ridge in the middle of the feature (Figure 19).

In August 2017, snowfields were present above the rock glacier. At the upslope interface of bedrock and rock glacier head, a pool of water was present on top of solid ice. Newly created protalus ramparts were observed at the head of this rock glacier that had formed from rockfall being carried over a retreating snowfield (Figure 20). Although



Figure 20. Protalus rampart at the head of the Varden Creek 1 rock glacier (outlined in blue). Note the exposed bedrock revealed by the melting snow field (2017).

this rock glacier shows a heterogeneous mix of material and is thus talus in origin, a possible origin for this rock glacier could be creep of a moraine or protalus rampart.

Two constant offset (CO) GPR transects were recorded on VC1, one longitudinal (280 m) and one transverse (155 m) (Figures 21 and 22). The longitudinal profile spans the entire length of the rock glacier from its head to its toe, and the transverse profile covers the entire width of the rock glacier. Processing techniques included DEWOW, SEC gain, and background subtraction before hyperbola-fitting and migration and topographic correction after average velocity was determined. In addition, a bandpass filter was applied to the data.

A near reflector is prominent in both the longitudinal and transverse profiles which is interpreted as the base of the active layer (Monnier and Kinnard, 2013, 2015). The depth to the near reflector varies between 1.9 and 6.7 m throughout both transects. On the longitudinal profile the depth gradually increases further away from the head of the rock glacier with an average of 3.4 m. On the transverse profile, an increase in depth to the near reflector occurs on pressure ridges.

A high occurrence of diffracting points in the GPR profile indicates a heterogeneous mix of material along with high EM velocities ($>0.160 \text{ m/ns}^{-1}$) signify this rock glacier has an interstitial mix of ice and debris and is talus in origin validating Lillquist and Weidenaar's (in preparation) classification. Stacked hyperbolas in the beginning of the profile are a result of the transect passing over liquid water (Krainer et al., 2012; Monnier and Kinnard, 2015).

An increase in the amount of dipping reflectors occurs from approximately 165 m to 235 m on the longitudinal profile which indicates thrust planes and compressional

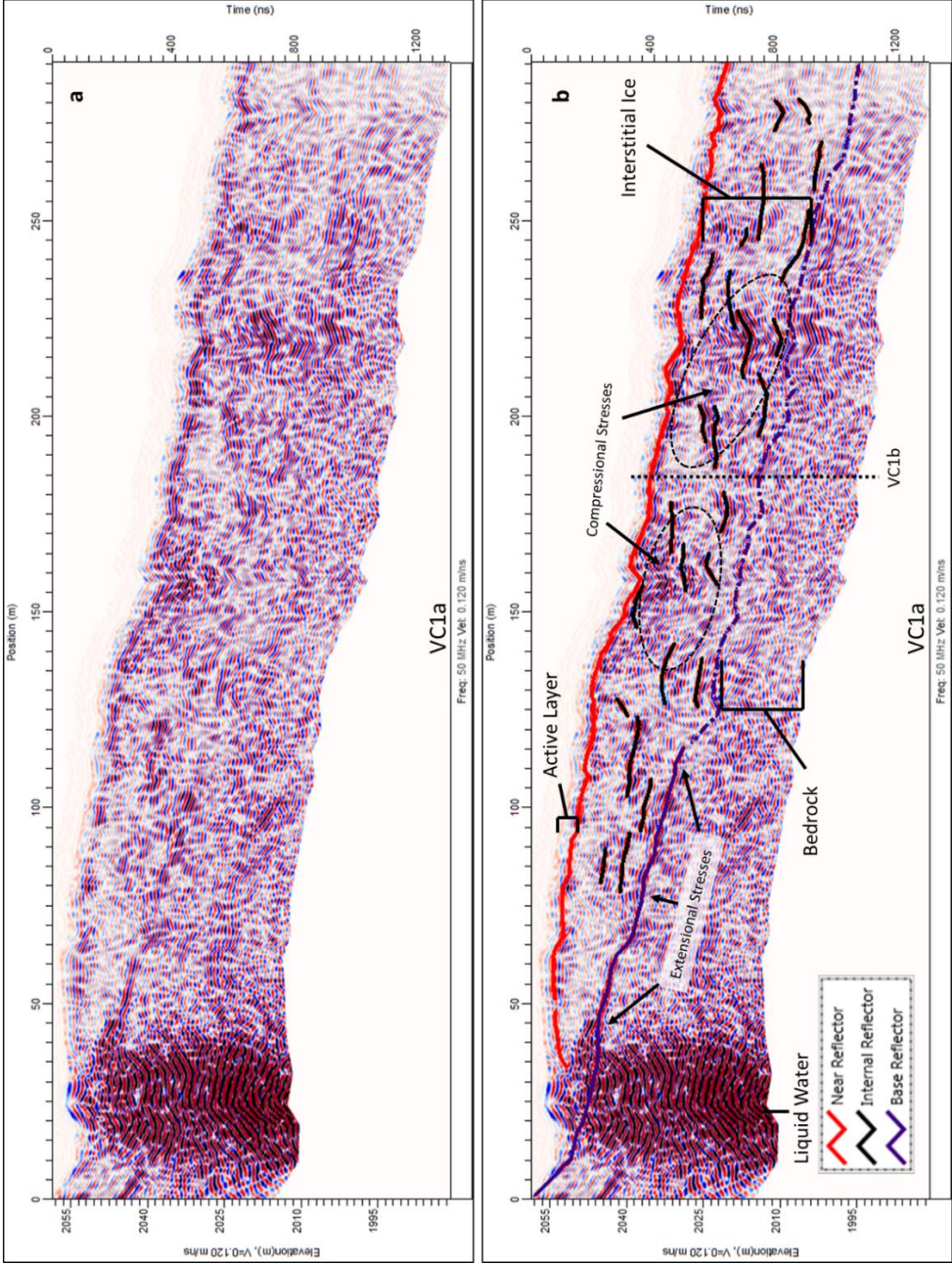


Figure 21. Migrated and topographically corrected longitudinal GPR profile of VC1a without interpretations (a) and with interpretations (b). Dotted line on (b) indicates intersection of transverse profile VC1b.

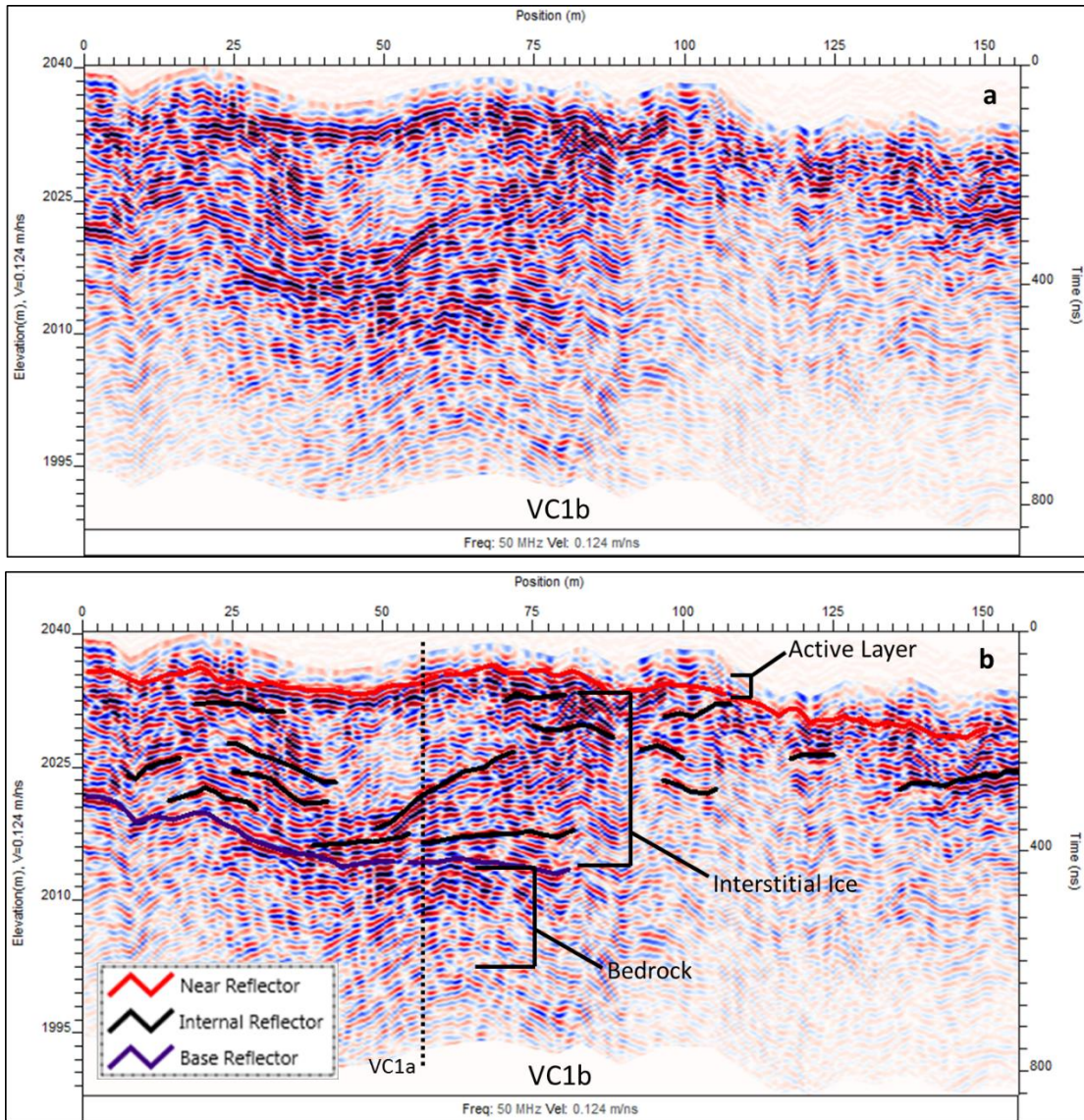


Figure 22. Migrated and topographically corrected transverse GPR profile of VC1b without interpretations (a) and with interpretations (b). Dotted vertical line on (b) indicates intersection of longitudinal profile VC1a.

stresses (Monnier et al., 2008, 2011). This corresponds to a decreased surface slope angle which causes a decrease in flow rate. Darker locations indicated by circles highlight these areas of compressional forces (Figure 21).

The longitudinal profile starts at the head of the rock glacier on bedrock for the first 15 m. This was important because it is apparent in the beginning of the GPR profile

that the dipping basal reflector is the bedrock (Figure 21). This basal reflector is prominent until about 125 m into the longitudinal profile and then the signal starts to fade. By increasing the gain level it becomes easier to detect this reflector. In addition, given the LRF measurements from the top of the toe to the base the depth to bedrock must exceed at least 25 m verifying the estimation in depth measurements for the approximate bedrock depth. Bedrock outcrops on either side of the rock glacier in this area support this as well. Also, it is externally apparent that there is marked thickening of the entire feature toward the toe. Base depth varies from 0 m at the head to 30 m at the toe with an average depth of 21.9 m. At the point in which the two transects intersect the basal reflector on both is less prominent but still distinguishable. The depth to this basal reflector corresponds at this point of intersection. Low EM velocities ($<0.10 \text{ m/ns}^{-1}$) suggest an unfrozen saturated layer near the bedrock underneath the permafrost-rich layer which could indicate basal shear as a creep mechanism (Burger et al., 1999).

Varden Creek 2

Varden Creek 2 (VC2) is an active, talus, tongue-shaped rock glacier (Table 4) (Figure 23). This rock glacier flows northeast from the same headwall as VC1 and is less than 100 m directly west of VC1 located within the Methow River watershed in the Northeastern Cascades. Although adjacent to VC1, this rock glacier has many different characteristics. Both are tongue-shaped rock glaciers but where VC1's toe has a horseshoe shape, VC2 has a V-shape. This could be due to slightly different topographies including a steeper slope on VC2. In addition, the two rock glaciers differ in color with VC1 having a noticeable oxidized beige color and VC2 matching the surrounding grey talus.

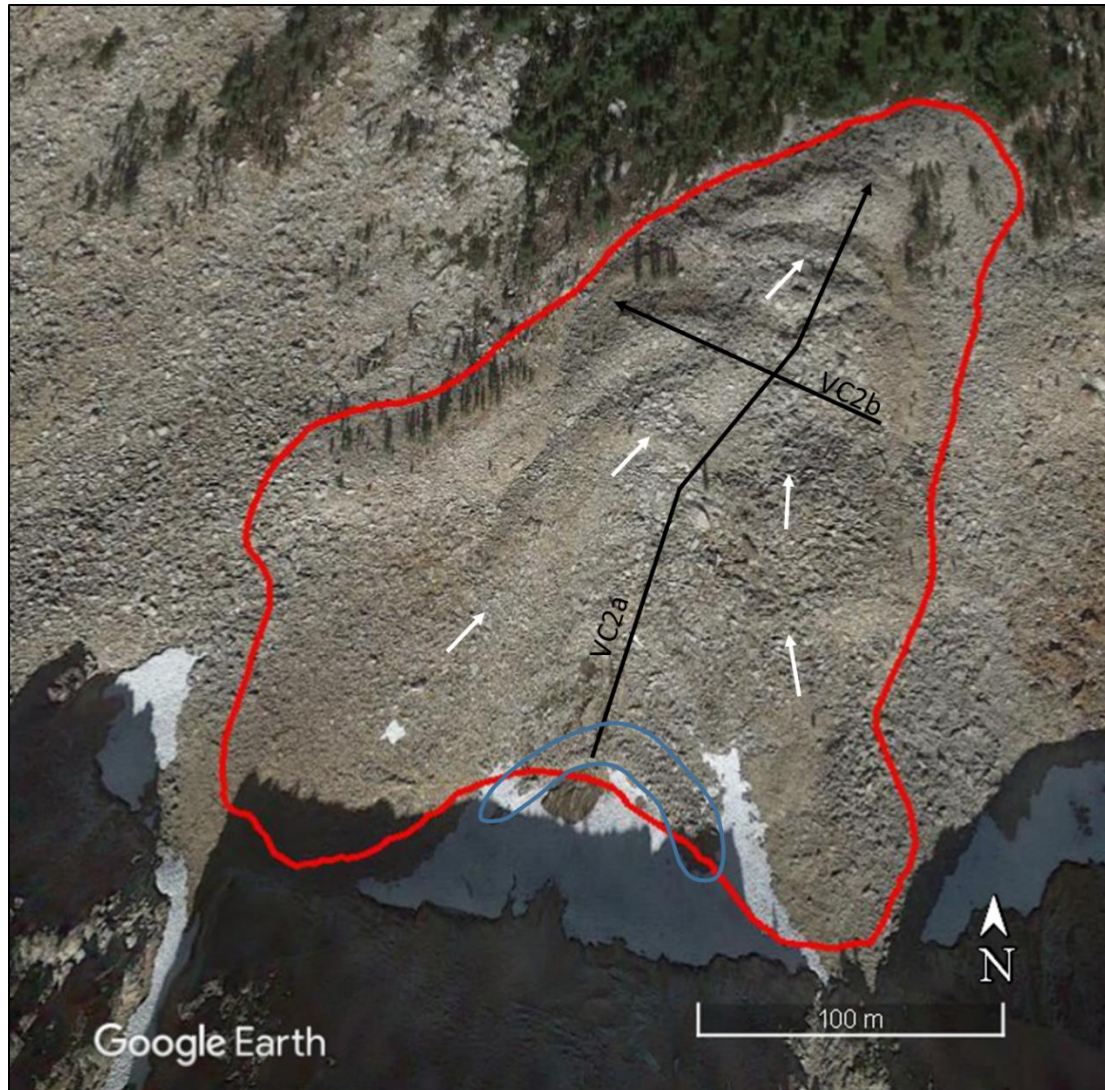


Figure 23. Google Earth image of VC2. Black lines depict location and direction of GPR profiles, white arrows indicate direction of flow, red line indicates rock glacier boundary, and blue line outlines protalus rampart. Note snowfields near the head and larch trees, shown by their shadows, toward the toe.

This rock glacier is 344 m long and 185 m wide and consists of fractured granite (Stoffel and McGroder, 1990). Surface rock diameter averaged approximately 2 m. However, on the tops and fronts of pressure ridges, finer-grained material is present. Once again, several larch trees are present in these locations. These are areas where finer grained material creates more favorable growing conditions. No other vegetation was

present on this rock glacier. Several streams were observed emerging from the toe of VC2 in mid-August 2017.

A small protalus rampart is present on the bedrock at the head of the VC2 rock glacier (Figure 23). This feature is still active in that it had a snow patch directly above it and there was much evidence of recent rockfall contributing to its mass. This suggests that this rock glacier began as a protalus feature. In addition, the empty portion at the head of VC2 highlights the importance of snowfields for the delivery of talus.

Two GPR profiles were collected on this rock glacier, one longitudinal profile (260 m) and one transverse profile (150 m) (Figures 24 and 25). Processing included DEWOW and SEC gain before hyperbola fitting. Migration, topographic correction, background subtraction and a bandpass filter were applied with an average velocity of 0.127 m/ns^{-1} .

The near reflector does not appear as clear as on VC1 but is still present. This near reflector, which is interpreted to be the base of the active layer, ranges from 2 m to over 5 m thick with an average of 3.4 m. This is attributed to thickening on pressure ridges which is common on all rock glaciers in this study. In addition, the thickness of the active layer increases toward the toe.

The series of stacked hyperbolae beneath the bedrock at 65 m on the longitudinal profile are a result of the GPR passing over liquid water (Figure 24) (Krainer et al., 2012; Monnier and Kinnard, 2015). This point corresponds to water visible from the surface. In addition to water, permafrost was also observed under the water (Figure 26) indicating the base of the active layer approximately 2.5 m from the surface.

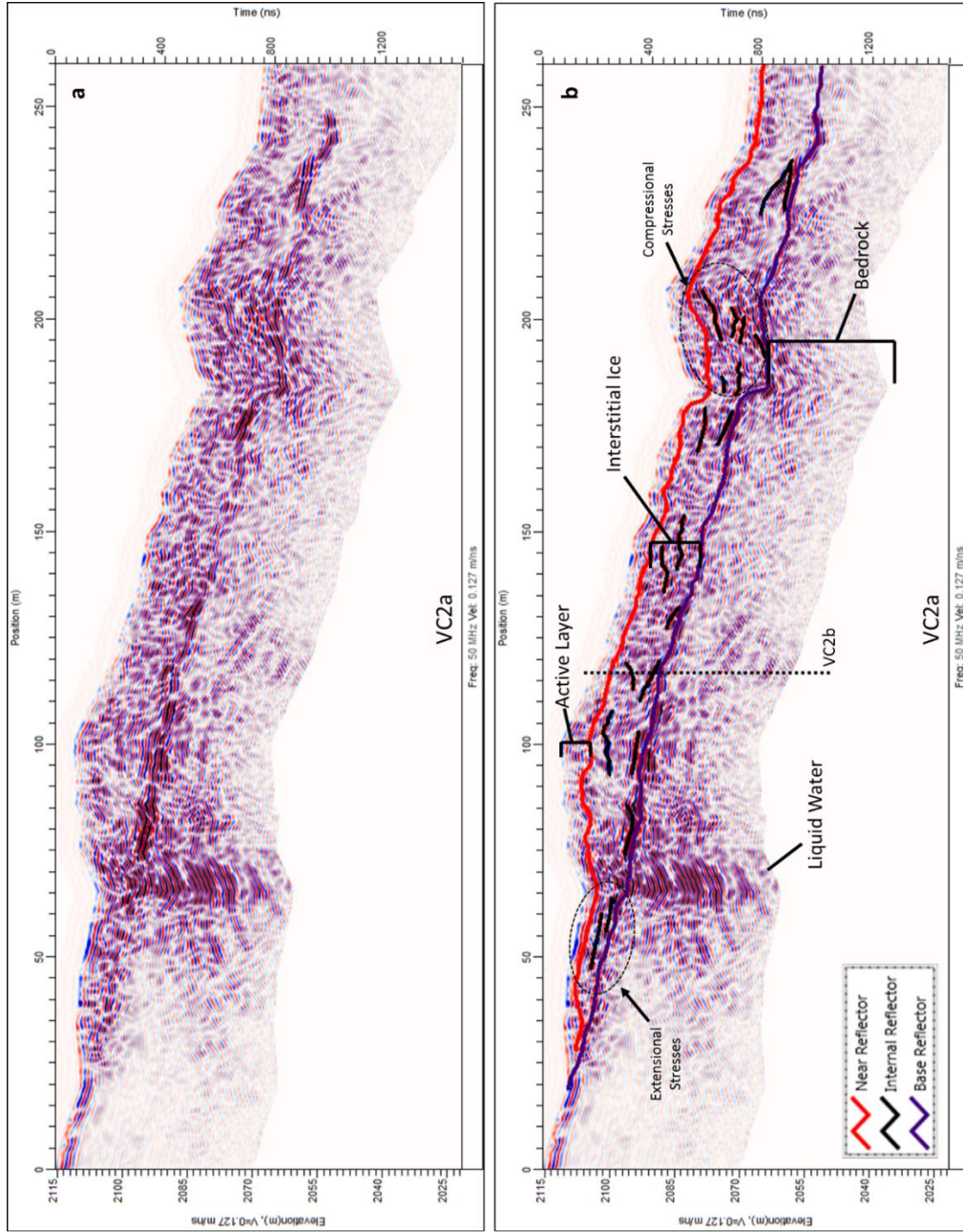


Figure 24. Migrated and topographically corrected longitudinal GPR profile of VC2a without interpretations (a) and with interpretations (b). Dotted line on (b) indicates intersection of transverse profile VC2b.

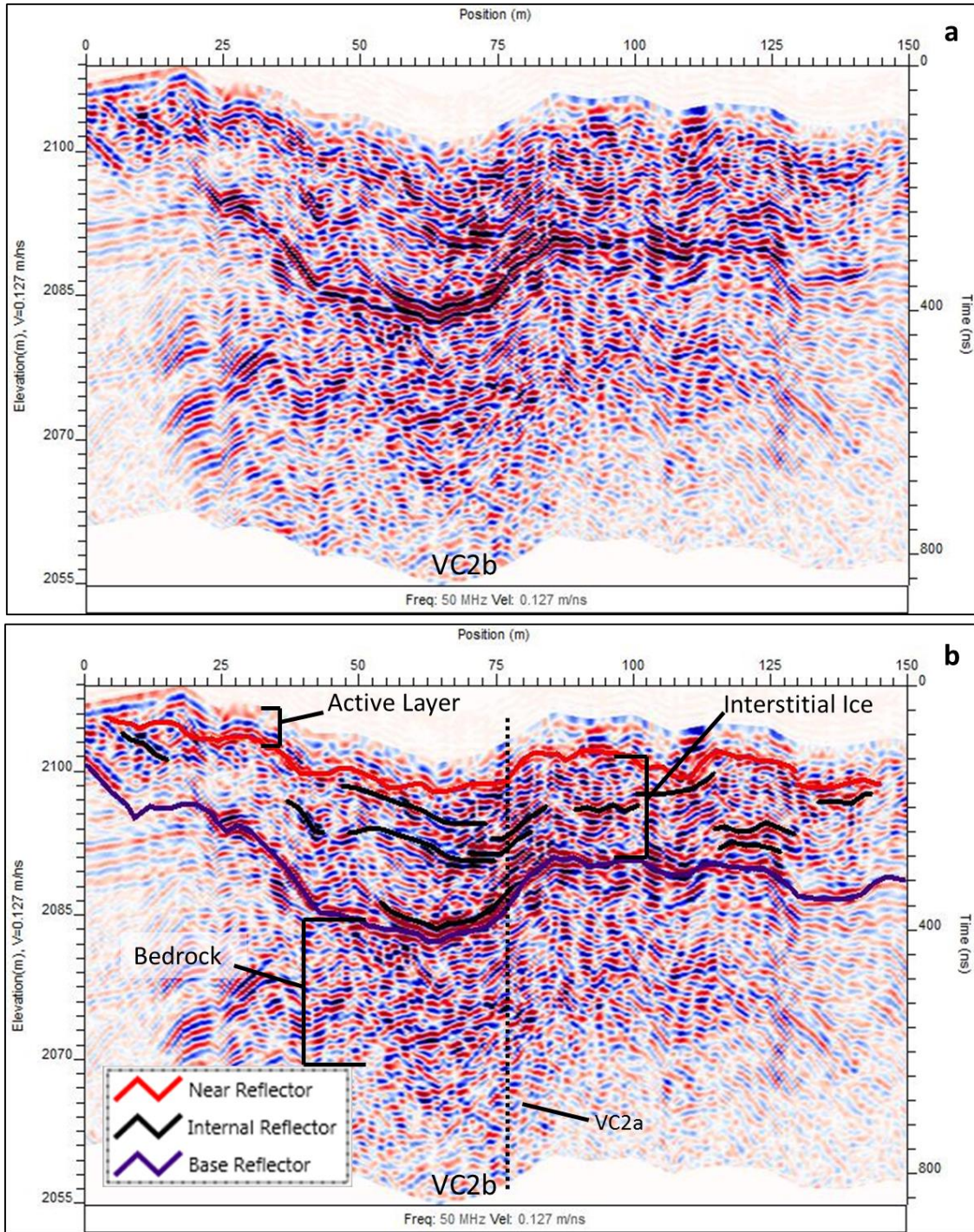


Figure 25. Migrated and topographically corrected transverse GPR profile of VC2b without interpretations (a) and with interpretations (b). Dotted vertical line on (b) indicates intersection of longitudinal profile VC2a.

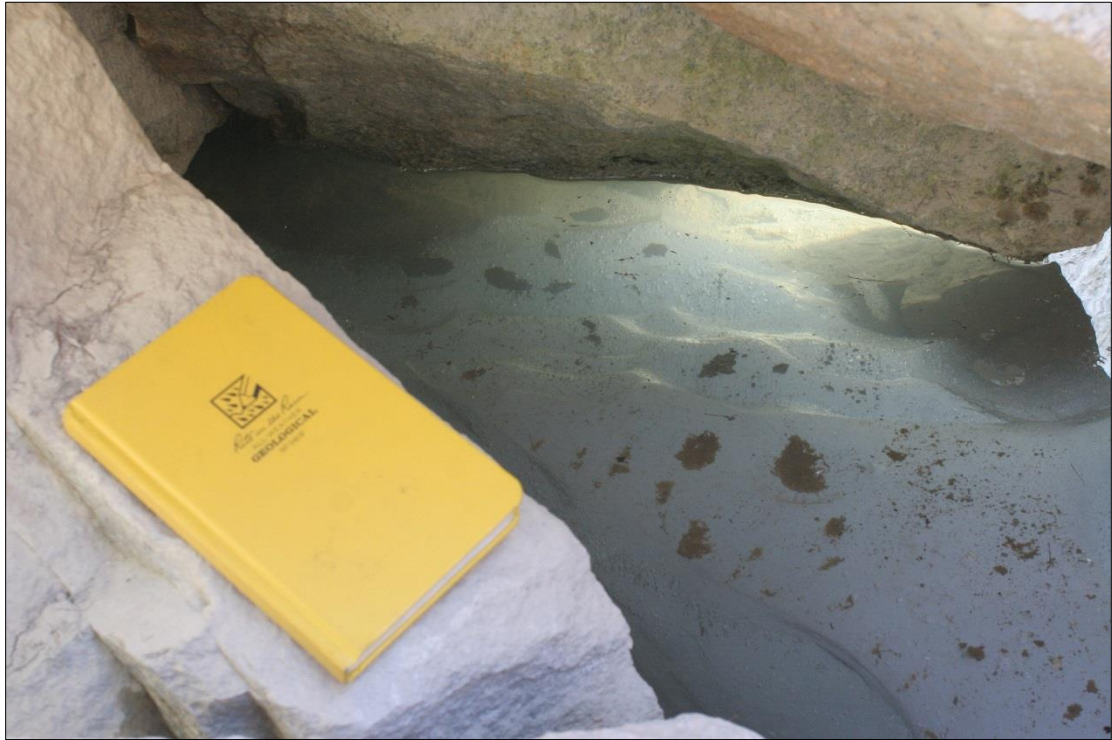


Figure 26. Water over permafrost on VC2. Longitudinal profile of VC2 intersects this point at 65 m. August, 2017.

Surface parallel reflectors in the upper portion of the longitudinal profile exhibit thrust planes in the form of extensional stress (Figure 24) (Hausmann et al., 2012). Small upward-dipping reflectors on the longitudinal profile from 100 m to 175 m mirror small pressure ridges and larger stacked toplapping reflectors near 200 m show more extreme stress due to a sharp decrease in slope angle (Monnier et al., 2008, 2011). This is a direct result of the bedrock angle which levels out in this section. Reflectors on the transverse profile display thrust planes that mirror bedrock topography (Figure 25).

The longitudinal profile begins at the head of the rock glacier and continues down to the top of the toe. Similar to VC1, the profile for this rock glacier also begins on

bedrock for the first few meters. This indicates that the basal reflector, which is prominent throughout the entirety of the profile, is the bedrock reflector. Base depths range from 0 m at the head of the rock glacier where the bedrock is exposed to just over 21 m at the last large pressure ridge before the toe. Combined base depths from the transverse and longitudinal profiles average 15.1 m. The depth to bedrock and to the active layer correspond on the intersecting longitudinal and transverse profiles. Similar to VC1, low EM velocities ($<0.10 \text{ m/ns}^{-1}$) near the bedrock suggest an unfrozen saturated layer associated with basal shear (Burger et al., 1999).

Bridge Creek 1

The Bridge Creek 1 (BrC1) feature was first identified as an active, glaciogenic, lobate-shaped rock glacier (Lillquist and Weidenaar, in preparation). It is located in the Northeastern Cascades within the Stehekin and Chelan River watersheds. From satellite imagery it appears as a large lobate rock glacier with many pressure ridges (Figure 27). However, on the ground these pressure ridge-like features are uniform in slope on both the up- and down-slope sides. In addition, the surface material consists of poorly sorted fines, cobbles and boulders. This differs greatly from that of traditional rock glacier surface material which consists of sorted, larger blocky material with finer grains concentrated more toward the front of pressure ridges and the toe. Further, it did not appear inflated which shows no internal ice. With these factors present BrC1 appears more as a series of overlapping end moraines left by the Lyall Glacier which has retreated into the cirque above rather than an expression of permafrost creep in the form of a rock glacier. If any portion were to be considered a rock glacier it would be the lowest portion, outlined in white in Figure 27. This portion has more blocky material at the tops of the

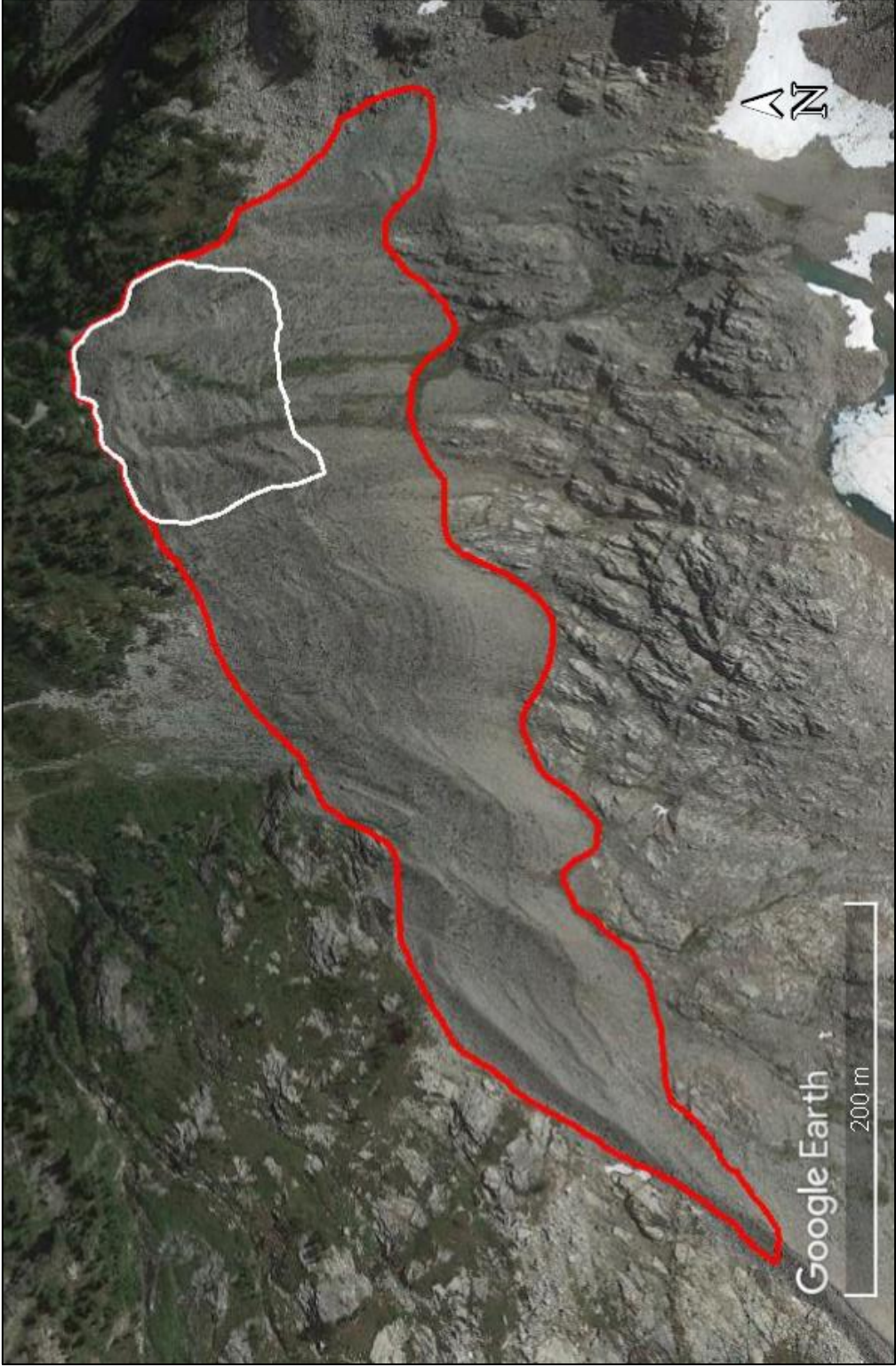


Figure 27. Google Earth image of BrC1. Red line indicates total feature boundary and white line indicates lower portion.

pressure ridge-like features that indicate frost-sorting which occurs with rock glacier creep. If this is a rock glacier it would have developed out of the end moraine material. In addition, jokulhaups (i.e., outburst floods) may have eroded the overlapping end moraines creating channels.

North Creek 1

The North Creek 1 (NC1) rock glacier is an active, talus, complex-shaped rock glacier (Table 4) (Figure 28). This rock glacier is located within the Twisp River Watershed in the Northeastern Cascades in a large northeast-facing cirque. From the head of the cirque NC1 flows north-northeast and is 386 m long and 321 m wide. Surface material on NC1 is medium in size with an average boulder diameter of approximately 1 m. However, rock size varies greatly from sands and fines to school bus-sized boulders. The parent material is comprised of andesite breccia (Dragovich and Norman, 1995).

NC1 was originally classified as a tongue-shaped rock glacier in Lillquist and Weidenaar's (in preparation) inventory. However, upon field investigation in late August 2017 it was determined that this rock glacier originates from multiple head sources and the convergence of two lobes forms one large tongue-shaped lobe at the toe. This fits one of Barsch's (1996) criteria of a complex rock glacier. In addition, this rock glacier was originally classified as glaciogenic as a result of being located in a cirque. However, a high concentration of diffracting points in the GPR profiles indicates a heterogeneous mix of material and thus talus origin.

Different colored rock from each lobe is apparent in satellite imagery and is striking in the field. Upon convergence of the two head sources a series of well-defined furrows run longitudinally down the center of the rock glacier (Figure 29). An abrupt

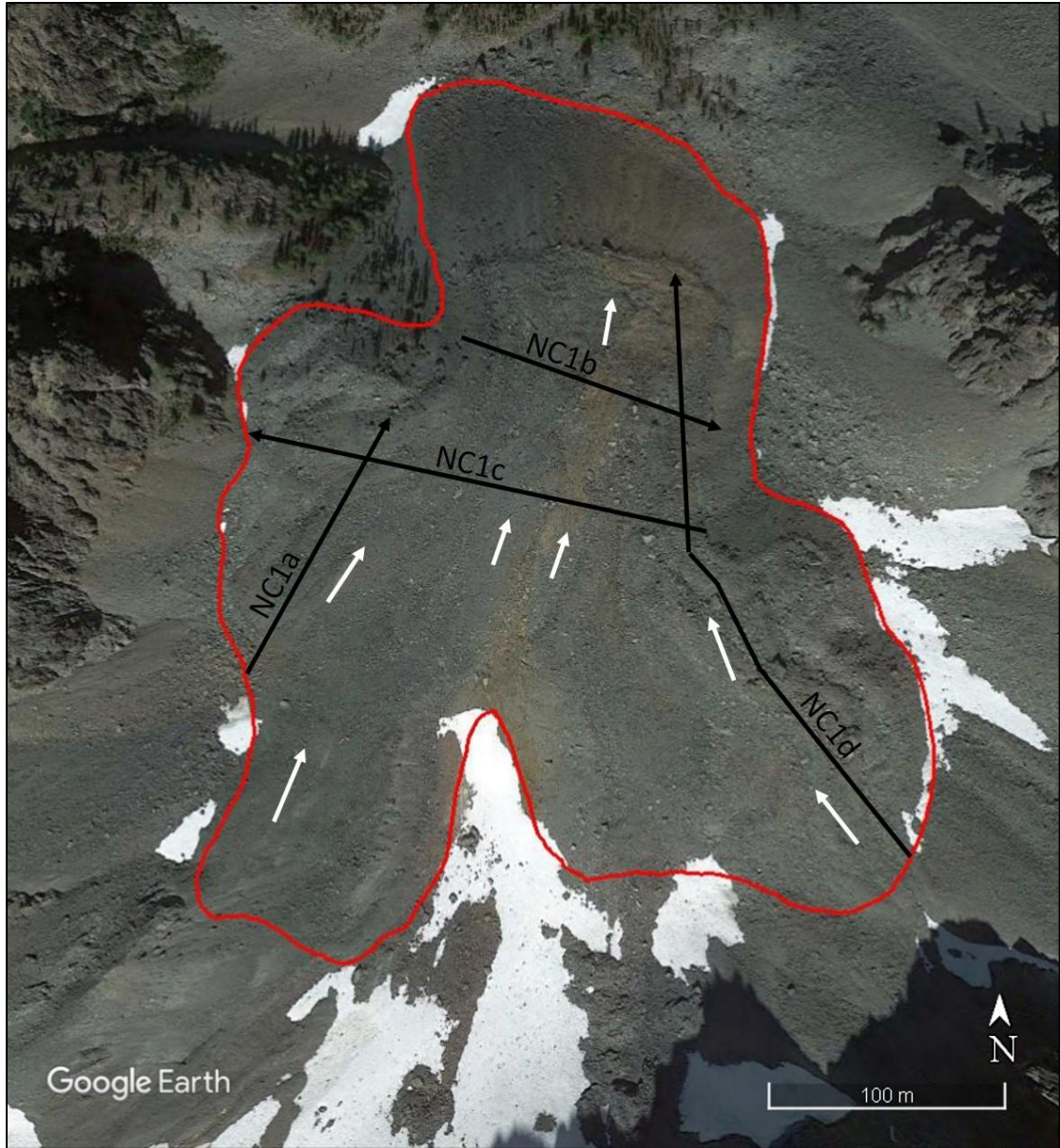


Figure 28. Google Earth image of NC1. Black lines depict location and direction of GPR profiles, white arrows indicate direction of flow, and red line indicates rock glacier boundary.



Figure 29. Ground photographs of NC1. A) Panoramic photo standing along the measuring tape for the longitudinal profile of the eastern lobe of North Creek 1. Note the linear furrows at the bottom left of the photo. B) View facing east taken on the western lobe of NC1 (arrow indicates location of photograph B). Note the color change in the middle of the furrows marking the convergence of the two lobes. Photograph A) taken by Angus Brookes and photograph B) taken by Adam Riffle, 2017.

change in color in the middle of these furrows marks the separation of the two lobes. The furrows run down and eventually end by a series of transverse pressure ridges that mark the convergence of the two lobes. The furrows are an expression of extensional stresses while the pressure ridges are a result of compressional stresses.

No streams were present at the front of this rock glacier. This is likely a result of the rock glacier potentially overriding a talus layer which allowed water to percolate beneath the surface. However, streams were observed further downslope where the talus dissipates.

Little vegetation was present on NC1. Only small plant species such as succulents and wild flowers were observed. These species were restricted to the lateral flanks of the rock glacier where finer-grained material is present to sustain growth. No larch trees were observed on the rock glacier but many were found in close proximity.

Four GPR profiles were surveyed on this rock glacier (Figure 30-33). A longitudinal transect was surveyed on each lobe and two transverse transects, one that ran across the western and eastern lobes, intersecting the furrowed section and one that ran across the pressure ridges of the toe. Before hyperbola fitting, processing included DEWOW and SEC gain. Migration, topographic correction, and background subtraction were applied with an average velocity of 0.129 m/ns^{-1} .

Near reflectors, indicating the base of the active layer, are present on all four GPR profiles. Near reflector depths range from 2.5 m at the head to 6.6 m near the toe with an average of 3.6 m. Similar to other profiles examined, greater depths to the active layer are found under pressure ridges. For example, depth increases under two large pressure ridges from approximately 100 m to 150 m in Figure 30.

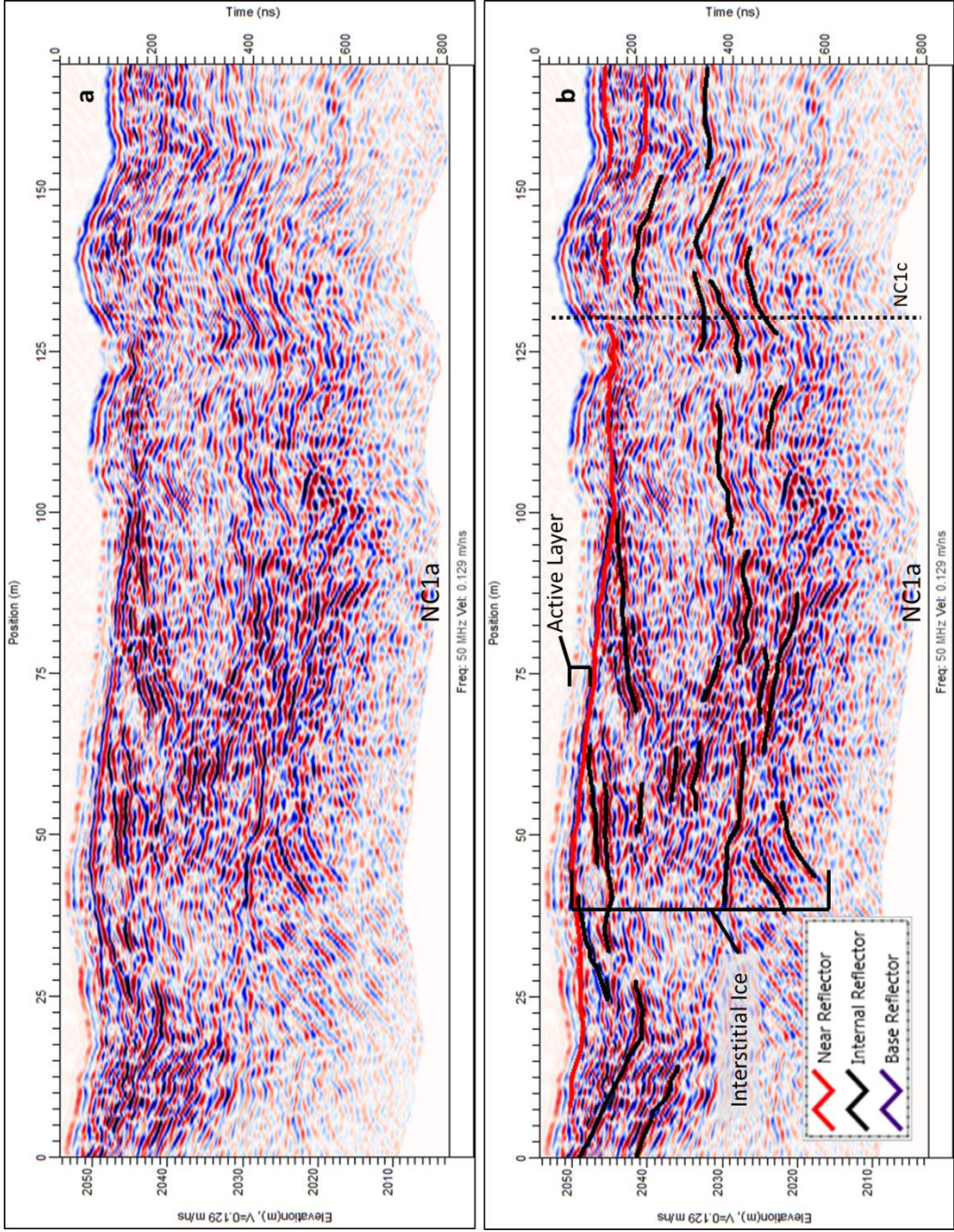


Figure 30. Migrated and topographically corrected longitudinal GPR profile of NC1a without interpretations (a) and with interpretations (b). Dotted vertical line on (b) indicates intersection of transverse profile NC1c.

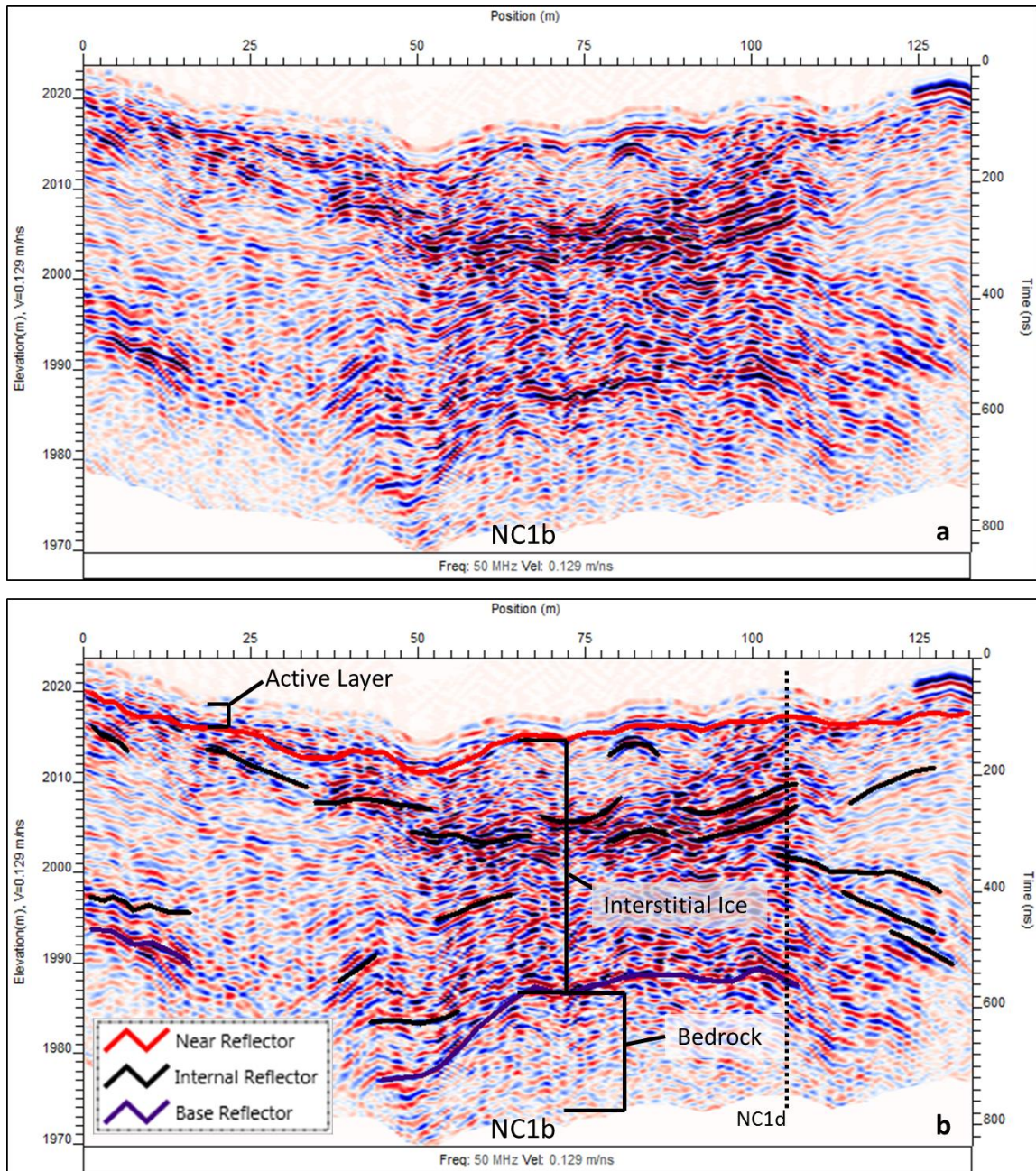


Figure 31. Migrated and topographically corrected transverse GPR profile of NC1b without interpretations (a) and with interpretations (b). Dotted vertical line on (b) indicates intersection of longitudinal profile NC1d.

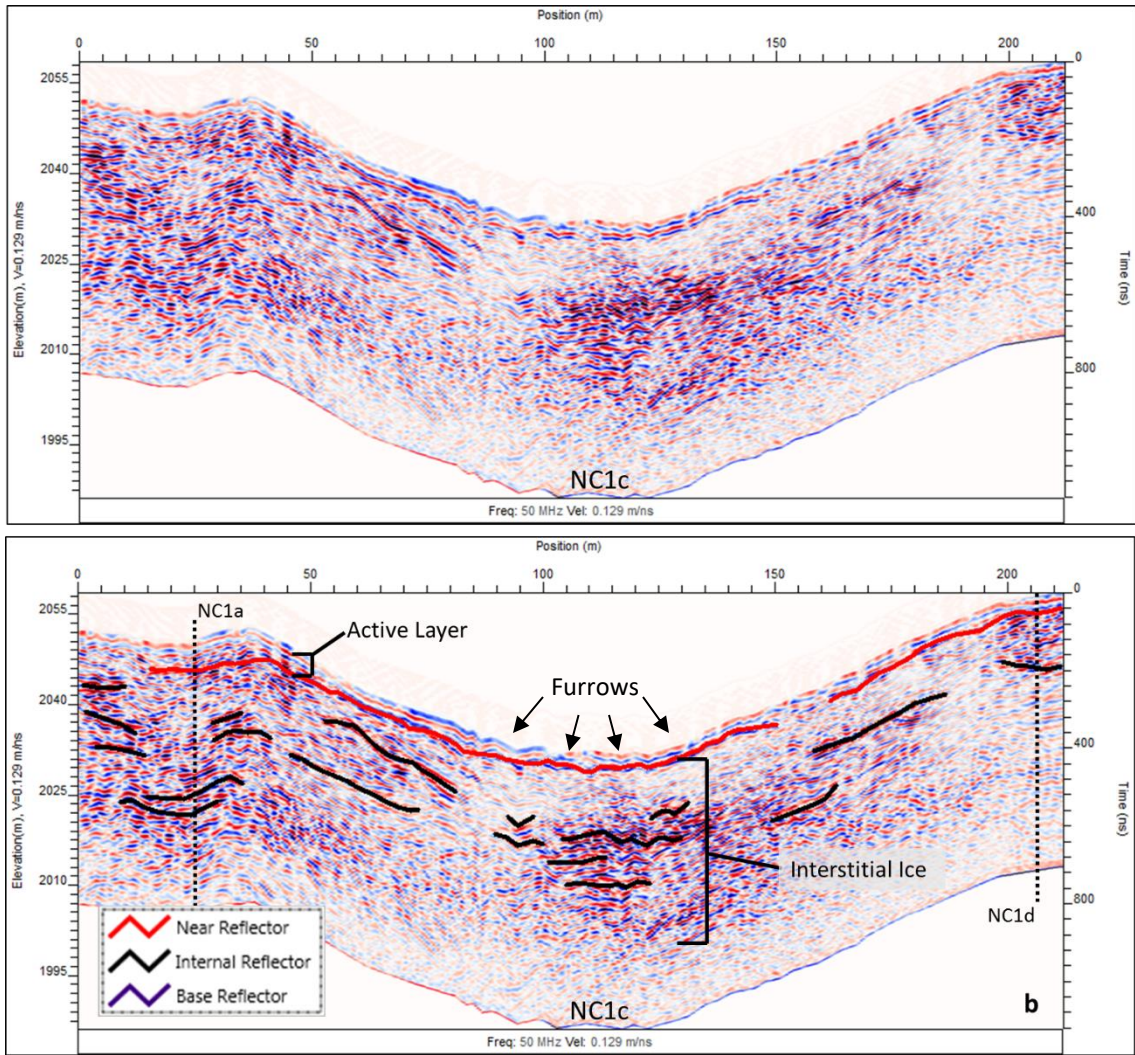


Figure 32. Migrated and topographically corrected transverse GPR profile of NC1b without interpretations (a) and with interpretations (b). Dotted vertical lines on (b) indicate intersections of longitudinal profiles NC1a and NC1d.

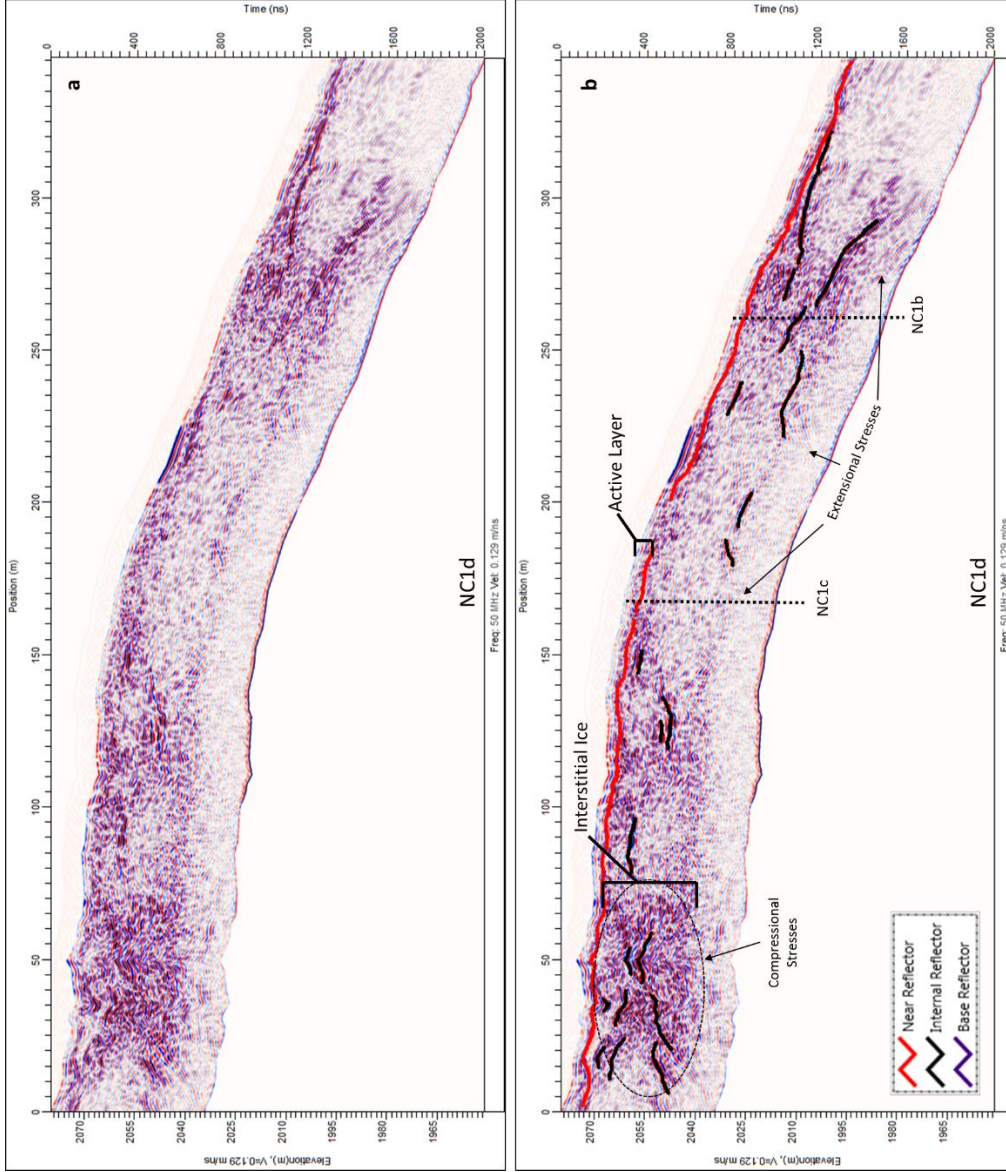


Figure 33. Migrated and topographically corrected longitudinal GPR profile of NC1d without interpretations (a) and with interpretations (b). Dotted vertical lines on (b) indicate intersections of transverse profiles NC1b and NC1c.

At the point where the furrows end and the transverse pressure ridges begin near the toe, a prominent reflector appears on the NC1d profile (at approximately 275 m) and runs roughly horizontal as it gradually converges with the surface of the rock glacier near the toe (Figure 33). This could indicate that the upper portion of the profile is a separate feature that is overriding a lower lobe (Monnier et al., 2011). In addition, under the furrowed section in the middle of NC1c profile stacked undulating reflectors mirror the furrowed topography. Surface parallel reflectors between 50 and 75 m and between 150 and 175 m on this same profile depict extensional planes where the eastern and western lobes slope down into each other (Figure 32). Surface parallel reflectors in the upper portion of NC1a and the lower portion of NC1d show extensional stress planes caused by increased slope angle (Figures 30 and 34) (Hausmann et al., 2012).

The only prominent basal reflectors was observed on the NC1b profile (Figure 31). Depths from this profile range from 17 m to 40 m with an average depth of 26.6 m. Absence of base reflectors in other parts of the profile suggest that part of this rock glacier is sitting atop either glacial debris or talus deposits and bedrock depths were greater than that attained during GPR surveying (Isaksen et al., 2000; Hausmann et al., 2007). This makes sense given the size of the talus fans, therefore the large amount of talus production, within this cirque. The basal reflector in NC1b could be the lip of the cirque which then drops off shown by a sharp increase in slope angle on the surface near the toe. In addition, this aligns with the absence of streams at the base of the toe. Talus under the frozen permafrost body allows water to percolate deeper and only appear further downslope where the talus ends. Furthermore, higher amounts of attenuation present throughout some of the profiles could preclude detection of the base layer.

West Fork Buttermilk Creek 3

The West Fork Buttermilk Creek 3 (WFBC3) rock glacier is an active, glaciogenic, complex-shaped rock glacier (Table 4) (Figure 34). This feature sits at the head of the West Fork Buttermilk Creek drainage within the Twisp River watershed in the Northeastern Cascades. Satellite imagery shows that its surface is inflated with pronounced surface morphology consisting of pressure ridges and furrows which was confirmed in the field. Its head originates in a northeast-facing cirque and it flows northeast downslope alongside an adjacent ridge out of the cirque. The rock glacier is 580 m long and 305 m wide. It flows as one body for approximately the first 450 m and then splits into two separate lobes that flow downslope.

The overall bedrock is orthogneiss (Bunning, 1992). In general, surface material was large and blocky with most boulders exceeding 2 m in diameter. Darker colors on rocks indicate weathering around the tops of pressure ridges. In most areas this is accompanied by unweathered, finer-grained material at the fronts of the pressure ridges which indicates that this material has been newly exposed. Several larch trees can be found on its surface in these areas of finer-grained material. In addition, several streams were present running from the toe of the rock glacier and running water could be heard beneath the surface of the rock glacier in several locations toward the head.

One 481 m longitudinal GPR transect was surveyed in early August 2017 (Figure 35). The profile originates at the head of the rock glacier and runs 430 m down to the toe of the western lobe. Data from portions of the beginning of the profile were lost due to user error so the resulting length of the profile is 457.5 m. Processing techniques included migration and topographic correction after hyperbola fitting. Based on hyperbola

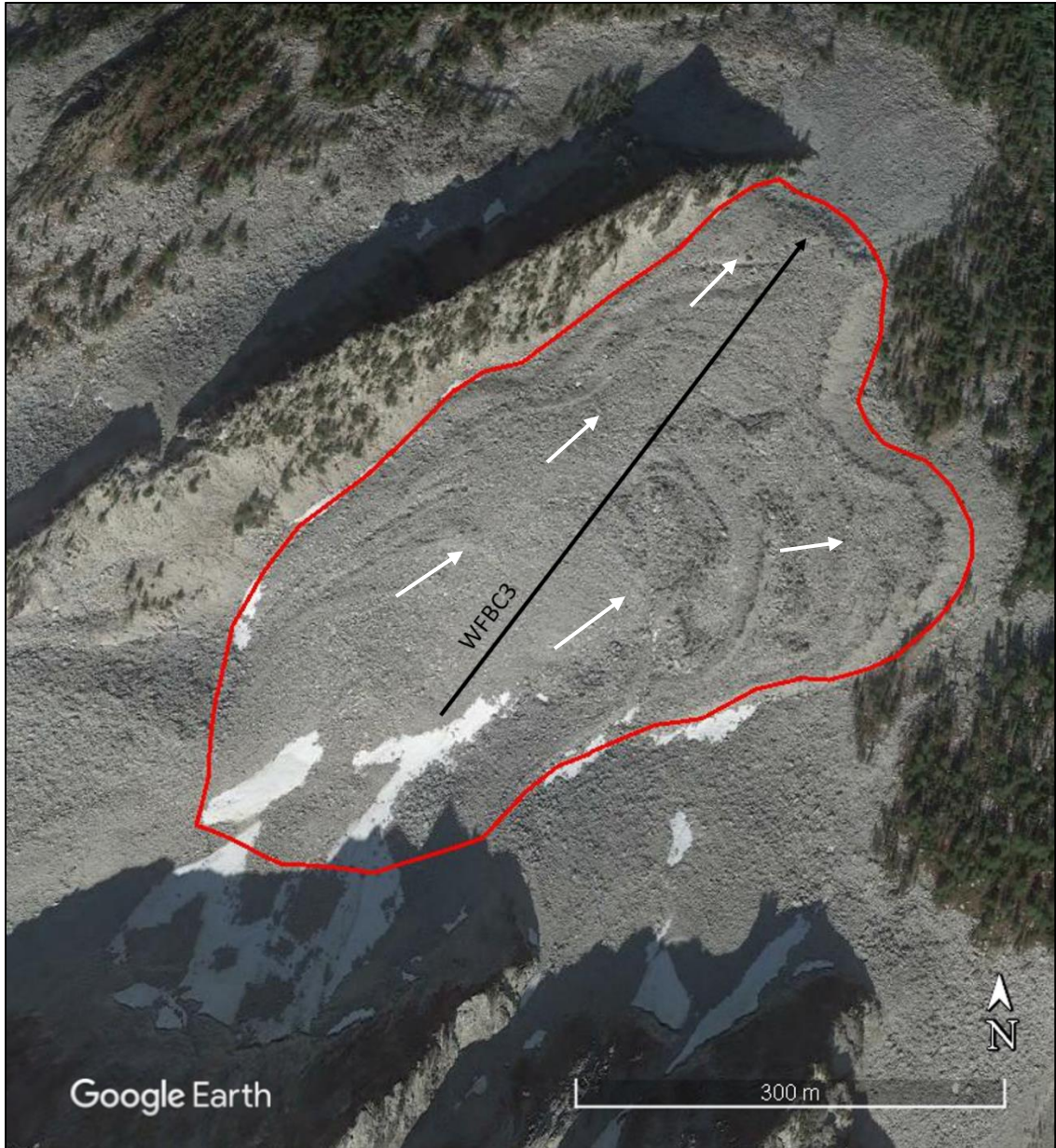


Figure 34. Google Earth image of WFBC3. Black line depicts location and direction of GPR profile, white arrows indicate direction of flow, and red line indicates rock glacier boundary.

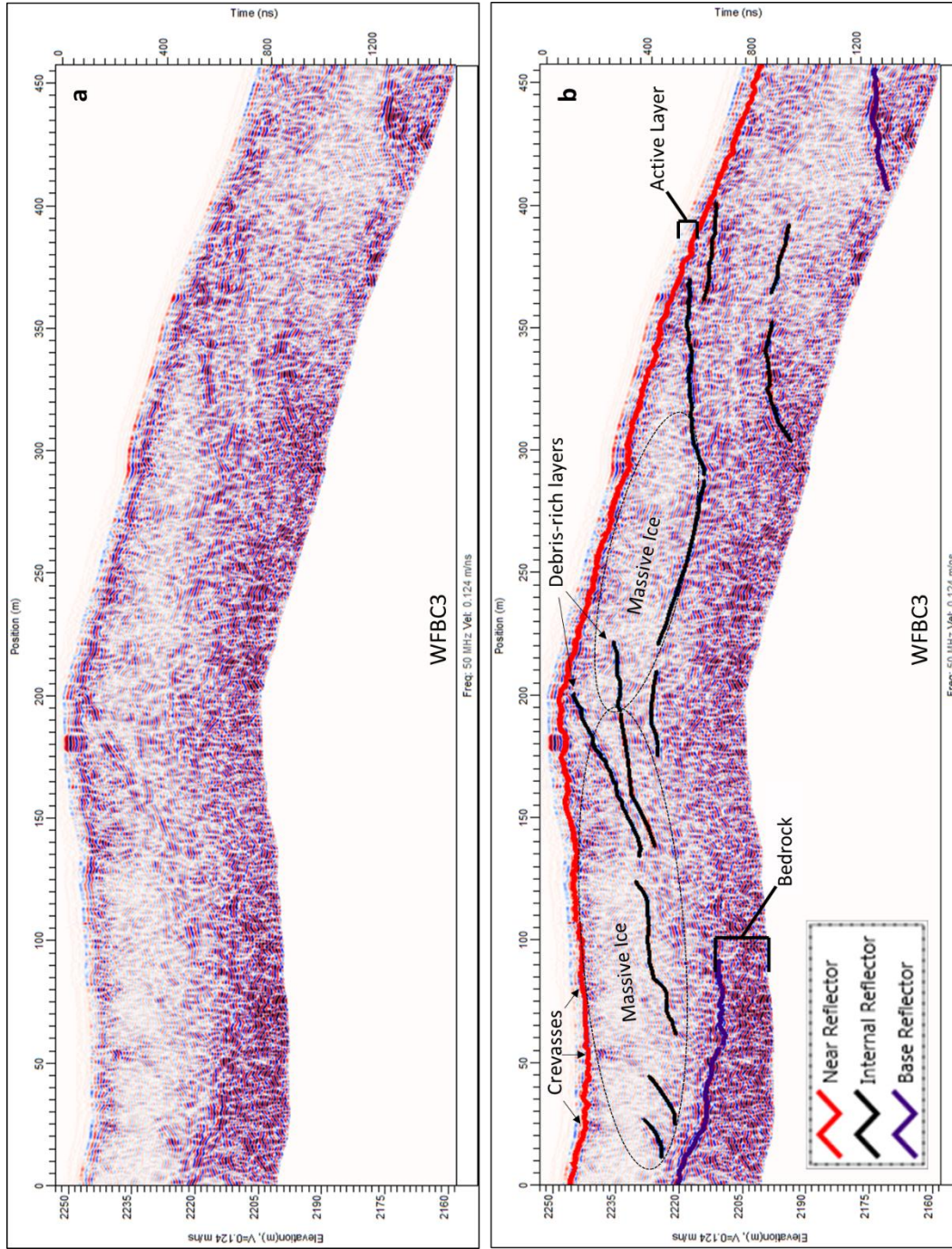


Figure 35. Migrated and topographically corrected longitudinal GPR profile of WFBC3 without interpretations (a) and with interpretations (b).

fitting the average velocity for WFBC3 is 0.124 m/ns^{-1} which was used for migration and topographic correction.

Multiple areas toward the surface of the rock glacier, indicated with arrows, show small concentrations of diffracting points (Figure 35b). These are interpreted as crevasses in the massive ice that have been filled with debris and are now part of the active layer (Guglielmin et al., 2018). The active layer ranges from 1.8 m near the head of the rock glacier to 4.4 m near the toe with an average of 3.1 m.

The GPR profile suggests that this rock glacier contains massive ice (Figure 20). The circled areas indicate regions that lack numerous diffracting points. In addition, these areas contain higher velocities ($>0.160 \text{ m/ns}^{-1}$) indicating that these sections could consist of more homogenous material (i.e., ice). They are separated by several upward-dipping reflectors from 130 m to 220 m (Figure 20). This could possibly be a coarse sediment layer or a layer of debris separating the two sections of massive ice (Monnier et al., 2011; Guglielmin et al., 2018). These reflectors are likely thrust planes that are debris-rich sediment layers which express compressional stresses likely due a slightly convex surface under the rock glacier before the slope steepens at 200 m (Monnier et al., 2008; Guglielmin et al., 2018). Unfortunately, no clear basal reflector is present in this section but this slight rise in elevation could be caused by the lip of cirque, marking the edge of the over-deepening created by the former cirque glacier. In addition, higher concentrations of diffracting points deeper in the profile suggest this massive ice core resides on top of underlying debris rather than directly on bedrock (Isaksen et al., 2000). The depth to the far reflector, interpreted as the base of rock glacier is on average 35.5 m.

This is deepest average depth to base of all the rock glaciers in this survey which likely corresponds to it also having the largest surface area (0.159 km²) of all surveyed rock glaciers.

West Fork Buttermilk Creek 4

The West Fork Buttermilk Creek 4 (WFBC4) rock glacier is an active, glaciogenic, complex-shaped rock glacier (Figure 36). This feature is located approximately 0.5 km southeast of the WFBC3 rock glacier within the Twisp River watershed in the Northeastern Cascades. This rock glacier flows out from a north-facing cirque and splits into two lobes qualifying it as a complex rock glacier. The eastern lobe of this rock glacier is partially deflated with small pressure ridges residing in the deflated area. Time restrictions allowed the surveying of only one lobe of the rock glacier in early August 2017. The western lobe was chosen because it was still inflated indicating it still contains permafrost. The western lobe is 300 m long and 172 m wide.

Similar to WFBC3, this rock glacier also consists of predominantly orthogneiss (Bunning, 1992). Interestingly, surface material was generally much smaller (i.e., ~1 m in diameter) than that found on the adjacent WFBC3 rock glacier. Small, angular, platy rocks were more common on this rock glacier as well. This suggests that WFBC4 has a different structure due to different weathering processes affecting its parent material. In addition, this rock glacier does not have pronounced pressure ridges like those observed on WFBC3 and is instead relatively flat.

Little vegetation was present on this rock glacier indicating an active state. On the outer slopes of the eastern lobe, several small larch trees grow; however, no notable



Figure 36. Google Earth image of WFBC4. Black line shows GPR transect, white arrows indicate flow path and red line shows rock glacier outer limits. Dotted arrow indicates portion of transect lost after data collection.

vegetation grows on the western lobe. A stream was observed emerging from the toe of this rock glacier.

One longitudinal transect was surveyed on the western lobe of the WFBC4 rock glacier (Figure 37). This profile originally spanned the full length of the rock glacier (200 m), but the second 100 m section was lost after data collection. Processing techniques before hyperbola fitting included DEWOW, background subtraction, and SEC gain, while migration and topographic correction were applied after the average velocity of 0.133 m/ns^{-1} was determined.

A near reflector is evident at the base of the active layer, which ranged from 2.2 m near the head to 4.1 m in depth toward the toe. The average depth of the active layer is 2.97 m.

Similar to WFBC3, changes in subsurface material in the middle portion of this profile (circled in Figure 37) consists of few diffracting points, suggesting that WFBC4 consists of massive ice under a debris layer. The circled portion toward the north end of the profile shows few reflectors as well. In addition, there is an absence of diffracting points between and underneath the upward-sloping internal reflectors. These multiple linear upward-sloping reflectors suggest areas of ice-poor, debris-rich sediment layers within the massive ice that are likely thrust planes between different portions of the massive ice (Monnier et al., 2011; Guglielmin et al., 2018). Lillquist and Weidenaar (in preparation) had originally classified WFBC4 as a talus rock glacier, but this evidence points toward a glacial origin.

This is the only profile in which a series of reflectors parallel to the basal reflector are depicted at depth. An explanation for this could be that these are mirrored reflectors

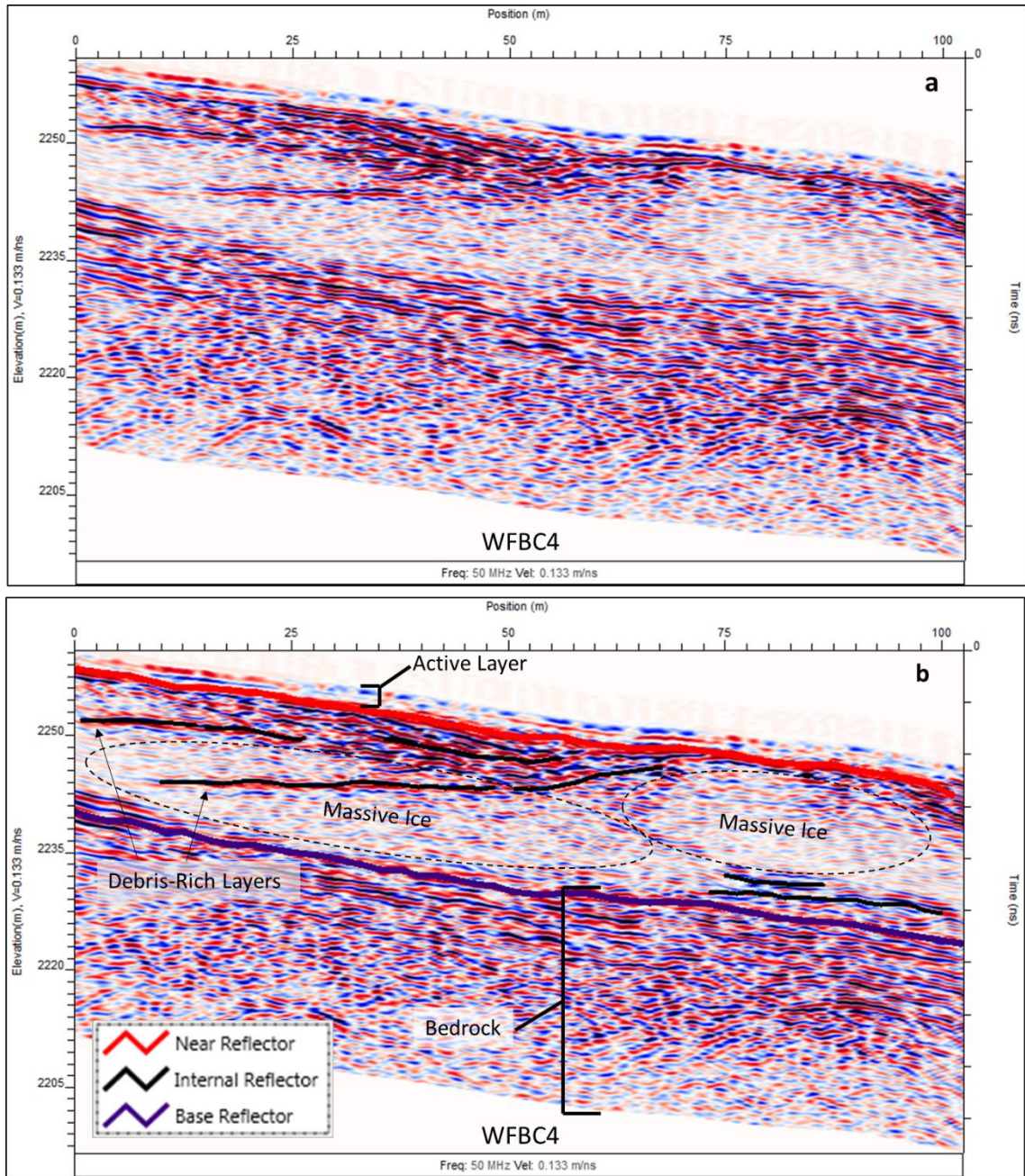


Figure 37. Migrated and topographically corrected longitudinal GPR profile of WFBC4 without interpretations (a) and with interpretations (b).

from the bedrock reflector above. Bedrock outcrops were observed on the west side of the rock glacier at a similar elevation as the first reflector in the series of these mirrored reflectors. The basal reflector has a minimum depth of 18.7 m and a maximum depth of

24.1 m with an average of 21.1 m. Low EM velocities ($<0.10 \text{ m/ns}^{-1}$) near the bedrock reflector suggest basal shear for this glaciogenic rock glacier.

East Fork Buttermilk Creek 2

The East Fork Buttermilk Creek 2 (EFBC2) rock glacier is an active, glaciogenic, complex-shaped rock glacier (Table 4) (Figure 38). It is located in a north-facing cirque beneath Mount Bigelow within the Twisp River watershed in the Northeastern Cascades. From its head source the rock glacier splits at about 180 m into two separate lobes. The western lobe was excluded from field surveying in mid-August 2017 due a steep gradient making the terrain dangerous for data collection. The eastern lobe is 457 m long and 137 m wide.

This rock glacier is located just over 4 km southwest of WFBC3 and WFBC4, and is made up of predominately orthogneiss (Bunning, 1992). Average surface boulder diameter was approximately 2 m. The eastern lobe of EFBC2 in particular has pronounced surface topography marked by large pressure ridges. Similar to WFBC3, these ridges have steep fronts that consist of more fine grained, unweathered material.

About 200 m down the longitudinal profile permafrost was observed (Figure 39). This permafrost was found about 2 m below the surface. Large boulders on the surface created cavities that allowed crew members to access. Here, permafrost was observed interstitially mixed between all the rocks and boulders beneath. This was interpreted to be the top of the active layer which supports the active classification. Also, the permafrost had flowing water moving across its surface. This is possibly meltwater from either the snowfields above or the melting of the active layer itself. In addition, the permafrost was

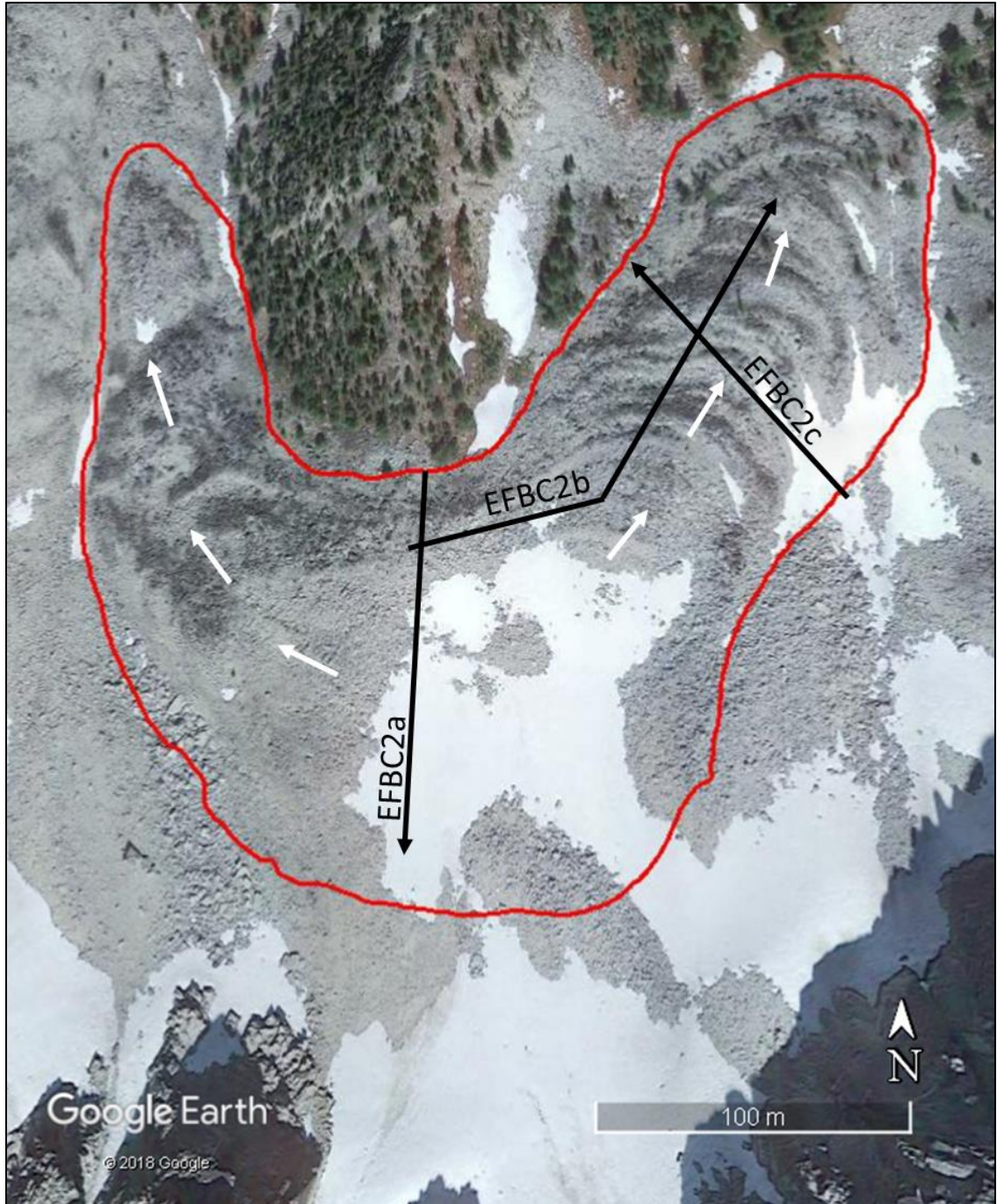


Figure 38. Google Earth image of EFBC2. Black lines depict location and direction of GPR profiles, white arrows indicate direction of flow, and red line indicates rock glacier boundary. Note larch trees, shown by their shadows, toward the toe of the eastern lobe.



Figure 39. Permafrost found beneath surface of EFBC2. Permafrost is overridden by flowing water. Note the fine sediment buildup atop the permafrost indicated by the arrow. Location of photo indicated in GPR profile in Figure 43.

covered in certain spots by fine sediment, likely deposited by wind and transported down by the flowing water.

This rock glacier was originally classified as inactive which Lillquist and Weidenaar (in preparation) determined from satellite imagery due to the dark weathering and lichen growth on much of the surface. Its western lobe also flows into a much older lobe that has significant soil development and tree growth. On the eastern lobe a series of larch trees are growing among the pressure ridges near the toe. Typically tree growth indicates stable conditions and therefore an inactive state. However, in the Northeastern Cascades, Goshorn Maroney (2012) showed movement of a rock glacier using LiDAR

where larches are present. To further support this, many of the larches on EFBC2 have been distorted or tilted (Figure 40).

One longitudinal and two transverse GPR transects were recorded on the eastern lobe of this rock glacier (Figures 41-43). The longitudinal transect runs 320 m from the middle of the lobe down its center to its toe. The elbow shape is a result of following the direction of flow. In addition, two transverse profiles were surveyed. One transverse transect was recorded across the top lobe oriented north-south and runs 155 m toward the headwall. The second transverse profile, 158 m in length, was surveyed toward the toe of the eastern lobe. This profile was oriented approximately perpendicular to the longitudinal (Figure 42) profile.

GPR results confirm that this rock glacier consists of a heterogeneous mix of rock, saturated sediment, and permafrost therefore confirms Lillquist and Weidenaar's (in preparation) talus classification. Overall thickening of the rock glacier is observed at about 175 m down the longitudinal profile. This is where the slope angle lessens and the extensional forces become compressional. This is apparent on the surface with the development of pronounced pressure ridges and in the EFBC2b profile with multiple stacked upward-dipping reflectors (Figure 42).

The near reflector is apparent on all three profiles. The average depth to the near reflector is 3.15 m with a minimum depth of 1.65 m and a maximum depth of 6 m. Depth to the near reflector thickens toward the toe and also along pressure ridges with thinning occurring in troughs between these features.



Figure 40. Toe of eastern lobe of EFBC2. Note the tilted tree on the front slope (indicated with white arrow) and streams originating from rock glacier toe (blue arrows). Field assistants (black arrow) for scale at bottom left of toe.

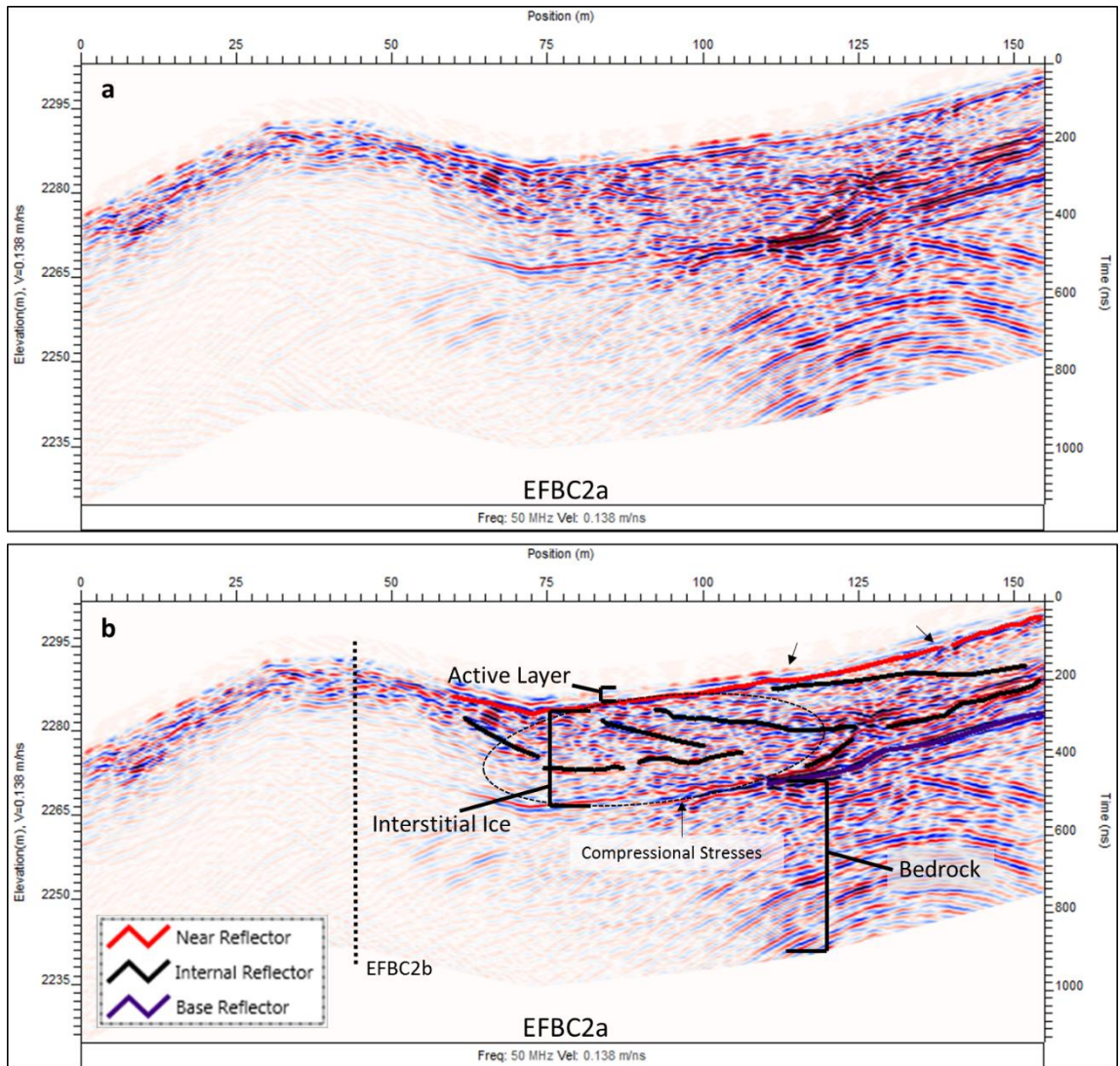


Figure 41. Migrated and topographically corrected top transverse GPR profile of EFBC2a without interpretations (a) and with interpretations (b). Dotted line indicates intersection with longitudinal profile EFBC2b.

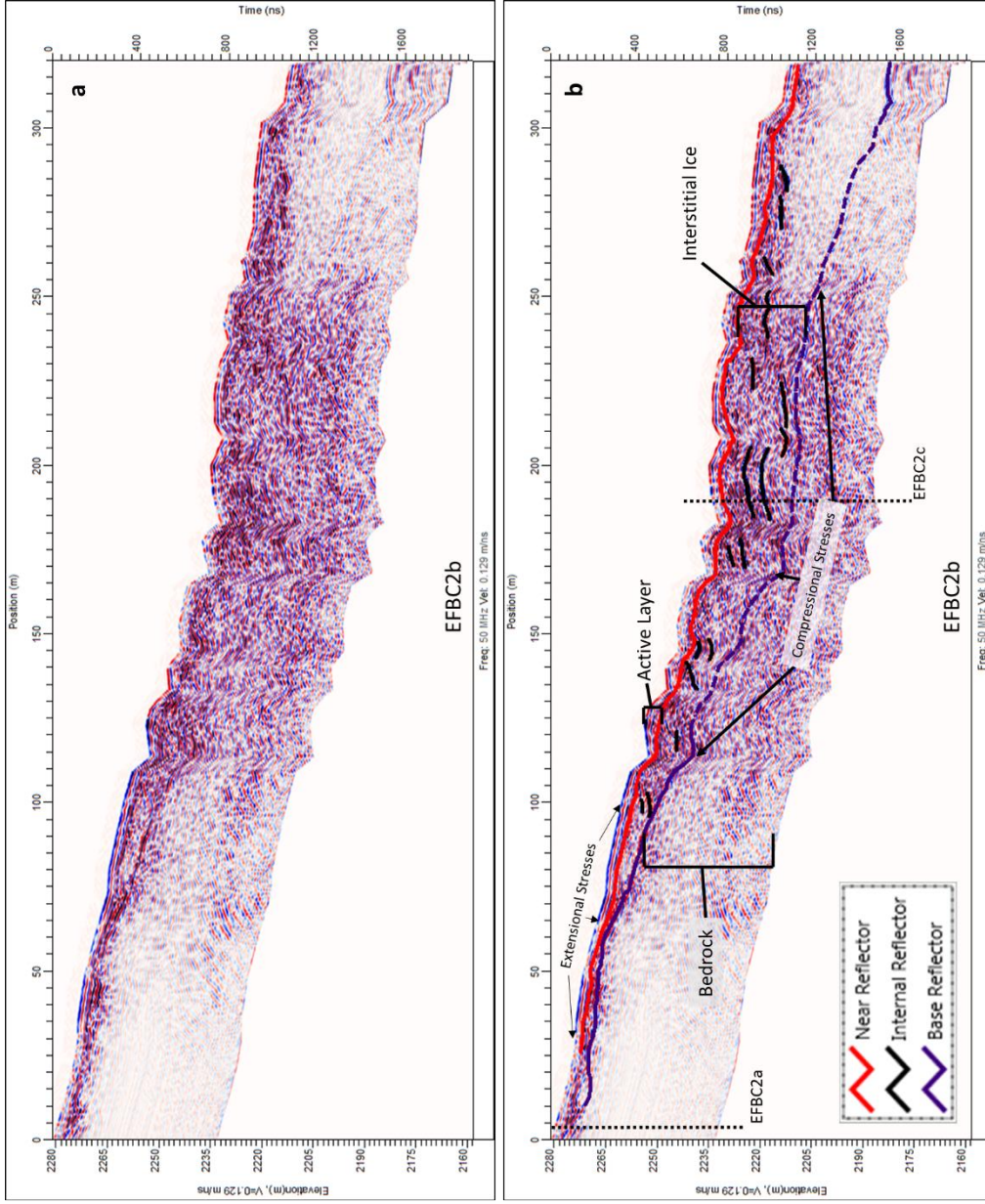


Figure 42. Migrated and topographically corrected longitudinal GPR profile of EFBC2b without interpretations (a) and with interpretations (b). Dotted lines indicated intersections with transverse profiles EFBC2a and EFBC2c.

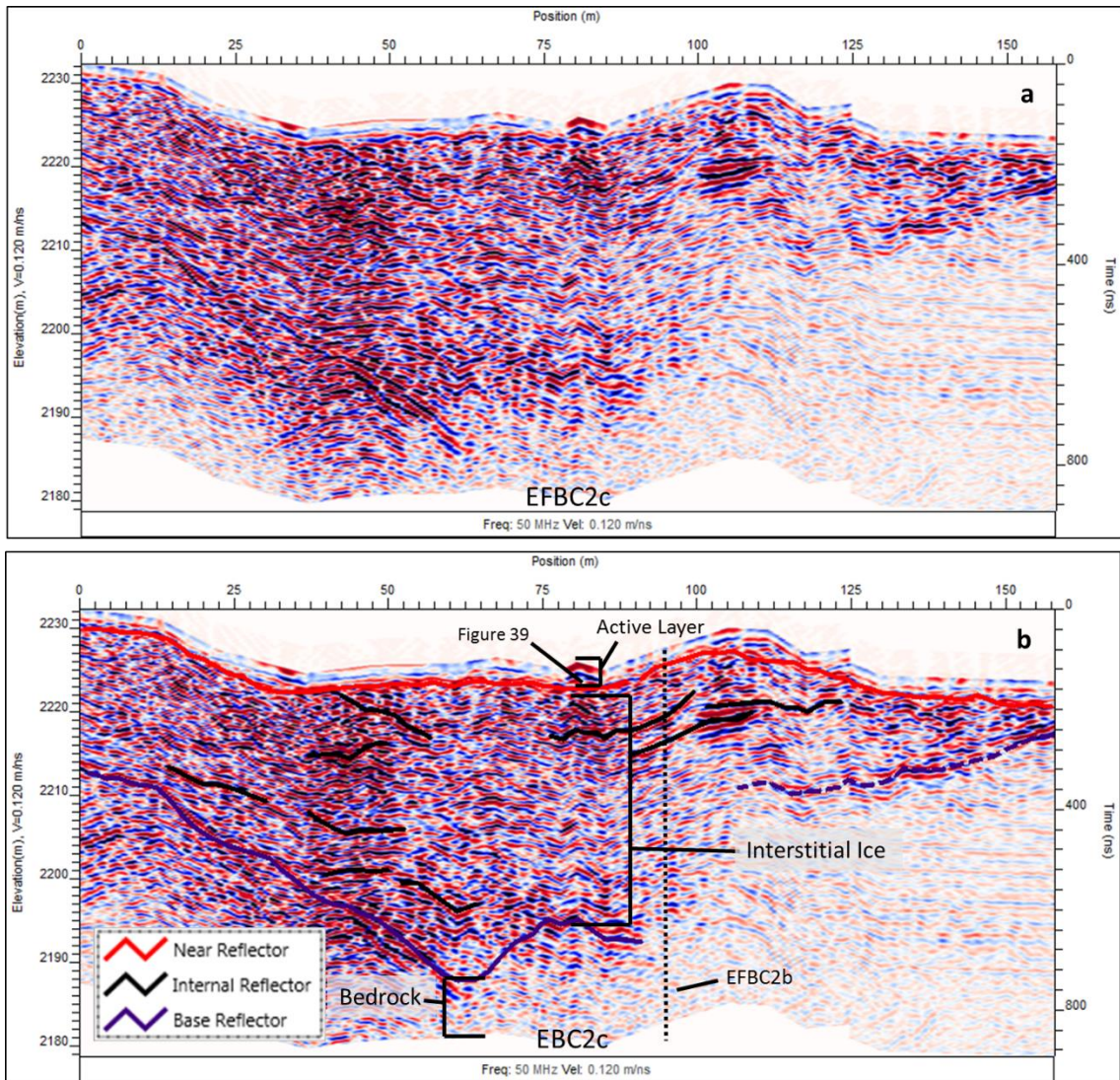


Figure 43. Migrated and topographically corrected bottom transverse GPR profile of EFBC4c without interpretations (a) and with interpretations (b). Dotted line indicates intersection with longitudinal profile EFBC2b.

Upward dipping reflectors on the upper transverse profile indicate compression from debris accumulation in this area (Figure 41) (Monnier et al., 2008, 2011). This portion sits below several avalanche chutes and, as this portion accumulates avalanche and rockfall debris, it is forced east or west as a result of the ridge in the center of the cirque. Shallow base depths in the beginning of the longitudinal profile along with

surface parallel reflectors indicate extensional forces (Figure 42) (Hausmann et al., 2012). This is caused by the steeper slope angle at the head of the rock glacier. Pressure ridges begin after this portion where slope angle decreases. Internal stacked reflectors throughout the longitudinal profile correspond with these pressure ridges and indicate thrust planes (Monnier et al., 2008).

In addition, the base reflector is easily distinguished in the first 125 m of the longitudinal profile but loses strength until the last 20 m. By increasing the gain value this reflector was able to be detected throughout the remainder of the profile and is estimated with a dashed black line (Figure 42). Measurements of the clear basal reflector on the bottom transverse profile correlate to the estimated base depth on the longitudinal profile. Base depths were averaged from all three profiles for a mean depth of 16.1 m. Maximum depths were recorded to 37.6 m near the toe, while minimum base depths reached as low as 2.6 m. The basal reflector on the bottom transverse profile (EFBC2b) clearly shows the bedrock surface sloping down on either side toward the middle of the rock glacier. This shows that the rock glacier is following the center of the valley drainage.

Tronsen Creek 1

The Tronsen Creek 1 (TC1) rock glacier is an inactive, talus, tongue-shaped rock glacier (Table 4) (Figure 44). This rock glacier is located within the Wenatchee River watershed in the Northeastern Cascades. TC1 flows west due to an east-west orientation of the drainage. This is also due to it being sufficiently shaded by surrounding higher terrain (i.e., Diamond Head) and therefore experiences decreased insolation. TC1 is approximately 258 m long and 41 m wide. Several longitudinal furrows extend from the

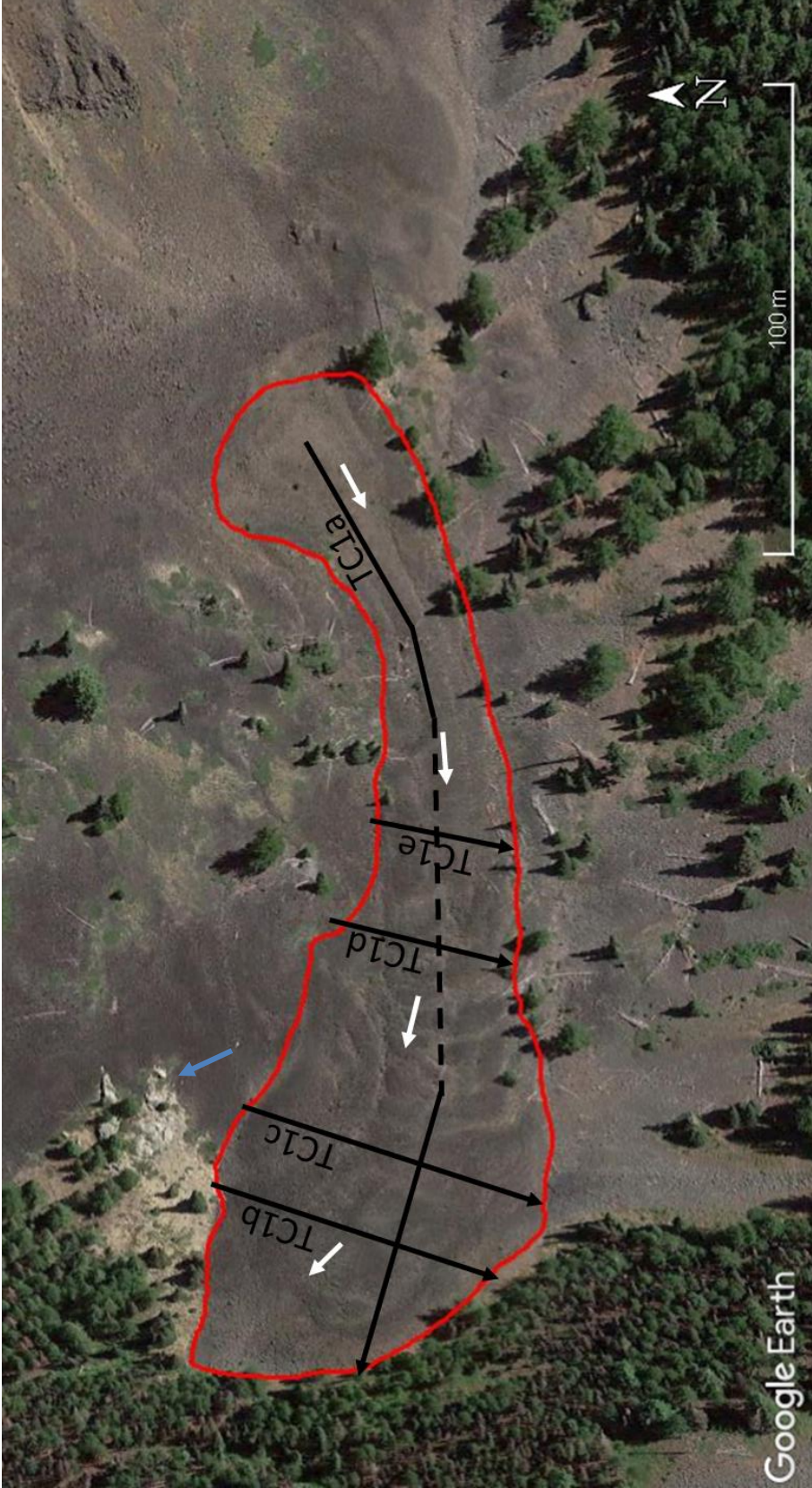


Figure 44. Google Earth image of TC1. Black arrows depict location and direction of GPR profiles, white arrows indicate direction of flow, red line indicates rock glacier boundary, and blue arrow points to sandstone outcrop. In addition, dotted line indicates portion of longitudinal GPR transect that was lost after data collection.

head of the rock glacier. These furrows end as the gradient decreases where a series of transverse pressure ridges mark a buildup of material.

The TC1 rock glacier consists of basalt. Tronsen Basin itself consists of basalt on the south and west portions of the basin and transitions into sandstone on the northeastern portion (Tabor et al., 1989). Directly adjacent to TC1 a sandstone outcrop is present (Figure 44). It is probable that the rock glacier consists of basaltic material that has flowed over the sandstone bedrock. Surface material consists of basalt rocks that average 0.5 m in diameter.

A stream flows from the toe of TC1 year round. In addition, vegetation is limited to several small juniper bushes and some trees that are restricted to the outskirts of the rock glacier.

One longitudinal and four transverse transects were recorded on this rock glacier (Figures 45-50). The longitudinal transect was recorded in June 2017 and the transverse transects were recorded in mid-July 2017. Ease of access allowed for an increase in the amount of transects. A Forest Service road that is open in the summer allows vehicle access to within less than 0.5 km from the rock glacier. In addition, this rock glacier is located close to CWU and is small in size which allows for quicker transect recording.

GPR profiles show a heterogeneous mix of material with high EM velocities ($>0.160 \text{ m/ns}^{-1}$) indicating talus origin. Processing included DEWOW and SEC gain before hyperbola fitting. Migration, topographic correction, and background subtraction were applied with an average velocity of 0.136 m/ns^{-1} .

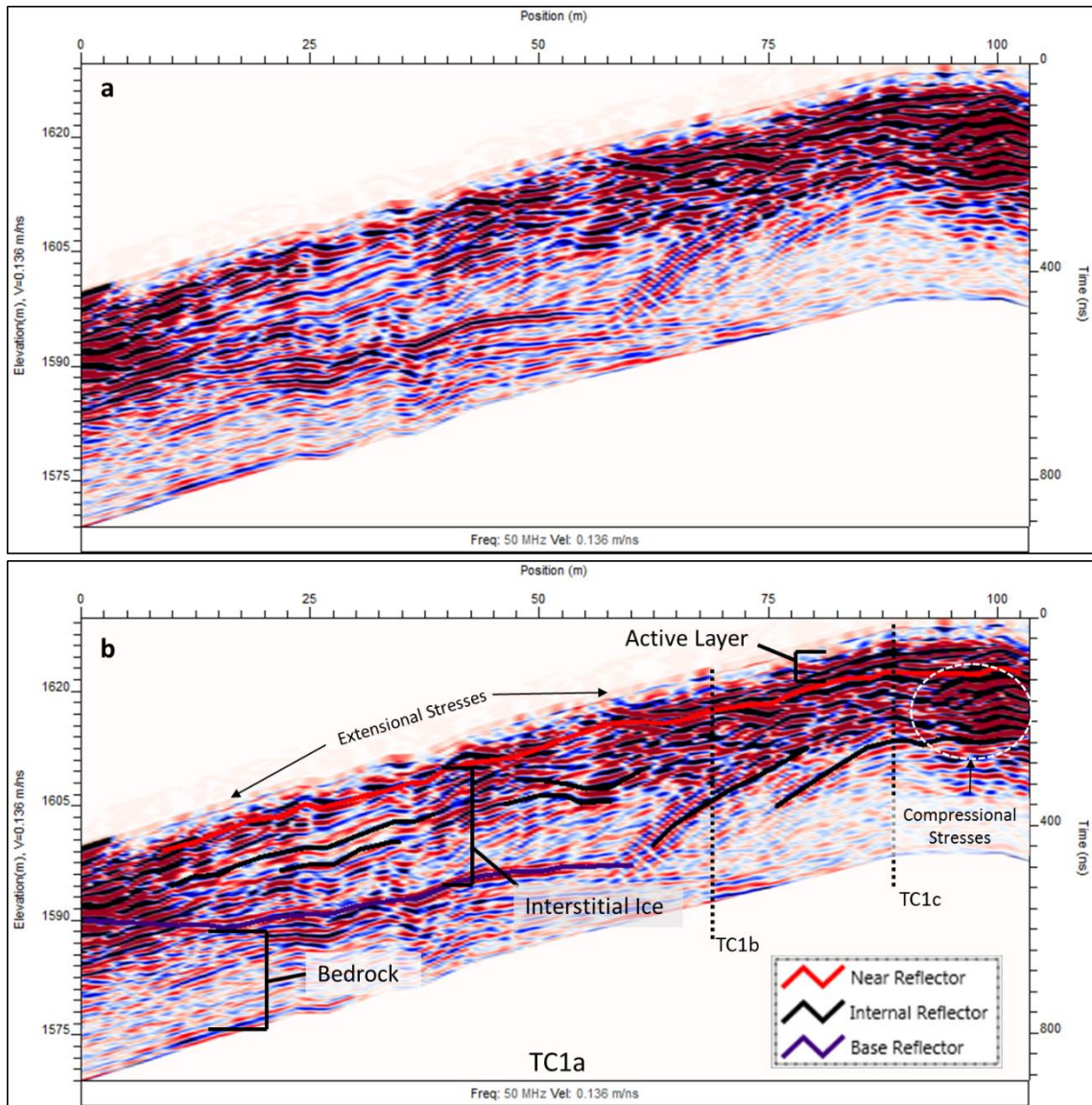


Figure 45. Migrated and topographically corrected lower longitudinal GPR profile of lower TC1a without interpretations (a) and with interpretations (b). Dotted lines indicate intersections with transverse profiles TC1b and TC1c.

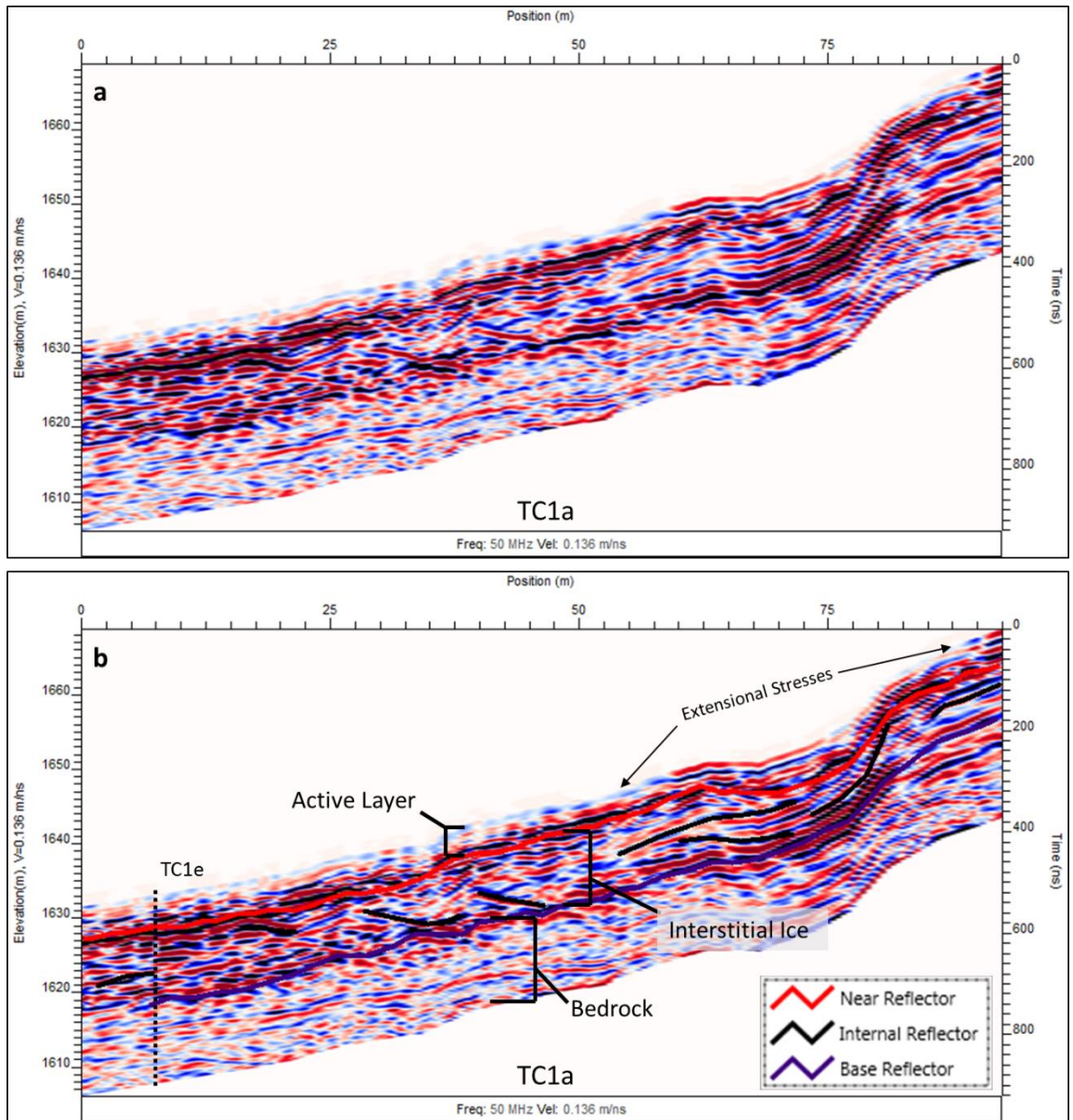


Figure 46. Migrated and topographically corrected upper longitudinal GPR profile of TC1a without interpretations (a) and with interpretations (b). Dotted line indicates intersection with transverse profile TC1e.

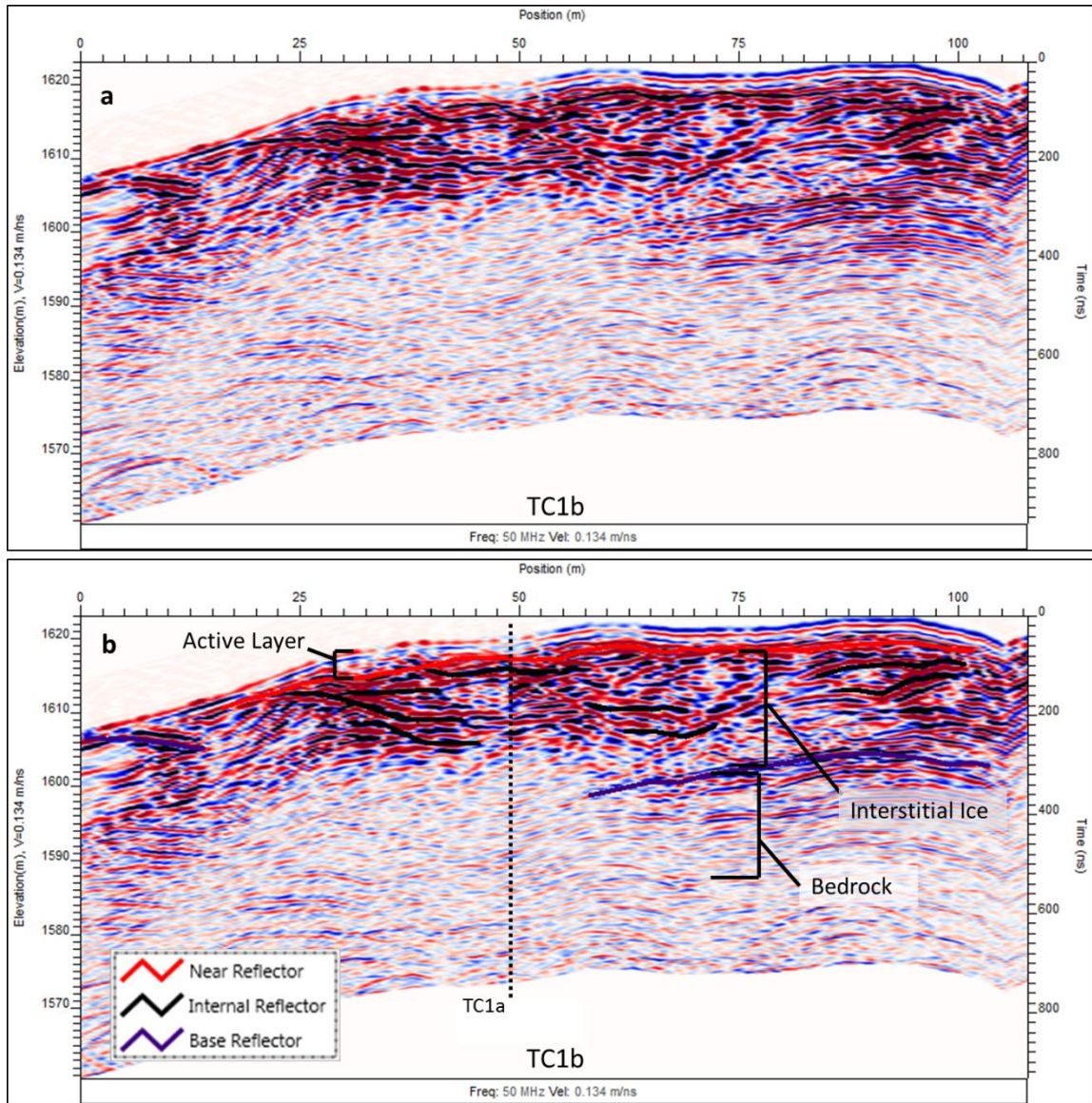


Figure 47. Migrated and topographically corrected transverse GPR profile of TC1b without interpretations (a) and with interpretations (b). Dotted line indicates intersection with longitudinal profile TC1a.

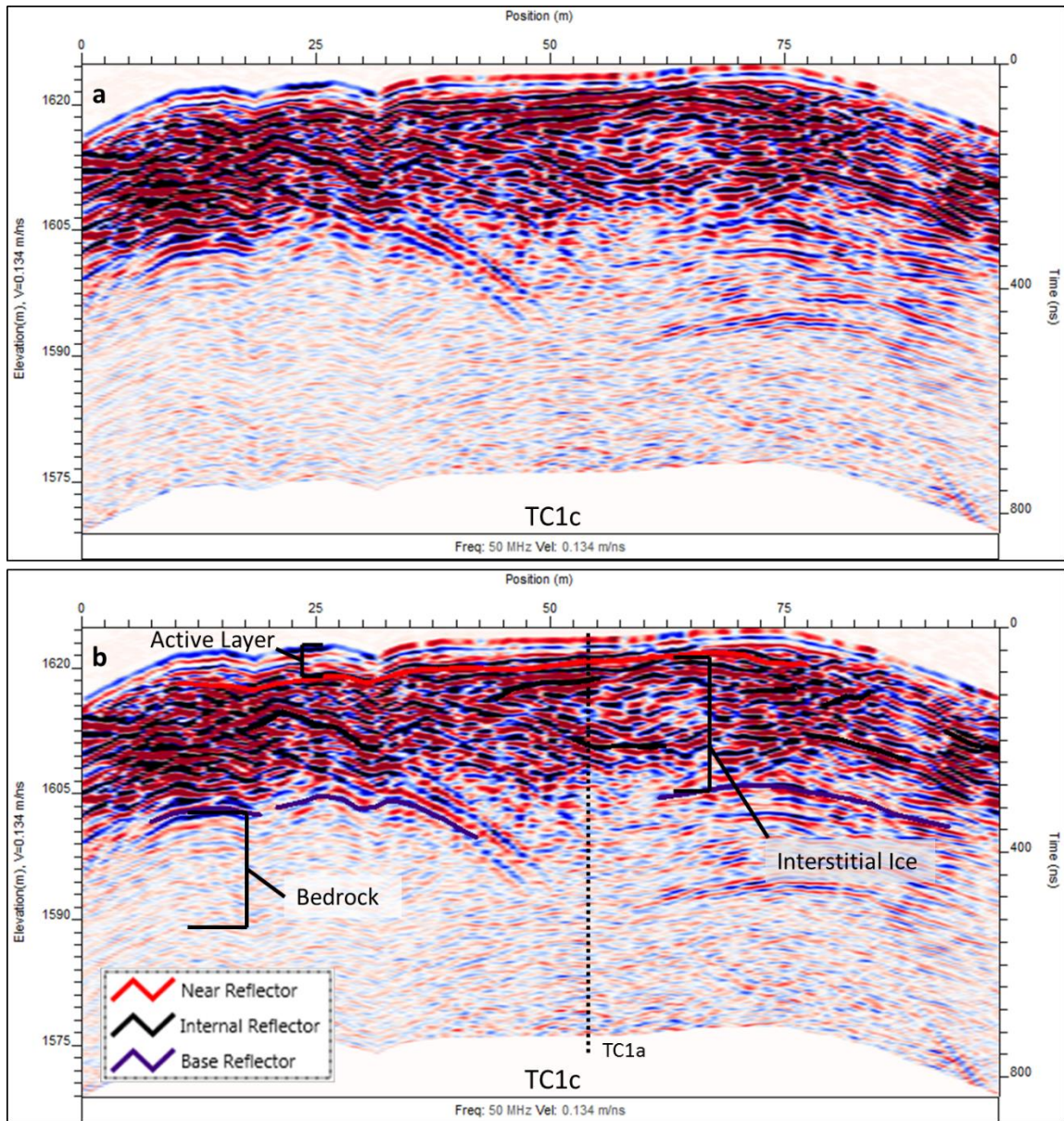


Figure 48. Migrated and topographically corrected transverse GPR profile of TC1c without interpretations (a) and with interpretations (b). Dotted line indicates intersection with longitudinal profile TC1a.

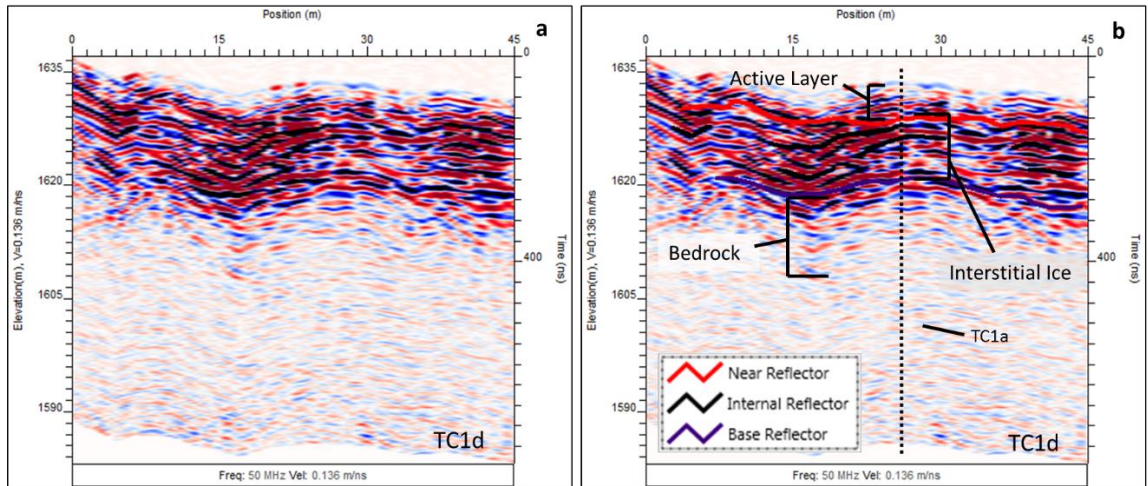


Figure 49. Migrated and topographically corrected transverse GPR profile of TC1d without interpretations (a) and with interpretations (b). Dotted line indicates intersection with longitudinal profile TC1a.

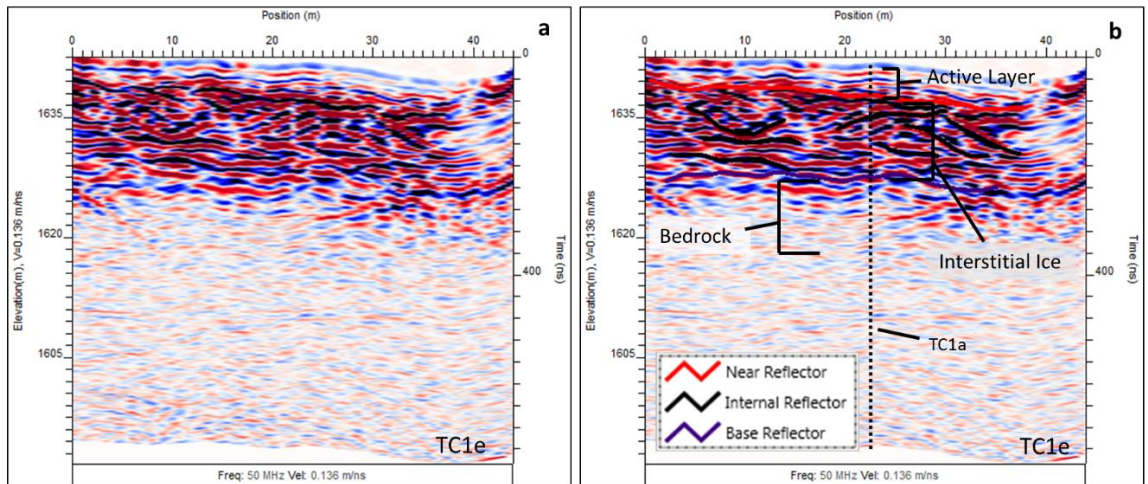


Figure 50. Migrated and topographically corrected transverse GPR profile of TC1e without interpretations (a) and with interpretations (b). Dotted line indicates intersection with longitudinal profile TC1a.

The longitudinal profile was surveyed using the older Pulse_EKKO 100 system. This was the first GPR transect surveyed in this study. Like most of the longer transects in this study, this was recorded as separate lines totaling approximately 100 m each. These lines were recorded with different time windows and, as a result, they cannot be

merged together. In addition, the middle 100 m section of this profile was lost during data processing and is not depicted.

A near reflector is prevalent in all the profiles. Depth to this near reflector increases toward the toe and ranges from 4 m to just over 8 m with an average depth of 5.6 m. These depths are greater than those found on the other rock glaciers in this study. An overall thicker active layer possibly indicates degrading permafrost and support Lillquist and Weidenaar's (in preparation) classification of inactive.

In addition, high velocities (>0.160 m/n1) present within the profile indicate the presence of permafrost. This is significant because it shows permafrost at a low elevation (1,585 m) for its position east of the Cascade Crest. This highlights the impact of favorable microclimate conditions.

Surface parallel reflectors are present in the upper portion of the upper longitudinal profile (Figure 46). These indicate extensional stresses which is reinforced by lateral furrows observed on the surface in the same region. Upward-dipping reflectors can be seen throughout the rest of the profile indicating thrust planes as areas of compressional stresses (Monnier et al., 2008, 2011; Hausmann et al., 2012). These correspond to a decrease in slope gradient where the furrows end and transverse pressure ridges begin.

A basal reflector is present in most of the profiles. However, this reflector is not as strong as some of the other basal reflectors observed on other rock glaciers. This could indicate that it is a change in substrate material and is possibly the sandstone that is observed in outcrops on the rock glacier's north flank. Sandstone has different EM

properties than basalt which could explain this weaker signal (Martinez and Byrnes, 2001). Base depths vary from 14 m to 30 m with an average of 19.5 m.

Spruce Creek 5

The Spruce Creek 5 (SC5) rock glacier is an inactive, talus, tongue-shaped rock glacier. It flows north off an east-west oriented ridge located in the Teton River watershed in the Southeastern Cascades. This rock glacier is approximately 170 m in length and 80 m wide, and is made of basalt (Schasse, 1987). Size of average surface material is >0.5 m.

No streams were observed at the toe of this rock glacier. A large tree island was found on its eastern middle portion. In addition, a small pond was observed next to the tree island. It is possible that this tree island and pond are the result of a mass wasting event that deposited sediment on top of the rock glacier. This would explain such extensive vegetation development in this concentrated area.

Two GPR transects were recorded on this rock glacier, one longitudinal (177.5 m) and one transverse (89 m) profile. Unfortunately, the data from both of these transects is very poor quality. A low depth of penetration and a high rate of attenuation were experienced throughout both transects which created low resolution. Rainfall and snowfall during data collection in mid-September 2017 caused water to infiltrate between the antenna and transmitter and receiver which likely had an effect on data recording.

Bear Creek 1

The Bear Creek 1 (BC1) rock glacier is an inactive, talus, tongue-shaped rock glacier (Figure 51). BC1 flows northeast out of a northeast-facing cirque within the Teton River watershed in the Southeastern Cascades. This rock glacier is approximately



Figure 51. Google Earth image of BC1. White outline indicates full extent of BC1 and red outline indicates extent of active portion of BC1. Black arrows depict location and direction of GPR profiles and white arrows indicate direction of flow.

704 m in length and 219 m in width and is comprised of andesite (Schasse, 1987).

Surface material averages about 1 m in diameter.

It is possible that this rock glacier has different lobe ages. The upper portion of BC1 is sparsely vegetated but the lower portion is heavily vegetated with large trees. The vegetation is mostly confined to the tops of pressure ridges. This vegetation cover indicates an inactive or a relict state in the lower reaches but it is possible that the upper

non-vegetated portion is still active. If this is the case, this rock glacier would be considered a complex rock glacier by Barsch's (1996) classification. However, only the upper 260 m was surveyed due to time constraints in early September 2017. In addition, since the upper portion of the rock glacier was the focus of this survey, the toe of this rock glacier was not visited to observe if any streams or springs were present.

One longitudinal (260.5 m) and one transverse transect (138.5 m) were surveyed at BC1 (Figures 52 and 53). Processing on these transects included trace editing, background removal, and SEC gain. Migration and topographic correction were also performed after hyperbola analysis at 0.124 m/ns^{-1} .

Both profiles show the existence of a near reflector indicating the base of the active layer. The average depth to the near reflector is 2.4 m with a minimum of 1.6 m and a maximum depth of 4.1 m. This is thinnest average depth of the active layer of all the rock glaciers surveyed in this study which supports the classification of active on its upper portion. On the longitudinal profile the near reflector depth gradually increases from the head of BC1 toward the toe. Depths stay relatively consistent throughout the transverse profile. Where depths do vary on the transverse profile, shallower depths are often associated with troughs between pressure ridges.

High concentrations of diffracting points within both profiles depict a heterogeneous mix of material which indicates talus origin. In the transverse profile a curious middle reflector starts at approximately 40 m and gradually rises toward the surface. This internal bounding reflector could indicate a separation between an upper permafrost-poor layer and a lower permafrost-rich layer. It is known from core sampling that permafrost, even in a talus rock glacier with a heterogeneous mix of material, is not

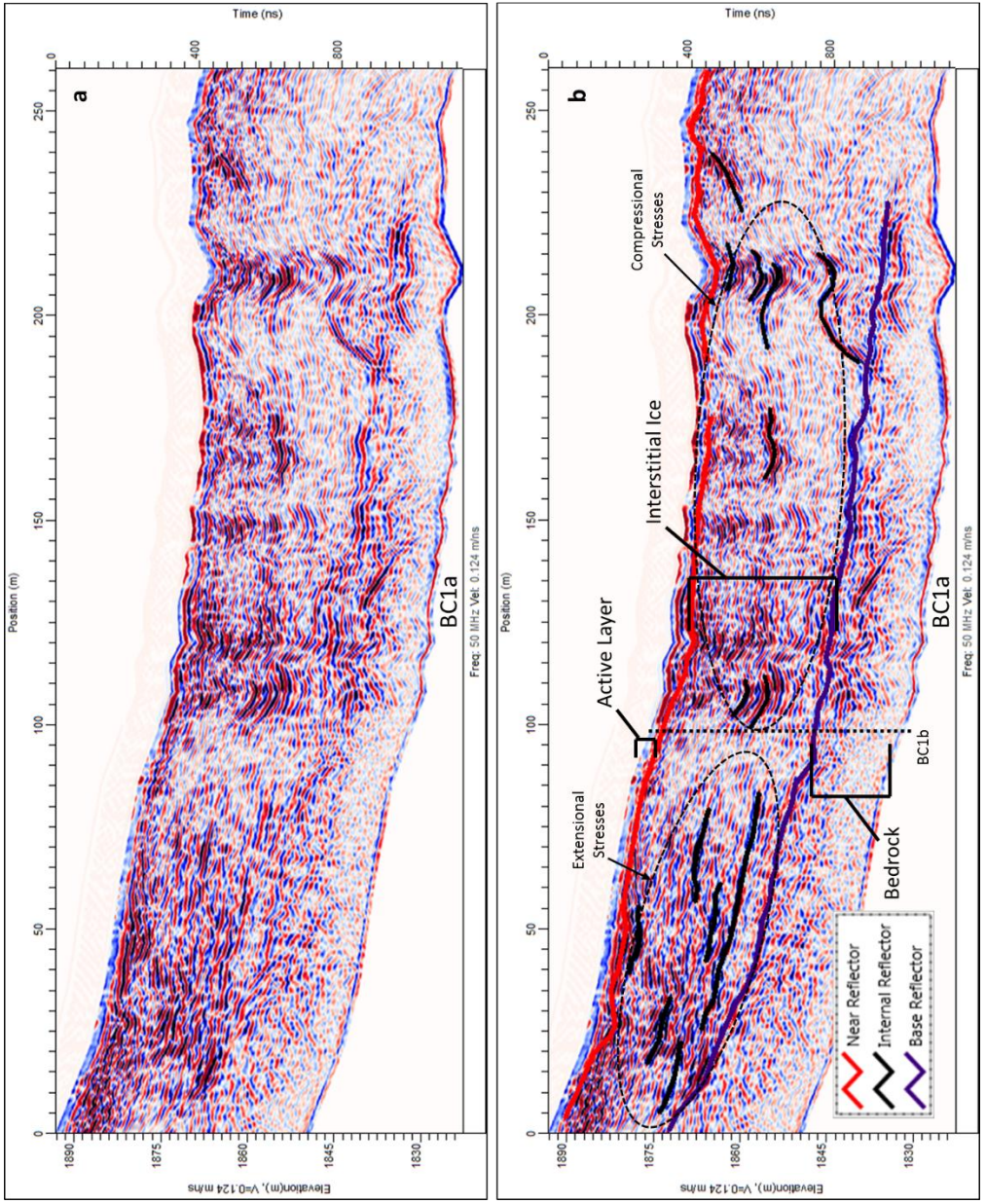


Figure 52. Migrated and topographically corrected longitudinal GPR profile of BC1a without interpretations (a) and with interpretations (b). Dotted line indicates intersection with transverse profile BC1b.

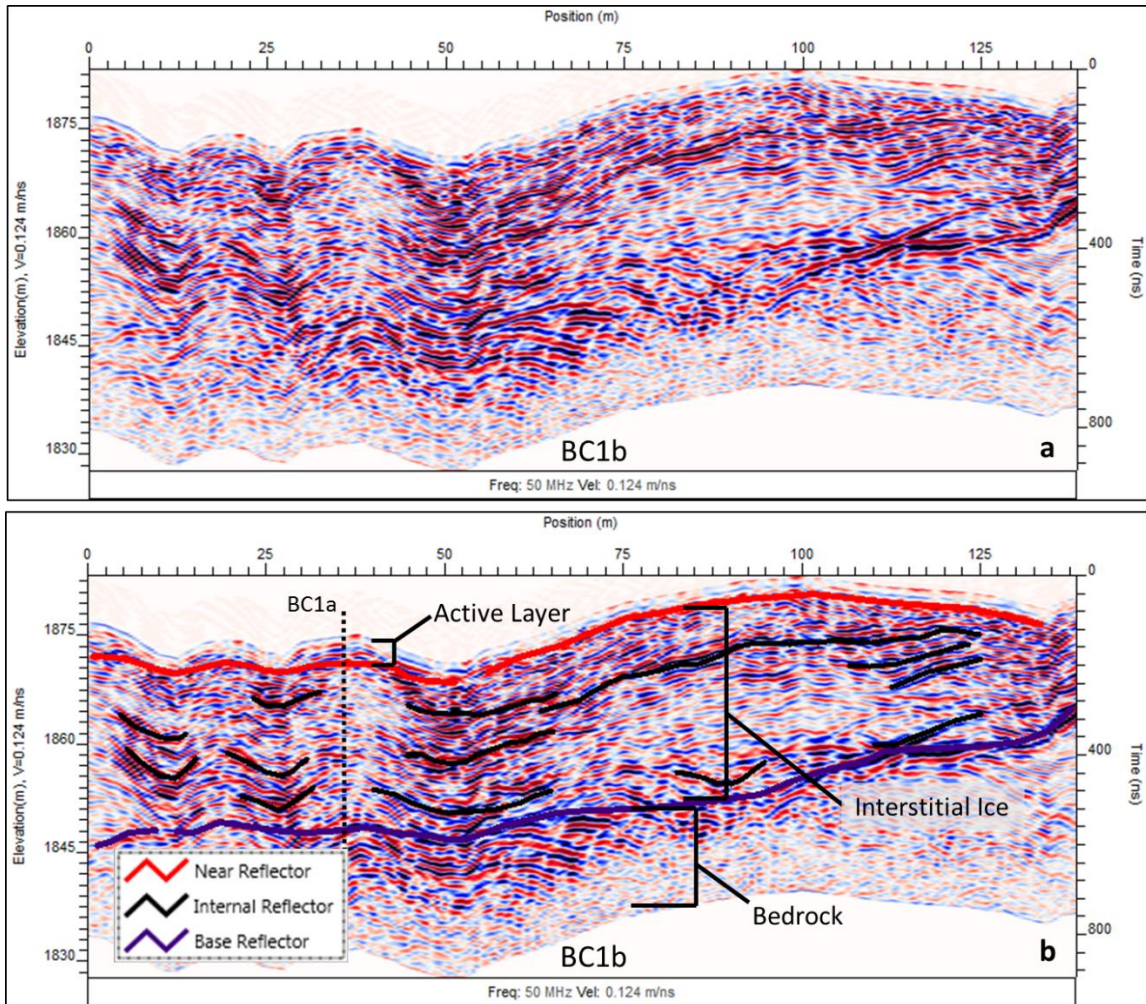


Figure 53. Migrated and topographically corrected transverse GPR profile of BC1b without interpretations (a) and with interpretations (b). Dotted line indicates intersection with longitudinal profile BC1a.

evenly distributed (Maurer and Hauck, 2007). In addition, this could also be a permafrost-free, sediment-dense layer or an ice-rich permafrost layer but is difficult to determine without further investigation (Hausmann et al., 2012).

The first 100 m of the longitudinal profile is marked by surface parallel reflectors which indicate extensional flow (Hausmann et al., 2012). After the first 100 m a series of stacked and undulating reflectors suggests compressional stresses which aligns with the start of a series of pressure ridges seen on the surface (Figure 52) (Monnier et al., 2008, 2011). The thickness of the rock glacier increases in this section indicating a buildup of material caused by a decrease in slope angle.

A strong far reflector, interpreted as bedrock, was detected in both profiles. A gradual increase in depth is seen toward the end of the longitudinal profile. Base depths range from 14.7 m to over 37 m with an average depth of 25.6 m.

Bear Creek 3

The Bear Creek 3 (BC3) rock glacier is an active, talus, lobate shaped rock glacier (Figure 54). Located in a north-facing cirque, it extends approximately 83 m north-northeast with a width of 242 m. This rock glacier is located 250 m southeast of BC1 within the Tieton River watershed in the Southeastern Cascades. Andesite is the dominant rock type on this rock glacier and surface material consists of boulders averaging 1 m in diameter (Schasse, 1987). This lobate rock glacier consists of multiple pressure ridges that extend almost its entire width. This was the only lobate rock glacier visited in this study.

No trees are present on the surface of BC3 and vegetation is limited to small shrubs. Large amount of fine sediments are apparent on the rock glaciers in this basin, including BC1 and BC3. These are attributed to the deposition of tephra during the 1980 eruption of Mount St. Helens. In addition, no streams were observed running from the toe of the rock glacier. This landscape is extremely porous. In mid-August 2017, even with

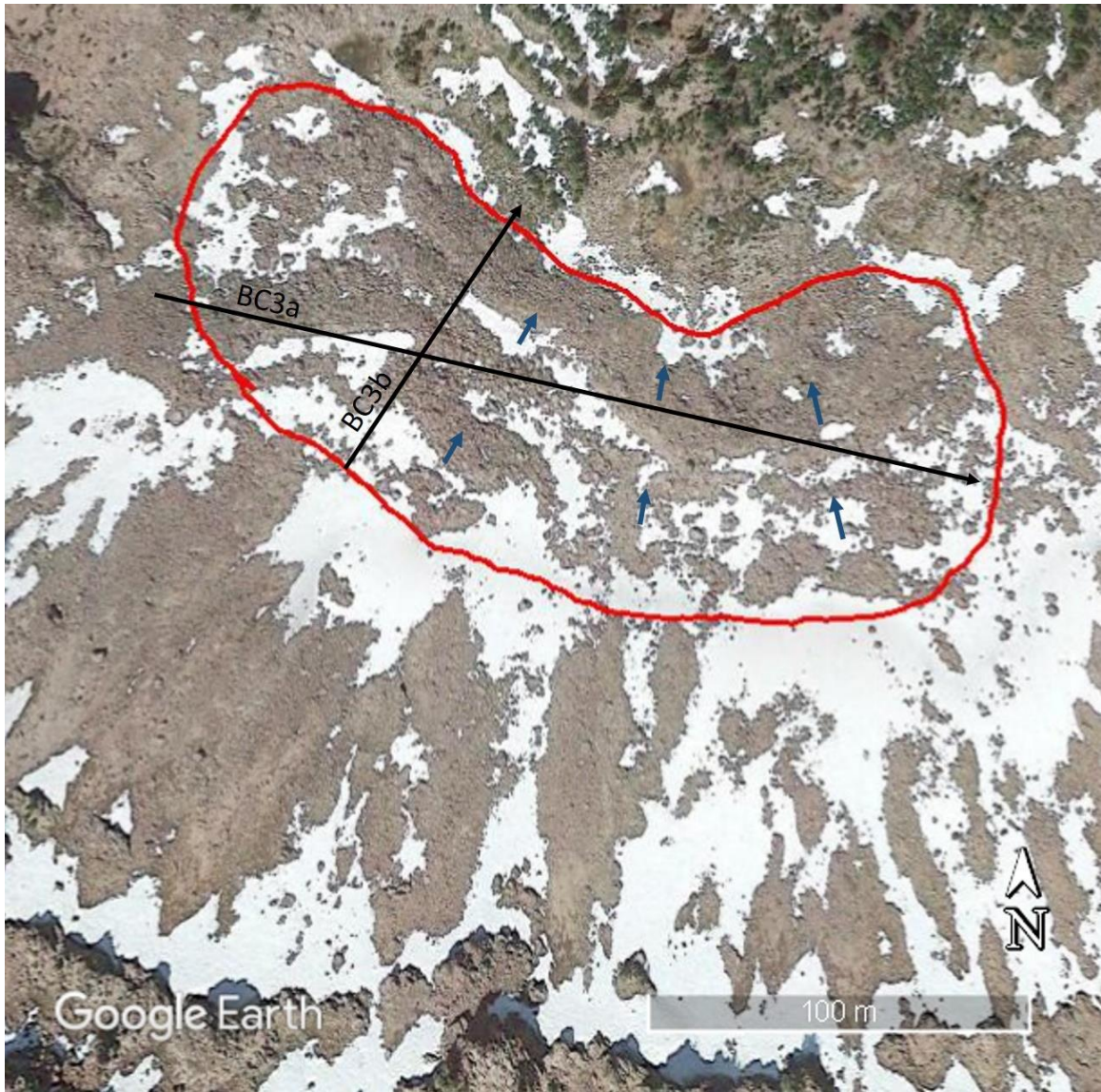


Figure 54. Google Earth image of BC3. Black lines depict location and direction of GPR profiles, blue arrows indicate direction of flow, and red lines indicate rock glacier boundary.

multiple snow fields present, streams were scarce indicating that snowmelt infiltrates rather than running off.

Two GPR transects were recorded on BC3, one longitudinal (100 m) and one transverse (261 m) (Figures 55 and 56). Both transects have a condensed array of diffraction hyperbola throughout which indicates a heterogeneous mix of material. This

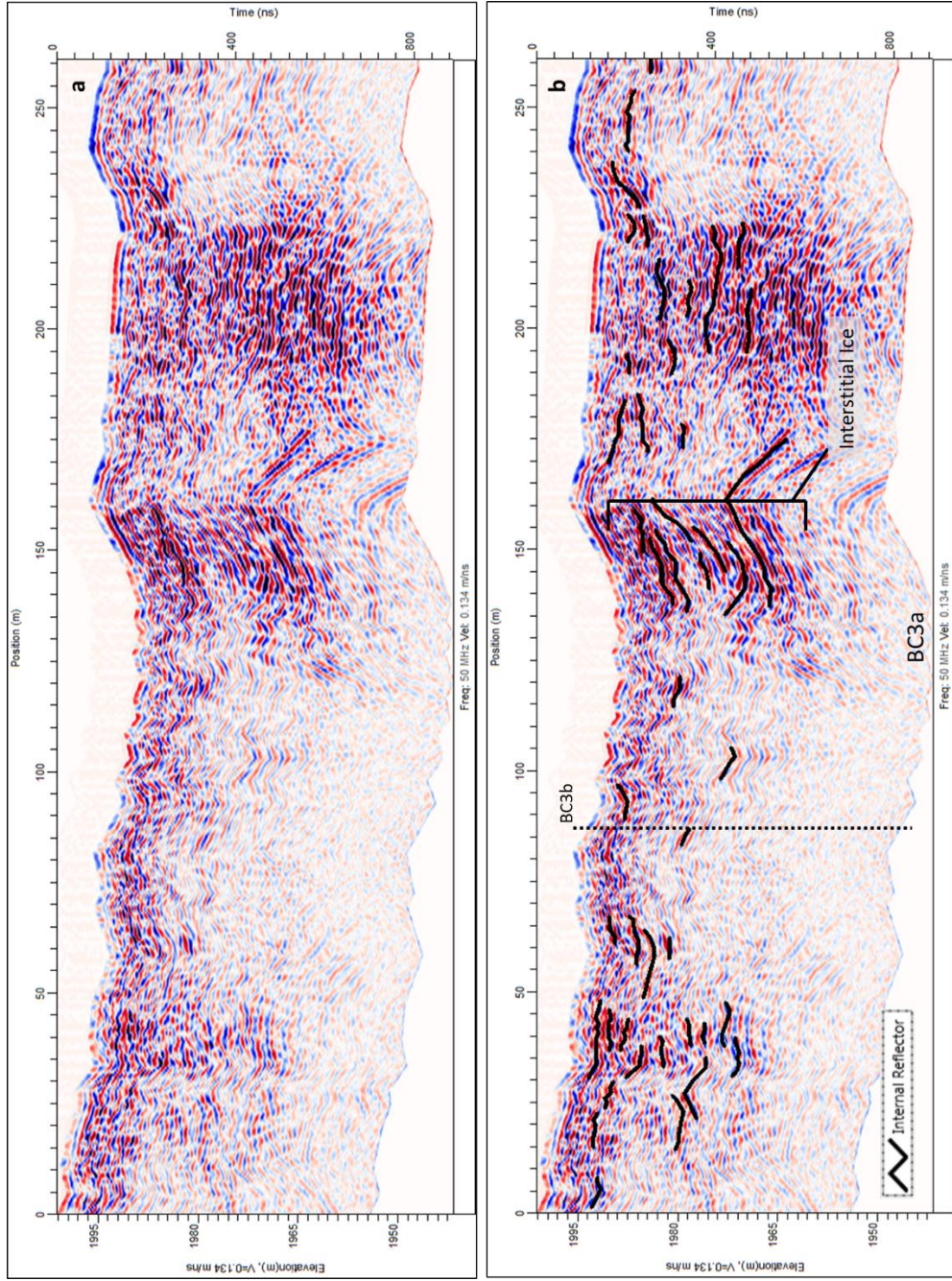


Figure 55. Migrated and topographically corrected transverse GPR profile of BC3a without interpretations (a) and with interpretations (b). Dotted line indicates intersection with longitudinal profile BC3b.

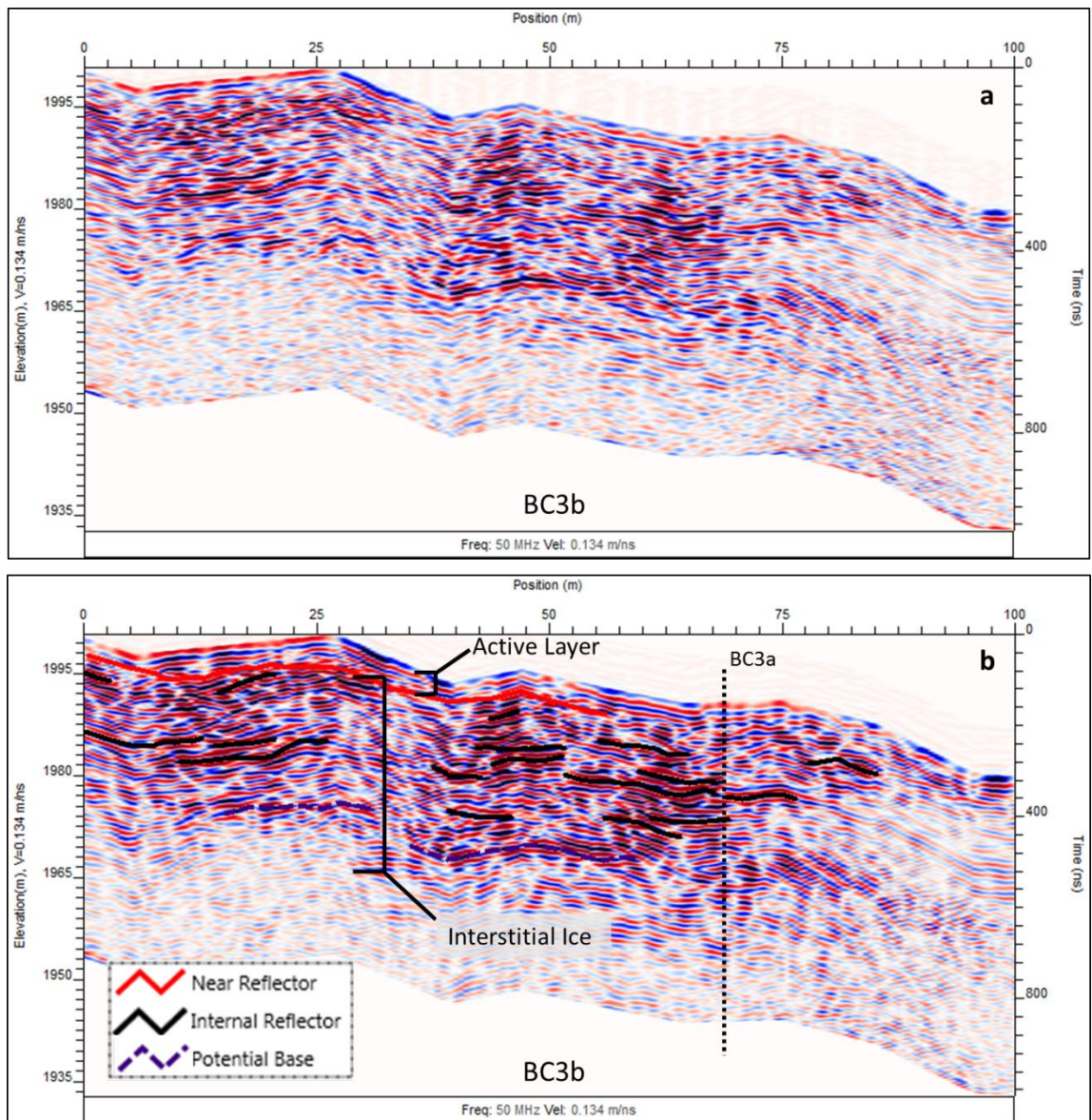


Figure 56. Migrated and topographically corrected longitudinal GPR profile of BC3b without interpretations (a) and with interpretations (b). Dotted line indicates intersection with transverse profile BC3a.

interpretation supports Lillquist and Weidenaar's (in preparation) classification of talus origin.

Near and far reflectors were much less defined on BC3 compared to other rock glaciers in this study. A defined near reflector that is interpreted as the base of the active

layer is shown in the longitudinal profile; however, it only persists for the first 55 m. This could indicate less permafrost toward the toe of the rock glacier. Several stronger reflectors were detected at depth but were not continuous which does not provide strong evidence that these are basal reflectors. In addition, no strong near or basal reflectors were detected in the longitudinal profile. Only a faint near reflector is present on the longitudinal profile and is apparent on the transverse profile for only the first 30 m. However, this was not the case for BC1 where GPR portrayed clear near and far reflectors.

On the longitudinal profile reflectors slightly mirror pressure ridges on the surface. Few upward-dipping reflectors are present to indicate strong compressional stresses (Figure 56). However, on the transverse profile a series of undulating and upward-dipping reflectors are present (Figure 55). These possibly indicate areas of thrust planes portraying compressional stresses.

Minimal detection of internal reflectors could be a result of the EM properties of the andesite. This might introduce more attenuation which would dilute the signal at greater depths. Further, the fiber optic cables that connect the transmitter and receiver to the DVL are highly sensitive. If the inner fiber optic cables are not flush with the end of the connector it introduces high amounts of attenuation and penetration depth as well as overall resolution can be greatly affected. This is a likely scenario for data collected on this rock glacier given that high quality data was collected on BC1 which has the same geologic makeup.

Composition and Structure Synthesis

Ground penetrating radar proved to be a successful tool for depicting internal stratigraphy of rock glaciers. As a whole, GPR profiles of Eastern Cascade rock glaciers showed many similarities.

The Active Layer

The presence of a near reflector was common among the GPR profiles and is interpreted as the base of the active layer and top of the permafrost body (Monnier and Kinnard, 2015). Measurements from the surface of three rock glaciers to the top of observable permafrost matched depth measurements in the corresponding GPR profiles from the surface to the base of the near reflector. The active layer is thickest during the summer melt season. Since these surveys were completed during the mid-to-late summer they provide a better overall representation of the active layer thickness and the permafrost-rich layer than surveys conducted during the winter when the depth to the base of the active layer is shallower due to seasonal refreezing (Trombotto and Borzotta, 2009). In general, active layer measurements were thickest at the toe of the rock glacier and thinnest near the head, which is common among all rock glaciers due to higher elevations and more shading provided by cirque or valley walls at the head (Barsch, 1996).

The average active layer depth of 5.5 m on TC1, an inactive rock glacier, is almost 2 m thicker than the next deepest average active layer depth. This is a result of this rock glacier being located at a lower elevation than others in this study. This suggests that inactive rock glaciers have a thicker active layer than active rock glaciers which aligns with previous research (Barsch, 1996).

Active layer thickness varied within each rock glacier but average thicknesses among active rock glaciers were relatively similar (2.4-3.6 m). Average active layer thickness ranged from 2.4 m on BC1 to 5.6 m on TC1 with an overall average of 3.4 m. All active rock glaciers in the Northeastern Cascades have an average active layer thickness ≥ 3.0 m. However, in the Southeastern Cascades the upper, active portion of BC1 has an average thickness of 2.4 m. Unfortunately, no active layer thickness data was obtained from similar rock glaciers in the region to see if this is a common occurrence.

Also, a common pattern in the Eastern Cascades is that thickness increases on pressure ridges and declines in the troughs between these features. This is similar to rock glaciers in the Alps where snowpack in the troughs lasts longer into the summer providing more insulation (Barsch, 1996). This is evident on longitudinal profiles as well as transverse profiles. In addition, active layer depths correspond at intersections of transverse and longitudinal profiles.

No notable difference was observed between active layer depths on rock glaciers with larger, blockier surface material compared to rock glaciers that have smaller surface material. This is the case between WFBC3 and WFBC4 which are adjacent to each other at similar elevations but have noticeably different-sized surface material. This aligns with rock glaciers in the Andes where high elevations allow active layers consisting of finer surface material to be generally thinner than that in other mountain ranges (Janke et al., 2015). In addition, at high latitudes, like Svalbard, active layers are also thinner on average than lower elevation, mid-latitude mountain ranges (Farbrot et al., 2005). This shows that impacts of latitude and elevation on temperature remain the major

contributing factors dictating active layer thickness in the Eastern Cascades. This further explains a larger average thickness of the active layer on TC1 which is located over 200 m below the lowest active rock glacier (BC1) at 1,662 m.

All ice that was observed in the field was paired with water. It is likely that the presence of water is due to seasonal melt. This melt could be from the active layer but also could be from seasonal snow patches found at the heads of the rock glaciers where permafrost and water was observed. This could also be an indication of permafrost degradation and a transformative state from active to inactive.

Permafrost and EM Velocity

Within the rock glacier matrix on GPR profiles, high EM velocities (>0.160 n/ms⁻¹) indicate the presence of permafrost. This is reinforced by interstitial permafrost exposures at multiple rock glaciers. Along with this, low EM velocities (<0.10 n/ms⁻¹) at lower depths on most profiles indicate a saturated layer between the ice-rich permafrost body and the bedrock. Where low velocities combined with prominent bedrock reflectors are found, like on VC1, VC2, and WFBC4, this saturated sub-permafrost layer could play a role in the movement of these features by allowing basal shear along the bedrock (Burger et al., 1999). Further, this layer likely acts as an aquifer for meltwater and groundwater, especially in rock glaciers where strong bedrock reflectors were not detected (Burger et al., 1999).

In addition, a high concentration of diffracting points within GPR profiles indicates a heterogeneous mix of material, therefore a talus origin for rock glaciers. Areas with few diffracting points imply homogenous material and could indicate massive ice layers indicating a glacial origin for the rock glacier. This is reinforced if these areas also

exhibit high velocities ($>0.160\text{m/ns}^1$) like that found in WFBC3 and WFBC4. In addition, using GPR measurements of active layer and base depths the overall average permafrost thickness is 19.2 m.

High EM velocities ($>0.160\text{m/ns}^1$) are found within the one inactive rock glacier sampled (TC1). Permafrost distribution in the Cascades has not been extensively studied. The presence of permafrost within an inactive rock glacier shows that permafrost distribution may be more extensive and at lower elevations than previously assumed. Permafrost within the inactive TC1 rock glacier indicates that permafrost can exist as low as 1,662 m and as far east as 66 km from the Cascade Crest.

Internal Structures

Internal reflectors depict stratigraphy and show expressions of movement throughout all GPR profiles. Surface parallel reflectors are found in areas of extensional stresses on longitudinal profiles. They are often found near the rock glacier head where talus begins to accumulate. These reflectors are also observed in areas with increased slope angle (Hausmann et al., 2012). On transverse profiles surface parallel reflectors depict areas of uniform stratigraphy. Long, continuous reflectors have been described as areas of uniform material, possibly areas where seasonal snowpack has been buried by rockfall and compressed into ice (Hausmann et al., 2012).

Upward or downward-dipping reflectors represent thrust planes and are found in areas experiencing compressional stresses (Maurer and Hauck, 2007; Fukui et al., 2008; Monnier et al., 2008, 2011). These are typically found in areas along profiles where slope angle decreases and transverse pressure ridges form. This is often associated with overall thickening of the rock glacier (Monnier et al., 2008, 2011).

Rock Glacier Base

Clear, linear far reflectors were detected on over half of the surveyed rock glaciers. Similar reflectors were identified on a rock glacier in the Andes by Monnier and Kinnard (2015) and were interpreted as bedrock. In addition, adjacent bedrock outcrops helped to verify the far reflector as the bedrock layer on multiple rock glaciers. Further, starting GPR profiles on bedrock at the head of the VC1 and VC2 rock glaciers verified this layer as bedrock on the GPR profiles during data analysis.

The absence of a basal reflector on GPR profiles could be due to multiple factors. Absence could indicate that the rock glacier is thicker than depths obtained during GPR surveying which varied between approximately 40 to 50 m. For example, on the WFBC3 rock glacier, a basal boundary is apparent in the beginning and end of the profile but is absent in the middle. This middle portion appears to be thicker than the penetration depth of the GPR. Absence of a basal reflector could also indicate that the rock glacier has overridden talus or moraine thus the boundary between the base of the rock glacier and underlying sediment does not appear as strong as a bedrock reflector (Isaksen et al., 2000). This is likely the case on both the NC1 and WFBC3 rock glaciers. In addition, absence of a basal reflector could be caused by higher rates of attenuation due to system noise, material type, or reflections from adjacent rock walls (Guglielmin et al., 2018). This might be an explanation for absence of a basal reflector on the transverse transect on BC3.

Comparing Lillquist and Weidenaar's Inventory

Three rock glacier classifications changed from Lillquist and Weidenaar (in preparation) based on field observations. First, bent and distorted tree growth on EFBC2

indicated an active state rather than inactive state. Second, analysis of surface topography and direction at NC1 revealed it is the convergence of two separate lobes making it a complex rock glacier. Third, sorted fines and cobbles showed that BrC1 is not a rock glacier but is likely a series of overlapping end moraines from the retreated Lyall Glacier above. This research showed that ground observations remain an important step for accurately identifying rock glacier type.

Further, GPR has helped to clarify the origin of these features. Two rock glacier classifications changed from Lillquist and Weidenaar (in preparation) based on internal structure. Often, glaciogenic classification is associated with location of a rock glacier within a cirque and in contact with an end moraine. WFBC4, which is located in a cirque, changed from talus to glaciogenic origin based on indications of massive ice presence in the GPR profile. Conversely, NC1, which is located in a well-defined cirque, changed from glaciogenic to talus origin due to a higher concentration of diffracting points indicating interstitial ice. This indicates that rock glaciers located within a cirque could have talus origin.

Two rock glaciers, VC1 and VC2, showed signs of formation from protalus ramparts/lobes. Active protalus ramparts were present at the head of both rock glaciers. This would technically be classified as a talus origin but it suggests a subclass of talus origin to be identified in future research. Along with this, BC1 adds a complication to the classification scheme because the feature has a lower inactive or relict section but an active upper portion. The upper portion has a thin active layer (thinnest of all surveyed rock glaciers) and is devoid of heavy vegetation that exists on the lower portion. This suggests different lobe ages and according to Barsch (1996) this would be classified as a

complex rock glacier. However, different lobe ages are difficult to determine from satellite imagery, further highlighting the importance of field investigations.

Vegetation Implications

The common presence of larch trees on active rock glaciers in the Northeastern Cascades is worthy of discussion. Larch trees are located wherever there is sufficient soil to support vegetation. This was mostly found on the upper-front of pressure ridges or on the rock glacier front itself. In addition, the EFBC2 rock glacier showed multiple larch trees that are bent at the base. These trees have not started growing vertically again to compensate for this shift. This indicates recent movement of the lobes on this rock glacier. Further, larch trees are known to grow on talus slopes and in unfavorable conditions where other types of vegetation may not persist (Arno, 1984). Tree growth on rock glaciers typically indicates an inactive state; however, as discussed previously, Goshorn-Maroney (2012) showed movement of a rock glacier that has several larch trees on its surface (Barsch, 1996).

Water Content

Rock Glacier Study Sites

Eight of the surveyed rock glaciers provided data on base depth, permafrost presence, and active layer thickness (Table 5). These rock glaciers ranged in size from the TC1 rock glacier with a surface area of 0.017 km² to the WFBC3 rock glacier with an area of 0.159 km². The total area of these eight rock glaciers is 0.615 km². They comprise approximately 9 percent of the total rock glacier surface area of the Eastern Cascades. Ice volume for eight rock glaciers, calculated using GPR measurements with 50 percent ice

Table 5. Ice-water equivalence of eight rock glacier study sites calculated using GPR measurements compared to using Brenning's (2005) empirical formula.

Rock Glaciers	Area (km ²)	GPR Avg. Permafrost Depth (m)	Brenning Avg. Permafrost Depth (m)	GPR Ice Volume (km ³)	Brenning Ice Volume (km ³)	GPR Water Equivalent (km ³)	Brenning Water Equivalent (km ³)	Percent Difference
VC1	0.083	18.6	30.4	0.00077	0.00126	0.00071	0.00115	64%
VC2	0.062	11.7	28.7	0.00036	0.00089	0.00033	0.00082	145%
NC1	0.116	22.9	32.5	0.00134	0.00189	0.00122	0.00174	42%
WFBC3	0.159	32.5	34.6	0.00258	0.00275	0.00237	0.00252	7%
WFBC4	0.052	18.2	27.7	0.00048	0.00073	0.00044	0.00067	53%
EFBC2	0.082	13.0	30.3	0.00053	0.00124	0.00049	0.00114	134%
TC1	0.017	14.0	22.0	0.00009	0.00015	0.00008	0.00013	58%
BC1	0.044	23.2	26.8	0.00225	0.00350	0.00206	0.00321	16%

content for active rock glaciers and 40 percent ice content for inactive rock glaciers, totals 0.0067 km³ with a 0.0061 km³ or 4,945 acre-feet (AF) water equivalent.

Using Brenning’s (2005) empirical equation, permafrost thickness for these same eight rock glaciers averaged 29.1 m. Their total ice volume, calculated using Brenning’s (2005) empirical equation with 50 percent ice content for active rock glaciers and 40 percent ice content for inactive rock glaciers, was 0.0095 km³ with a 0.0087 km³ (7,053 AF) water equivalent (Table 6). Brenning’s equation resulted in an average overestimation of over 60 percent for the average permafrost thickness for each surveyed rock glacier compared to the results using GPR measurements. In addition, Brenning’s equation resulted in an overestimate of 43 percent for total ice volume and water equivalency for these eight rock glaciers.

Several reasons could explain such a large overestimation. First, Brenning’s equation was not supported by sufficient field observations. In addition, the equation does not take into account lesser ice contents for inactive rock glaciers. Another cause could be thinner active layers found in High Andes, which would increase the permafrost

Table 6. Total ice-water equivalence: Brenning compared to GPR. Calculated through GPR measured active layer and base depths compared to values calculated using Brenning’s (2005) empirical formula.

	Avg. Permafrost Depth (m)	Ice Volume (km ³)	Water Equivalent (km ³)
GPR	19.2	0.0067	0.0061
Brenning	29.1	0.0095	0.0087

thickness. However, subtracting the active layer from permafrost thicknesses is not mentioned in the methods for the development of the equation (Brenning, 2005; Azocar and Brenning, 2010).

Glacier Inventory

The Eastern Cascades of Washington contains 218 ice glaciers that cover a combined area of 46.51 km² (Sitts et al., 2010; Carisio, 2012; Heard, 2012). The individual sizes of glaciers in the Eastern Cascades range from small, unnamed cirque glaciers with areas of 0.01 km² to large glaciers such as the Chickamin Glacier (48°18'36.39"N, 121°00'58.91"W) which has an area of 4.27 km². Results show that Eastern Cascade ice glaciers have a total ice volume of 1.17 km³ (948,536 AF), which translates to a water equivalence of 1.074 km³ (870,707 AF).

Rock Glacier Inventory

Washington's Eastern Cascades contains 130 active and inactive rock glaciers with a total area of 5.57 km² (Lillquist and Weidenaar, in preparation). Individual rock glaciers in this region range in size from 0.004 km² to 0.187 km². Using areal measurements from Lillquist and Weidenaar's (in preparation) inventory and Brenning's (2005) empirical formula for rock glacier volume, Eastern Cascade rock glaciers contain 0.070 km³ (56,750 AF) of ice. This converts to a total of 0.064 km³ (51,886 AF) potential water stored in these features.

However, based on the results of the current GPR analysis, Brenning's equation appears to overestimate the thickness of the permafrost-rich layer thus the total ice content. As such, a 64 percent decrease was applied to all of the permafrost thickness calculations from Brenning's equation. This adjustment results in Eastern Cascade rock

glaciers containing 0.025 km³ (20,268 AF) of ice which converts to 0.023 km³ (18,646 AF) of water equivalence.

Water Content Synthesis

This study identified a 1:8 ratio of Eastern Cascade rock glacier surface area to Eastern Cascade ice glacier surface area. This equates to a 1:46 ratio of rock glacier to ice glacier water equivalence in the Eastern Cascades (Table 7). To compare the results of rock glacier to ice glacier water equivalence in the Eastern Cascades to other studies unadjusted results from Brenning's equation are used since these other studies use his same techniques (Table 8). This indicates that the relationship of water equivalence of rock glaciers to ice glaciers in Washington's Eastern Cascades falls between that of similar studies from other mountain ranges. Brenning (2005) estimated, using data from Barsch (1996), the ratio of rock glaciers to ice glacier water volume to be 1:83 in the Swiss Alps. Rangecroft et al. (2015) estimated the ratio of rock glacier to ice glacier water volume to be 1:33 for the Bolivian Andes. A higher ratio of 1:9 was shown in the Himalayas of Nepal (Jones et al., 2018). A similar ratio of 1:8 was found in the Argentinean Andes (Perruca and Esper Angillieri, 2011). However, the arid Andes of Chile are estimated to have the highest ratio of 1:2.7 which is mainly due to less glacial coverage in that area (Azocar and Brenning, 2010). Using Brenning's (2005) unadjusted empirical formula, the ratio seen in the Eastern Cascades of 1:17 falls in between that of Rangecroft et al. (2015) of the Bolivian Andes and Jones et al. (2018) of the Himalayas of Nepal. Overall, this suggests that more continental locations have higher ratios of rock glaciers to ice glaciers. This is generally due to less glacial coverage in these areas along with less snowfall and more favorable climate conditions for permafrost.

Table 7. Ice-water equivalence of Eastern Cascade rock glaciers and ice glaciers. “Adjusted” indicates where the 64 percent decrease from GPR findings was applied.

	Total Area (km ²)	Ice Volume (km ³)	Water Volume (km ³)
Glaciers	46.51	1.171	1.074
Adjusted Rock Glaciers (A)	5.57	0.025	0.023
Brenning Rock Glaciers (B)	5.57	0.070	0.064
Ratio of rock glaciers to ice glaciers	1:8	(A) 1:46 (B) 1:17	(A) 1:46 (B) 1:17

Table 8. Results from previous studies compared to results from GPR.

	<u>Brenning</u> : ratio of rock glacier to ice glacier volume	<u>Adjusted</u> : ratio of rock glacier to ice glaciers volume	Source
Swiss Alps	1:83	1:244	(Brenning, 2005)
Bolivian Andes	1:33	1:97	(Rangecroft et al., 2015)
Eastern Cascades, WA	1:17	1:46	(Current work)
Himalayas of Nepal	1:10	1:29	(Jones et al., 2018)
Argentinean Andes	1:8	1:24	(Perruca and Esper Angillieri, 2011)
Chilean Andes	1:2.7	1:9	(Azocar and Brenning, 2010)

In addition, if all these studies are adjusted to reflect the GPR results of ice content from this study the Eastern Cascades would still rank in the same position (Table 8). This shows that in spite of the Cascades being a maritime mountain range with a high presence of glaciers on its eastern drier side, it still ranks closely with dry mountain ranges around the globe.

Furthermore, if all the studies that utilize Brenning's equation are adjusted in the same way based on the rock glaciers surveyed in the Eastern Cascades then this would indicate less significance for rock glaciers as water storage world-wide. Additionally, as Duguay et al. (2015) point out, the hydrology of rock glaciers is complex and, by definition, permafrost does not melt seasonally. The internal permafrost only melts seasonally when it is degrading which would qualify a rock glacier as inactive. Therefore, on active rock glaciers, only the seasonal thaw of the active layer contributes to streamflow (Arenson and Jakob, 2010). Inactive rock glaciers contribute to streamflow through the degradation of internal permafrost as well as the melting of the active layer. This means that inactive rock glaciers potentially contribute more to streamflow annually than active rock glaciers.

Moving into the future, an increase in annual temperatures due to global warming could cause the melting of internal permafrost in inactive rock glaciers to contribute more to streamflow temporarily. Also, as temperatures increase, currently active rock glaciers will eventually transition to an inactive state. However, most of the rock glaciers in the Eastern Cascades are currently inactive which means that their next transition will be to a relict state in which they will no longer contribute to streamflow. In turn, runoff from rock glaciers will increase with increasing MAAT which will make them a more significant water source in the short term that will eventually diminish in the long run. Rock glaciers react slowly to climate change and their internal ice will outlast that of ice glaciers but the uncertainty lies in how long these features will ultimately last in reaction to rapidly increasing temperatures (Arenson et al., 2002; Degenhardt, 2009).

Rock glaciers will be able to prolong the transition from active to inactive and eventually to relict by insulation provided by the thick, rocky debris of the active layer. Glaciers, on the other hand, are melting at an alarming rate with less help from an insulating layer to prolong their recession. Rock glaciers, either active or inactive, will potentially outlast ice glaciers in the Eastern Cascades. This means that future rock glacier runoff will contribute more percentage-wise to water supplies and base flow than currently observed. In terms of late summer baseflow, this is important because although these features will contribute runoff, and potentially more as time goes on, they will not fill the void after glaciers disappear in this region (Table 7). This emphasizes the inevitable diminishing water resources faced in the Eastern Cascades of Washington and many other regions worldwide. This research aligns with numerous other studies focused on climate change by signifying the importance of current water resources and their inevitable change brought on by a warming climate.

CHAPTER VI

MANAGEMENT IMPLICATIONS AND FURTHER RESEARCH

Management Implications

Determining the water storage capacity of rock glaciers fills a void in the current research and provides a more definitive picture on water sources in the Eastern Cascades in a warming world. While rock glacier runoff will likely increase due to rising annual temperatures, these features will not compensate for the complete loss of glacial runoff. Also, decreasing snowpack that results in decreasing snowmelt will further stress the mountain hydrologic system. In turn, this means that water managers in this region must prepare for a sharp decrease in water supply over the next century and beyond. This will have an enormously negative impact on countless resources including the agricultural industry, generation of hydroelectric power, and native salmon populations. This information concerns local water managers and other stakeholders, which include irrigation districts, the Bureau of Reclamation, local municipalities, Native American tribes, and numerous environmental organizations.

Future Research and Improvements

Further research on rock glaciers in the Eastern Cascades would be very useful for revealing more about their hydrological significance. Minimal studies have been conducted on rock glaciers in this area, which provides a wealth of options to explore. In addition, improvements in data collection can help in similar future investigations.

First, in terms of GPR data collection, it is important to properly manage files within the GPR and back up all data as soon as possible after collection. Also, it is important to make sure to shut down the instrument properly after data collection. Data

were lost on BC3 due to improper shut down and on TC1 due to not backing up files. In addition, the use of GPR during precipitation events is not recommended. Rainfall and snowfall during surveying on SC5 made for low quality data due to infiltration of water into parts of the antennas.

To improve measurements determined in this study acquiring high resolution orthophoto or light detection and ranging (LiDAR) imagery to create accurate digital elevation models (DEMs) of rock glaciers will give a better total volume of these structures. This would provide more accurate measurements of total ice content. In addition, adding other geophysical methods could be useful to determine ice content of the rock glaciers surveyed in this study. While GPR provided information on structure and composition, it was not able to reveal specific ice content. However, seismic and electromagnetic surveys can reveal more about the distribution of material within the rock glacier. In conjunction with accurate GPR measurements of depth of the active layer and of the rock glacier base, seismic and electromagnetic surveys can quantify ice content (Farbrot et al., 2005; Hausmann et al., 2007; Maurer and Hauck, 2007).

While this study provides information on future potential streamflow contribution, an important area that needs to be examined is current streamflow contribution, which can be achieved by monitoring rock glacier runoff. This will provide substantial information on year round fluctuation of runoff and a better picture of the yearly contribution to streamflow. Another way to quantify the yearly streamflow contribution is by examining the active layer (Duguay et al., 2015). Measuring active layer depths at other times of the year (i.e., winter, fall, and spring) to compare to measurements made in the summer in this study can provide more information on the volume that melts each

season. Further, measuring the size of surface material can provide a better estimate of the snow, firn, and ice distribution on the active layer.

An additional way to expand on this research is to expand the area and scope of the research. It would be beneficial to provide a look at the Cascades as a whole. Mapping rock glaciers in the Western Cascades would provide more insight into rock glacier distribution. Further, there are other permafrost features within the Cascades that could be included in future mapping and field investigations. These features include protalus ramparts and protalus lobes. These features have yet to be mapped extensively in the Eastern Cascades. Although much smaller than rock glaciers by nature, these features also contain permafrost and therefore have a role in the mountain hydrologic cycle (Richmond, 1962).

REFERENCES

- Annan, A. P. 2003. *Ground Penetrating Radar Principles, Procedures & Applications*. Mississauga: Sensors & Software Inc.
- Arenson, L. U., and M. Jakob. 2010. The significance of rock glaciers in the dry Andes – A discussion of Azocar and Brenning (2010) and Brenning and Azocar (2010). *Permafrost and Periglacial Processes* 21:282–285.
- Arenson, L. U., M. Hoelzle, and S. Springman. 2002. Borehole deformation measurements and internal structure of some rock glaciers in Switzerland. *Permafrost and Periglacial Processes* 13 (2):117–135.
- Arno, S. F. 1984. *Timberline: Mountain and Arctic Forest Frontiers*. Seattle: The Mountaineers.
- Azocar, G. F., and A. Brenning. 2010. Hydrological and geomorphological significance of rock glaciers in the dry Andes, Chile (27°-33°S). *Permafrost and Periglacial Processes* 21 (1):42–53.
- Barsch, D. 1996. *Rock-glaciers: Indicators for the Present and Former Geoecology in High Mountain Environments*. Berlin: Springer.
- Beckey, F. 1977. *Cascade alpine guide, Stevens Pass to Rainy Pass*. Seattle: The Mountaineers.
- Beckey, F. 2000. *Cascade Alpine Guide: Climbing & High Routes*. Seattle: The Mountaineers.
- Brazier, V., M. P. Kirkbride, and I. F. Owens. 1998. The relationship between climate and rock glacier distribution in the Ben Ohau Range, New Zealand. *Geografiska Annaler, Series A: Physical Geography* 80 (3–4):193–207.
- Brenning, A. 2005. Climatic and geomorphological controls of rock glaciers in the Andes of Central Chile: Combining statistical modelling and field mapping. PhD. Diss., Humboldt-Universität zu Berlin.
- Bunning, B. B. 1992. Geologic map of the east half of the Twisp 1:100,000 quadrangle, Washington. Washington Division of Geology and Earth Resources. Open File Report 90-9. Scale 1:100,000.

- Burger, K. C., J. J. Degenhardt, and J. R. Giardino. 1999. Engineering geomorphology of rock glaciers. *Geomorphology* 31 (1–4):93–132.
- Canaday, B. B., and R. W. Fonda. 1974. The influence of subalpine snowbanks on vegetation pattern, production, and phenology. *Bulletin of the Torrey Botanical Club* 101(6):340–350.
- Carisio, S. P. 2012. Evaluating areal errors in Northern Cascade glacier inventories. Master's thesis, University of Delaware.
- Charbonneau, A. 2012. Rock glacier activity and distribution in the southeastern British Columbia Coast Mountains. M.S. thesis, University of Victoria.
- Chen, J., and A. Ohmura. 1990. Estimation of alpine glacier water resources and their change since the 1870s. *Hydrology in Mountainous Regions* (193):127–136.
- Cossart, E., R. Braucher, M. Fort, D. L. Bourlès, and J. Carcaillet. 2008. Slope instability in relation to glacial debuitting in alpine areas (Upper Durance catchment, southeastern France): Evidence from field data and ¹⁰Be cosmic ray exposure ages. *Geomorphology* 95:3–26.
- Croce, F. A., and J. P. Milana. 2002. Internal structure and behaviour of a rock glacier in the arid Andes of Argentina. *Permafrost and Periglacial Processes* 13 (4):289–299.
- Degenhardt, J. J. 2009. Development of tongue-shaped and multilobate rock glaciers in alpine environments - Interpretations from ground penetrating radar surveys. *Geomorphology* 109 (3–4):94–107.
- Dragovich, J. D., and D. K. Norman. 1995. Geologic map of the west half of the Twisp 1:100,000 quadrangle, Washington. Washington Division of Geology and Earth Resources. Open File Report 95-3. Scale 1:100,000.
- Driedger, C. L., and P. Kennard. 1986. *Ice volumes on Cascade volcanoes: Mount Rainer, Mount Hood, Three Sisters, Mount Shasta*. U.S. Geological Survey Professional Paper 1365.

- Duguay, M. A., A. Edmunds, L. U. Arenson, and P. A. Wainstein. 2015. Quantifying the significance of the hydrological contribution of a rock glacier – A review. 68e *Conférence Canadienne de Géotechnique et 7e Conférence Canadienne sur le Pergélisol*, 20 au 23 septembre 2015, Québec, Québec. September, 2015.
- Evans, I. S. 1977. World-wide variations in the direction and concentration of cirque and glacier aspects. *Geografiska Annaler. Series A, Physical Geography* 59 (3/4):151-175.
- Farbrot, H., K. Isaksen, T. Eiken, A. Kääb, and J. L. Sollid. 2005. Composition and internal structures of a rock glacier on the strandflat of western Spitsbergen, Svalbard. *Norsk Geografisk Tidsskrift* 59:139–148.
- Fegel, T. S., J. S. Baron, A. G. Fountain, G. F. Johnson, and E. K. Hall. 2016. The differing biogeochemical and microbial signatures of glaciers and rock glaciers. *Journal of Geophysical Research: Biogeosciences* 121 (3):919–932.
- Florentine, C., M. Skidmore, M. Speece, C. Link, and C. A. Shaw. 2014. Geophysical analysis of transverse ridges and internal structure at Lone Peak rock glacier, Big Sky, Montana, USA. *Journal of Glaciology* 60 (221):453–462.
- Fountain, A. G., M. J. Hoffman, F. Granshaw, and J. Riedel. 2009. The “benchmark glacier” concept - Does it work? Lessons from the North Cascade Range, USA. *Annals of Glaciology* 50 (50):163–168.
- Fukui, K., T. Sone, J. A. Strelin, C. A. Torielli, J. Mori, and Y. Fujii. 2008. Dynamics and GPR stratigraphy of a polar rock glacier on James Ross Island, Antarctic Peninsula. *Journal of Glaciology* 54 (186):445–451.
- Geiger, S. T., J. M. Daniels, S. N. Miller, and J. W. Nicholas. 2014. Influence of rock glaciers on stream hydrology in the La Sal Mountains, Utah. *Arctic, Antarctic, and Alpine Research* 46 (3):645–658.
- Giardino, J. R., and S. G. Vick. Geologic engineering aspects of rock glaciers; In Giardino, J. R., J. F. Shroder, Jr., and J. D. Vitek. 1987. *Rock Glaciers*. Winchester, MA. Allen & Unwin, Inc. 265-287.
- Goshorn-Maroney, J. 2012. Thermal conditions and movement of rock glaciers in the North Cascades, Washington. Master’s thesis, Western Washington University.

- Granshaw, F. D., and A. G. Fountain. 2006. Glacier change (1958 – 1998) in the North Cascades National Park complex, Washington, USA. *Journal of Glaciology* 52 (177):251–256.
- Guglielmin, M., S. Ponti, and E. Forte. 2018. The origins of Antarctic rock glaciers: Periglacial or glacial features? *Earth Surface Processes and Landforms*.
- Haerberli, W. 1985. Creep of Mountain Permafrost: Internal structure and flow of alpine rock glaciers. *Mitteilungen der Versuchsanstalt für Wasserbau, Hydrologie und Glaziologie an der Eidgenössischen Technischen Hochschule, Nr. 77, Zurich*: 142.
- Haerberli, W., C. Guodong, A. P. Gorbunov, and S. A. Harris. 1993. Mountain permafrost and climatic change. *Permafrost and Periglacial Processes* 4:165–174.
- Haerberli, W., M. Hoelzle, A. Kääh, F. Keller, D. Vonder Müll, and S. Wagner. 1998. Ten years after drilling through the permafrost of the active rock glacier Murtèl, Eastern Swiss Alps: Answered questions and new perspectives. *PERMAFROST - Seventh International Conference* (55): 403–410.
- Haerberli, W., B. Hallet, L. Arenson, R. Elconin, O. Humlum, A. Kaab, V. Kaufmann, B. Ladanyi, N. Matsuoka, S. Springman and D. V. Muhl. 2006. Permafrost creep and rock glacier dynamics. *Permafrost and Periglacial Processes* 17:189–214.
- Harris, C., L. U. Arenson, H. H. Christiansen, B. Etzelmüller, R. Frauenfelder, S. Gruber, W. Haerberli, C. Hauck, M. Hölzle, O. Humlum, K. Isaksen, A. Kääh, M. A. Kernlutschg, M. Lehning, N. Matsuoka, J. B. Murton, J. Noetzli, M. Phillips, N. Ross, M. Seppälä, S. M. Springman, and D. Vonder Mühll. 2009. Permafrost and climate in Europe: monitoring and modelling thermal, geomorphological and geotechnical responses. *Earth-Science Reviews* 92:117–171.
- Harris, S. A., H.M. French, J.A. Heginbottom, G.H. Johnston, B. Ladanyi, D.C. Sego, R.O. van Everdingen. 1988. Glossary of permafrost and related ground-ice terms. Permafrost Subcommittee, National Research Council of Canada. Technical Memorandum (142): 156.
- Hausmann, H., K. Krainer, E. Brukl, and W. Mostler. 2007. Internal structure and ice content of Reichenkar rock glacier (Stubai Alps, Austria) Assessed by Geophysical Investigations. *Permafrost and Periglacial Processes* 18 (2007):351–367.
- Hausmann, H., K. Krainer, E. Brukl, and C. Ullrich. 2012. Internal structure, ice content and dynamics of Ölgrube and Kaiserberg rock glaciers (Ötztal Alps, Austria) determined from geophysical surveys. *Austrian Journal of Earth Sciences* 105(2): 12-31.

- Heard, J. A. 2012. Late Pleistocene and Holocene aged glacial and climate reconstructions in the Goat Rocks Wilderness, Washington, United States. Master's thesis, Portland State University.
- Heusser, C. J. 1972. Palynology and phytogeographical significance of a late-Pleistocene refugium near Kalaloch, Washington. *Quaternary Research* 2 (2):189—201.
- Hoelzle, M., S. Wagner, A. Kaab, D. V. M. 1998. Surface movement and internal deformation of ice-rock mixtures within rock glaciers at Pontresina-Schafberg, Upper Engadin, Switzerland. In PERMAFROST - Seventh International Conference, 465–471.
- Hopkins, K., 1966. Glaciation of Ingalls Creek Valley, East-Central Cascade Range, Washington. Unpublished M.S. Thesis, University of Washington.
- Humlum, O. 1982. Rock glacier types on Disko, central West Greenland. *Geografisk Tidsskrift* 82:59–66.
- . 2000. The geomorphic significance of rock glaciers: Estimates of rock glacier debris volumes and headwall recession rates in West Greenland. *Geomorphology* 35 (1–2):41–67.
- IPA (International Permafrost Association). 2015. Country reports: Reports from the Adhering Bodies of the International Permafrost Association. 84
- IPCC (International Panel on Climate Change). 2013: Summary for policymakers. Climate Change 2013: The Physical Science Basis. Contribution of Working Group I to the Fifth Assessment Report of the Intergovernmental Panel on Climate Change: 33.
- Isaksen, K., R. S. Odegard, T. Eiken, and J. L. Sollid. 2000. Composition, flow and development of two tongue-shaped rock glaciers in the permafrost of Svalbard. *Permafrost and Periglacial Processes* 11:241–257.
- Janke, J. R., A. C. Bellisario, and F. A. Ferrando. 2015. Classification of debris-covered glaciers and rock glaciers in the Andes of central Chile. *Geomorphology* 241:98–121.
- Jones, D. B., S. Harrison, K. Anderson, H. L. Selley, J. L. Wood, and R. A. Betts. 2018b. The distribution and hydrological significance of rock glaciers in the Nepalese Himalaya. *Global and Planetary Change* 160:123–142.

- Kellerer-Pirklbauer, A., M. Pauritsch, and G. Winkler. 2013. Relict rock glaciers as important aquifers in sensitive ecosystems: The example of the Natura 2000 protection area. 5th Symposium for Research in Protected Areas 5 (June): 373–378.
- Kerschner, H. 1978. Paleoclimatic inferences from late Wurm rock glaciers, Eastern Central Alps, Western Tyrol, Austria. *Arctic and Alpine Research* 10 (3):635–644.
- Krainer, K., K. Lang, and H. Hausmann. 2010. Active rock glaciers at Croda Rossa/Hohe Gaisl, Eastern Dolomites (Alto Adige/South Tyrol, Northern Italy). *Geografia fisica e dinamica quaternaria* 33 (1):25-36.
- Krainer, K., L. Mussner, M. Behm, and H. Hausmann. 2012. Multi-disciplinary investigation of an active rock glacier in the Sella Group (Dolomites; Northern Italy). *Austrian Journal of Earth Sciences* 105 (2):48–62.
- Krainer, K., and W. Mostler. 2002. Hydrology of active rock glaciers: examples from the Austrian Alps. *Arctic, Antarctic, and Alpine Research* 34 (2):142-149.
- . 2006. Flow velocities of active rock glaciers in the Austrian Alps. *Geografiska Annaler* 88 (4):267–280.
- Krainer, K., W. Mostler, and C. Spötl. 2007. Discharge from active rock glaciers, Austrian Alps: A stable isotope approach. *Austrian Journal of Earth Sciences* 100:102–112.
- Laser Technology, Inc. 2017. TruePulse 360R User’s Manual. Centennial, CO. Laser Technology, Inc.
- Leopold, M., M. W. Williams, N. Caine, J. Völkel, and D. Dethier. 2011. Internal structure of the Green Lake 5 rock glacier, Colorado Front Range, USA. *Permafrost and Periglacial Processes* 22 (2):107–119.
- Libby, W.G. 1968. Rock glaciers in the North Cascade Range, Washington (abstract of paper submitted for the meeting in Reno, Nevada, April 6-9, 1966). *Geological Society of America Special Paper* 101, p. 318-19.
- Lillquist, K., and M. Weidenaar. In preparation. Rock glaciers in the Eastern Cascade Range, Washington, USA.
- Long, W. A. 1975. Glacial studies in the Entiat River drainage basin, North-Central Washington. United States Forest Service.

- Martinez, A., and A. P. Byrnes. 2001. Modeling dielectric-constant values of geologic materials: An aid to ground-penetrating radar data collection and interpretation. *Current Research in Earth Sciences*, Bulletin 247 (1):1–16.
- Mass, C. 2008. *The Weather of the Pacific Northwest*. Seattle, WA: University of Washington Press.
- Mathews, W. H. 1955. Permafrost and its occurrence in the southern coast mountains of British Columbia. *The Canadian Alpine Journal* 7:94–98.
- Maurer, H., and C. Hauck. 2007. Instruments and methods: Geophysical imaging of alpine rock glaciers. *Journal of Glaciology* 53 (180):110–120.
- Menounos, B., G. Osborn, J. J. Clague, and B. H. Luckman. 2009. Latest Pleistocene and Holocene glacier fluctuations in Western Canada. *Quaternary Science Reviews* 28 (21-22): 2049-2074.
- Merrill, D.E. 1966. Glacial geology of the Chiwaukum Creek drainage basin and vicinity. M.S. thesis, University of Washington, Seattle.
- Millar, C. I., and R. D. Westfall. 2008. Rock glaciers and related periglacial landforms in the Sierra Nevada, CA, USA; inventory, distribution and climatic relationships. *Quaternary International* 188 (1):90–104.
- Mitchell, S. G., and D. R. Montgomery. 2006. Influence of a glacial buzzsaw on the height and morphology of the Cascade Range in central Washington State, USA. *Quaternary Research* 65 (1):96–107.
- Monnier, S., C. Camerlynck, and F. Rejiba. 2008. Ground penetrating radar survey and stratigraphic interpretation of the Plan du Lac rock glaciers, Vanoise Massif, Northern French Alps. *Permafrost and Periglacial Processes* 19:107–136.
- Monnier, S., C. Camerlynck, F. Rejiba, C. Kinnard, T. Feuillet, and A. Dhemaied. 2011. Structure and genesis of the Thabor rock glacier (Northern French Alps) determined from morphological and ground-penetrating radar surveys. *Geomorphology* 134 (3–4):269–279.
- Monnier, S., and C. Kinnard. 2013. Internal structure and composition of a rock glacier in the Andes (upper Choapa valley, Chile) using borehole information and ground-penetrating radar. *Annals of Glaciology* 54 (64):61–72.
- . 2015. Internal structure and composition of a rock glacier in the Dry Andes, Inferred from ground-penetrating radar data and its artefacts. *Permafrost and Periglacial Processes* 26:335–346.

- Moore, R.D., S. W. Fleming, B. Menounos, R. Wheate, A. Fountain, K. Stahl, K. H. and M. J. 2009. Glacier change in western North America: Influences on hydrology, geomorphic hazards and water quality. *Hydrological Processes* 23:42–61.
- NRCS (Natural Resources Conservation Service Snow Telemetry). 2018. NRCS SNOTEL. U. S. Department of Agriculture. <https://www.wcc.nrcs.usda.gov/snow/> (accessed 09 February 2018).
- O’Neal, M. A., B. Hanson, S. Carisio, and A. Satinsky. 2015. Detecting recent changes in the areal extent of North Cascades glaciers, USA. *Quaternary Research* (United States) 84 (2):151–158.
- Owen, L. A., and J. England. 1998. Observations on rock glaciers in the Himalayas and Karakoram Mountains of northern Pakistan and India. *Geomorphology* 26 (1–3):199–213.
- Paterson, W. S. B. 1994. *The Physics of Glaciers*, 3rd ed. Oxford: Pergamon.
- Pelto, M. S. 1993. Current behavior of glaciers in the North Cascades and effect on regional water supplies. *Washington Geology* 21 (2):3–10.
- . 2011a. Skykomish River, Washington: Impact of ongoing glacier retreat on streamflow. *Hydrological Processes* 25 (21):3356–3363.
- . 2011b. Methods for assessing and forecasting the survival of North Cascade, Washington glaciers. *Quaternary International* 235 (1–2):70–76.
- Pelto, M. S., and C. Hedlund. 2001. Terminus behavior and response time of North Cascade glaciers, Washington, U.S.A. *Journal of Glaciology* 47 (158):497–506.
- Perucca, L., and M. Y. E. Angillieri. 2011. Glaciers and rock glaciers’ distribution at 28° SL, Dry Andes of Argentina, and some considerations about their hydrological significance. *Environmental Earth Sciences* 64 (8):2079–2089.
- Porter, S. C. 1976. Pleistocene glaciation in the southern part of the North Cascade Range, Washington. *Bulletin of the Geological Society of America* 87:61–75.
- . 1977. Present and past glaciation thresholds in the Cascade Range, Washington, USA: Topographic and climatic controls, and paleoclimatic implications. *Journal of Glaciology* 18 (78):101–116.

- Post, A., D. Richardson, W. V. Tangborgn, and F. L. Rosselot. 1971. Inventory of glaciers in the North Cascades, Washington. Professional Paper 705-A, US Geologic Survey.
- Potter, N. 1972. Ice-cored rock glacier, Galena Creek, northern Absaroka Mountains, Wyoming. *Geologic Society of America Bulletin* 83 (10):3025–3058.
- Price, M. P., and A. C. Byers, D. A. Friend, T. Kohler, and L. W. Price. 2013. *Mountain Geography: Physical and Human Dimensions: Origin of Mountains*. Berkley: University of California Press, 378 pp.
- Rangecroft, S., S. Harrison, and K. Anderson. 2015. Rock glaciers as water stores in the Bolivian Andes: An assessment of their hydrological importance. *Arctic, Antarctic, and Alpine Research* 47 (1):89–98.
- Richmond, G. M. 1962. Quaternary stratigraphy of the La Sal Mountains, Utah. U.S. Geological Survey Professional Paper 324, 135 pp.
- Ritter, D., R. C. Kochel and J. R. Miller. 2011. *Process Geomorphology*. Long Grove, IL: Waveland Press, Inc.
- Sattler, K., B. Anderson, A. Mackintosh, K. Norton, and M. de Róiste. 2016. Estimating Permafrost Distribution in the Maritime Southern Alps, New Zealand, Based on Climatic Conditions at Rock Glacier Sites. *Frontiers in Earth Science* 4 (4):1–17.
- Schasse, H. W. 1987. Geologic map of the Mount Rainier quadrangle, Washington. Washington Division of Geology and Earth Resources. Open File Report 87-16. Scale 1:100,000.
- Scurlock, J. 2005. Glaciers, remnants, & rock glaciers of the Eastern North Cascades. <http://www.pbase.com/nolock/eastnclaciers>. (accessed 22 April 2018).
- Sensors & Software Inc. 2012. pulseEKKO PRO User’s Guide. Mississauga, ON. Sensors & Software Inc.
- Sensors & Software Inc. 2017. EKKO_Project Processing Module User’s Guide. Mississauga, ON. Sensors & Software Inc.
- Siler, N., G. Roe, and D. Durran. 2013. On the dynamical causes of variability in the rain-shadow effect: A case study of the Washington Cascades. *Journal of Hydrometeorology* 14 (1):122–139.

- Sinclair, K., and C. Pitz. 1999. Estimated baseflow characteristics of selected Washington rivers and streams: Water supply bulletin No. 60. Washington Department of Ecology. Publication No. 99-327.
- Sitts, D. J., A. G. Fountain, and M. J. Hoffman. 2010. Twentieth century glacier change on Mount Adams, Washington, USA. *Northwest Science* 84 (4):378–385.
- Steig, E. J., J. J. Fitzpatrick, N. Potter Jr., and D. H. Clark. 1998. The geochemical record in rock glaciers. *Geografiska Annaler, Series A: Physical Geography* 80A (3–4):277–286.
- Steinman, B. A., M. B. Abbott, M. E. Mann, N. D. Stansell, and B. P. Finney. 2012. 1,500 year quantitative reconstruction of winter precipitation in the Pacific Northwest. *Proceedings of the National Academy of Sciences* 109 (29):11619–11623.
- Stoelinga, M. T., M. D. Albright, and C. F. Mass. 2010. A new look at snowpack trends in the Cascade Mountains. *Journal of Climate* 23 (10):2473–2491.
- Stoffel, K. L., and McGroder. 1990. Geologic Map of the Robinson Mtn. 1:100,000 Quadrangle, Washington: Washington Division of Geology and Earth Resources, Open File Report 90-5. Scale 1:100,000.
- Tabor, R., Waitt, R., Frizzell, V., Swanson, D., Byerly, G., and Bentley, R., 1982. Geologic Map of the Wenatchee 1:100,000 Quadrangle, Central Washington: U.S. Geological Survey Miscellaneous Investigations Series Map 1-1311. 26 p., scale 1:100,000.
- Tabor, R. W., R. H. Haugerud, E. H. Brown, R. S. Babcock, R. B. Miller. 1989. Accreted terranes of the North Cascades Range, Washington. Field Trip Guidebook. Washington D.C., American Geophysical Union.
- Thompson, W.F., 1962. Preliminary notes on the nature and distribution of rock glaciers relative to true glaciers and other effects of the climate on the ground. In *North America*. IASH Commission of Snow and Ice, 58, 212-219.
- Treser, J. J. 2011. Historic glacier and climate fluctuations at Mount Adams, WA and effects on regional water supply. M.S. thesis, Central Washington University.
- Trombotto, D., and E. Borzotta. 2009. Indicators of present global warming through changes in active layer-thickness, estimation of thermal diffusivity and geomorphological observations in the Morenas Coloradas rockglacier, Central Andes of Mendoza, Argentina. *Cold Regions Science and Technology* 55 (3):321–330.

- Wahrhaftig, C., and A. Cox. 1959. Rock glaciers in the Alaska Range. *Geological society of America Bulletin* 70 (4):383–436.
- Weidenaar, M. 2013. Rock Glaciers in the Eastern Cascades, Washington. Undergraduate thesis, Central Washington University.
- Welter, S. 1987. Geomorphic character, age and distribution of rock glaciers in the Olympic Mountains, Washington. M.S. thesis, Portland State University.
- White, S. E. 1971. Rock glacier studies in the Colorado Front Range. 1961 to 1968, *Arctic Alpine Research*, 3:43–64.
- WRCC (Western Regional Climate Center). 2017. *Lake Cle Elum, Washington*. <http://www.wrcc.dri.edu/cgi-bin/cliMAIN.pl?wa4394> (accessed 09 February 2017).
- WRCC (Western Regional Climate Center). 2017. *Snoqualmie Pass, Washington*. <http://www.wrcc.dri.edu/cgi-bin/cliMAIN.pl?wa7781> (accessed 09 February 2017).
- WRCC (Western Regional Climate Center). 2017. *Stockdill Ranch, Washington*. <http://www.wrcc.dri.edu/cgi-bin/cliMAIN.pl?wa7781> (accessed 09 February 2017).

APPENDIXES

Appendix A. Active rock glaciers. From Lillquist and Weidenaar (in preparation).

	Name	Latitude	Longitude	Area (km ²)	Perm. Layer (m)	Ice (km ³)	Water (km ³)
1	Johnny Creek 2	48°49'02.40"N	120°27'20.86"W	0.028	4.39	0.00012	0.00011
2	Lease Creek 2	48°50'07.49"N	120°34'24.88"W	0.008	3.45	0.00003	0.00003
3	Lease Creek 3	48°50'07.76"N	120°32'27.29"W	0.105	5.73	0.00060	0.00055
4	Lease Creek 4	48°49'52.66"N	120°34'10.45"W	0.026	4.34	0.00011	0.00010
5	Monument Creek 1	48°47'47.43"N	120°32'03.18"W	0.139	6.06	0.00084	0.00077
6	Winthrop Creek 4	48°58'47.79"N	120°46'27.44"W	0.016	3.94	0.00006	0.00006
7	Auburn Creek 1	48°43'56.75"N	120°22'59.15"W	0.009	3.53	0.00003	0.00003
8	Auburn Creek 2	48°45'02.88"N	120°20'54.65"W	0.063	5.18	0.00033	0.00030
9	Eightmile Creek 1	48°45'57.91"N	120°20'24.27"W	0.105	5.74	0.00061	0.00055
10	Eightmile Creek 2	48°46'05.46"N	120°20'17.15"W	0.069	5.27	0.00036	0.00033
11	Huckleberry Creek 4	48°30'53.76"N	120°29'29.87"W	0.061	5.14	0.00031	0.00029
12	Varden Creek 1	48°33'12.11"N	120°33'14.64"W	0.080	5.42	0.00043	0.00040
13	Varden Creek 2	48°33'05.30"N	120°33'30.95"W	0.059	5.11	0.00030	0.00028
14	Wolf Creek 2	48°28'56.23"N	120°31'22.48"W	0.076	5.38	0.00041	0.00037
15	East Fork Buttermilk Creek 2	48°13'23.15" N	120°21'04.02"W	0.187	6.44	0.00121	0.00111
16	North Creek 1	48°29'04.99"N	120°34'29.02"W	0.105	5.73	0.00060	0.00055
17	Oval Creek 1	48°15'46.46"N	120°26'55.39"W	0.092	5.58	0.00051	0.00047
18	South Fork South Creek 1	48°23'55.35"N	120°37'6.47"W	0.004	3.01	0.00001	0.00001
19	West Fork Buttermilk Creek 1	48°17'27.10"N	120°24'56.48"W	0.072	5.31	0.00038	0.00035
20	West Fork Buttermilk Creek 2	48°15'21.11"N	120°26'1.11"W	0.048	4.90	0.00024	0.00022
21	West Fork Buttermilk Creek 3	48°15'10.83"N	120°25'02.96"W	0.160	6.24	0.00100	0.00092
22	West Fork Buttermilk Creek 4	48°14'57.31"N	120°24'12.63"W	0.087	5.53	0.00048	0.00044
23	West Fork Buttermilk Creek 5	48°14'50.42"N	120°23'50.41"W	0.043	4.80	0.00021	0.00019
24	Margerum Creek 1	48°18'02.13"N	120°44'29.94"W	0.030	4.46	0.00013	0.00012

	Name	Latitude	Longitude	Area (km ²)	Perm. Layer (m)	Ice (km ³)	Water (km ³)
25	Pass Creek 1	48°17'52.78"N	120°51'28.38"W	0.026	4.33	0.00011	0.00010
26	Pass Creek 2	48°18'01.28"N	120°51'44.30"W	0.012	3.74	0.00005	0.00004
27	Tumble Creek 1	48°07'54.13" N	120°39'54.82"W	0.017	4.00	0.00007	0.00006
28	Tumble Creek 2	48° 7'50.73"N	120°39'51.42"W	0.012	3.71	0.00004	0.00004
29	Mountaineer Creek 2	47°29'19.49"N	120°48'36.43"W	0.013	3.77	0.00005	0.00004
30	Rock Creek 1	48°02'04.77"N	120°44'09.98"W	0.004	2.95	0.00001	0.00001
31	Entiat River 1	48°08'53.74"N	120°47'36.88"W	0.062	5.16	0.00032	0.00029
32	Entiat River 2	48°08'31.36"N	120°46'44.91"W	0.014	3.83	0.00005	0.00005
33	Bear Creek 3	46°31'29.49"N	121°19'38.47"W	0.019	4.09	0.00008	0.00007
Total				1.852		0.01011	0.00927

Appendix B. Inactive Rock Glaciers. From Lillquist and Weidenaar (in preparation).

	Name	Latitude	Longitude	Area (km ²)	Perm. Layer (m)	Ice (km ³)	Water (km ³)
1	Birk Creek 1	48°49'49.86"N	120°35'29.13"W	0.014	3.05	0.00004	0.00004
2	Chuchawanteen Creek 1	48°55'40.08"N	120°42'18.69"W	0.028	3.51	0.00010	0.00009
3	Chuchawanteen Creek	48°56'37.69"N	120°44'45.33"W	0.030	3.58	0.00011	0.00010
4	Johnny Creek 4	48°50'01.47"N	120°26'31.79"W	0.007	2.64	0.00002	0.00002
5	Kid Creek	48°51'28.81"N	120°43'48.52"W	0.008	2.77	0.00002	0.00002
6	Monument Creek 2	48°47'57.80"N	120°31'11.55"W	0.153	4.95	0.00076	0.00070
7	Murphy Creek 1	48°51'21.57"N	120°27'43.43"W	0.102	4.56	0.00046	0.00043
8	Pinnacle Creek 2	48°47'07.00"N	120°25'58.84"W	0.053	4.00	0.00021	0.00019
9	Pinnacle Creek 3	48°46'52.95"N	120°25'47.27"W	0.032	3.62	0.00012	0.00011
10	Raven Creek 1	48°54'39.79"N	120°20'58.60"W	0.028	3.51	0.00010	0.00009
11	Rock Creek 1	48°52'34.42"N	120°43'5.23"W	0.071	4.24	0.00030	0.00027
12	Rock Creek 2	48°52'16.82"N	120°43'41.12"W	0.027	3.49	0.00009	0.00009
13	Shack Creek 1	48°49'21.45"N	120°38'53.69"W	0.035	3.67	0.00013	0.00012
14	W Fork Pasayton River 1	48°46'35.64"N	120°43'25.60"W	0.015	3.09	0.00005	0.00004
15	Winthrop Creek 2	48°58'58.99"N	120°46'12.33"W	0.018	3.24	0.00006	0.00005
16	Auburn Creek 5	48°44'27.19"N	120°23'32.27"W	0.029	3.56	0.00010	0.00010
17	Chewuch River 1	48°54'00.43"N	120°09'16.90"W	0.012	3.00	0.00004	0.00003
18	Copper Glance Creek 2	48°45'16.63"N	120°20'07.18"W	0.010	2.87	0.00003	0.00003
19	Copper Glance Creek 3	48°45'09.10"N	120°19'46.95"W	0.006	2.62	0.00002	0.00002
20	Copper Glance Creek 6	48°44'35.12"N	120°19'05.84"W	0.069	4.21	0.00029	0.00027
21	Copper Glance Creek 10	48°44'49.32"N	120°20'07.76"W	0.013	3.04	0.00004	0.00004
22	Cougar Creek 1	48°42'03.21"N	120°22'28.38"W	0.054	4.01	0.00022	0.00020
23	Diamond Creek 1	48°51'10.32"N	120°19'33.46"W	0.048	3.92	0.00019	0.00017
24	Eureka Creek 1	48°48'45.59"N	120°35'31.58"W	0.030	3.56	0.00011	0.00010
25	Eureka Creek 2	48°48'13.10"N	120°35'56.56"W	0.014	3.08	0.00004	0.00004
26	Eureka Creek 3	48°47'34.40"N	120°35'55.78"W	0.053	4.00	0.00021	0.00019

	Name	Latitude	Longitude	Area (km ²)	Perm. Layer (m)	Ice (km ³)	Water (km ³)
27	Fool Hen Creek 4	48°49'53.13"N	120°18'3.83"W	0.014	3.05	0.00004	0.00004
28	Fool Hen Creek 7	48°49'51.85"N	120°18'11.25"W	0.013	3.03	0.00004	0.00004
29	Hubbard Creek 1	48°27'46.84"N	120°28'50.98"W	0.048	3.93	0.00019	0.00017
30	Huckleberry Creek 5	48°30'28.60"N	120°27'48.61"W	0.053	4.00	0.00021	0.00019
31	Hurricane Creek 1	48°43'14.60"N	120°23'08.71"W	0.044	3.85	0.00017	0.00015
32	Hurricane Creek 3	48°42'28.63"N	120°23'34.22"W	0.050	3.96	0.00020	0.00018
33	Lost River 1	48°45'53.67"N	120°22'03.48"W	0.013	3.04	0.00004	0.00004
34	Lost River 2	48°53'37.31"N	120°27'7.52"W	0.017	3.18	0.00005	0.00005
35	Pat Creek 1	48°46'2.05"N	120°21'5.31"W	0.014	3.06	0.00004	0.00004
36	Panther Creek 1	48°42'48.30"N	120°22'15.96"W	0.020	3.29	0.00007	0.00006
37	Rommel Creek 1	48°55'55.52"N	120°12'11.95"W	0.018	3.21	0.00006	0.00005
38	Rommel Creek 4	48°55'36.79"N	120°11'28.76"W	0.042	3.83	0.00016	0.00015
39	South Fork Cedar Creek 1	48°29'30.44"N	120°31'41.03"W	0.038	3.74	0.00014	0.00013
40	South Fork Cedar Creek 3	48°29'59.59"N	120°31'54.86"W	0.020	3.30	0.00007	0.00006
41	South Fork Wolf Creek 1	48°27'12.99"N	120°29'10.03"W	0.035	3.68	0.00013	0.00012
42	Three Prong Creek 1	48°47'53.60"N	120°16'53.24"W	0.057	4.05	0.00023	0.00021
43	Varden Creek 3	48°33'29.10"N	120°34'44.54"W	0.092	4.47	0.00041	0.00038
44	Foggy Dew Creek 1	48°08'43.60"N	120°20'43.77"W	0.013	3.03	0.00004	0.00004
45	Mack Creek 1	48°19'39.21"N	120°32'33.53"W	0.059	4.09	0.00024	0.00022
46	Mack Creek 2	48°18'35.64"N	120°31'38.87"W	0.018	3.22	0.00006	0.00005
47	North Fork Libby Creek 1	48°14'32.25"N	120°19'52.16"W	0.042	3.83	0.00016	0.00015
48	Oval Creek 3	48°17'45.20"N	120°25'11.29"W	0.058	4.08	0.00024	0.00022
49	Reynolds Creek 1	48°22'49.87"N	120°34'47.08"W	0.043	3.84	0.00017	0.00015
50	South Creek 1	48°26'01.15"N	120°38'42.29"W	0.021	3.32	0.00007	0.00006
51	South Fork Twisp River 1	48°26'39.35"N	120°39'12.63"W	0.033	3.63	0.00012	0.00011
52	South Fork Twisp River 2	48°26'26.48"N	120°39'04.01"W	0.037	3.72	0.00014	0.00012

	Name	Latitude	Longitude	Area (km ²)	Perm. Layer (m)	Ice (km ³)	Water (km ³)
53	South Fork Twisp River 3	48°26'31.12"N	120°38'26.73"W	0.043	3.84	0.00017	0.00015
54	South Fork War Creek 1	48°18'13.93"N	120°29'55.72"W	0.038	3.75	0.00014	0.00013
55	South Fork War Creek 2	48°17'51.77"N	120°29'29.30"W	0.065	4.17	0.00027	0.00025
56	South Fork War Creek 3	48°18'1.99"N	120°29'1.62"W	0.014	3.08	0.00004	0.00004
57	South Fork War Creek 4	48°18'10.41"N	120°28'50.42"W	0.010	2.89	0.00003	0.00003
58	West Fork Buttermilk Creek 6	48°14'47.75"N	120°23'29.21"W	0.033	3.64	0.00012	0.00011
59	West Fork Buttermilk Creek 7	48°15'24.77"N	120°25'48.28"W	0.044	3.85	0.00017	0.00016
60	Castle Creek 4	48°15'18.16"N	120°43'41.83"W	0.008	2.73	0.00002	0.00002
61	East Fork Fish Creek 1	48°16'08.60"N	120°28'26.69"W	0.012	2.97	0.00004	0.00003
62	East Fork McAlester Creek 1	48°27'32.34"N	120°39'48.86"W	0.159	4.98	0.00079	0.00072
63	East Fork Prince Creek 3	48°09'45.92" N	120°21'52.67"W	0.096	4.51	0.00043	0.00040
64	Fourmile Creek 1	48°17'22.64"N	120°33'52.19"W	0.077	4.31	0.00033	0.00030
65	McAlester Creek 1	48°25'57.78"N	120°39'34.54"W	0.127	4.77	0.00061	0.00056
66	Park Creek 1	48°28'54.33"N	120°55'50.79"W	0.053	4.00	0.00021	0.00019
67	Prince Creek 2	48°13'57.02"N	120°23'21.72"W	0.012	2.97	0.00004	0.00003
68	Rainbow Creek 1	48°24'18.86"N	120°39'30.53"W	0.059	4.09	0.00024	0.00022
69	Tolo Creek 1	48°24'13.13"N	120°55'29.56"W	0.015	3.11	0.00005	0.00004
70	Box Creek 1	48°06'23.73"N	120°47'58.34"W	0.019	3.27	0.00006	0.00006
71	East Fork Mission Creek 1	47°17'12.74"N	120°26'23.42"W	0.054	4.01	0.00022	0.00020
72	East Fork Mission Creek 2	47°17'17.26"N	120°25'44.15"W	0.031	3.60	0.00011	0.00010
73	East Fork Mission Creek 3	47°17'33.18"N	120°25'13.12"W	0.008	2.71	0.00002	0.00002
74	Frosty Creek 1	47°39'50.78"N	120°57'03.09"W	0.043	3.83	0.00016	0.00015

	Name	Latitude	Longitude	Area (km ²)	Perm. Layer (m)	Ice (km ³)	Water (km ³)
75	Jack Creek 1	47°28'51.83" N	120°55'27.18"W	0.131	4.80	0.00063	0.00058
76	Leland Creek 1	47°36'27.06"N	121°04'11.52"W	0.031	3.61	0.00011	0.00010
77	Leland Creek 2	47°37'27.03" N	121°03'32.21"W	0.014	3.05	0.00004	0.00004
78	Tronsen Creek 1	47°18'41.27" N	120°33'42.72"W	0.014	3.06	0.00004	0.00004
79	Trout Creek 1	47°32'08.50"N	120°54'45.94"W	0.115	4.67	0.00054	0.00049
80	Trout Creek 2	47°33'44.91"N	120°52'26.30"W	0.025	3.44	0.00009	0.00008
81	Trout Creek 5	47°32'18.05"N	120°53'41.10"W	0.020	3.29	0.00006	0.00006
82	Fortune Creek 1	47°27'56.67" N	120°57'55.33"W	0.018	3.22	0.00006	0.00005
83	Fortune Creek 2	47°27'55.60"N	120°57'31.97"W	0.012	2.97	0.00004	0.00003
84	Little Salmon la Sac Cr 1	47°21'41.81"N	121°03'43.94"W	0.016	3.13	0.00005	0.00004
85	DeRoux Creek 1	47°26'16.47"N	120°58'38.57"W	0.032	3.61	0.00011	0.00011
86	Barton Creek 1	46°50'23.53"N	121°15'52.41"W	0.012	2.97	0.00004	0.00003
87	Little Hoodoo Creek 1	46°45'20.84"N	121°14'32.50"W	0.053	4.00	0.00021	0.00019
88	Little Rattlesnake Creek 1	46°43'34.52"N	121° 5'29.56"W	0.005	2.46	0.00001	0.00001
89	S Fork Quartz Creek 1	47°01'07.13"N	121°02'11.84"W	0.048	3.93	0.00019	0.00017
90	Bear Creek 1	46°31'50.52"N	121°19'31.69"W	0.175	5.08	0.00089	0.00082
91	Bear Creek 4	46°31'39.50"N	121°20'22.70"W	0.009	2.78	0.00002	0.00002
92	Bear Creek 6	46°33'28.58"N	121°19'06.18"W	0.008	2.72	0.00002	0.00002
93	Scatter Creek 1	46°35'22.35"N	121°23'13.93"W	0.033	3.63	0.00012	0.00011
94	Spruce Creek 3	46°33'52.87"N	121°11'26.32"W	0.017	3.18	0.00005	0.00005
95	Spruce Creek 4	46°33'58.89"N	121°11'36.12"W	0.004	2.41	0.00001	0.00001
96	Spruce Creek 5	46°33'35.53"N	121°11'37.02"W	0.012	2.98	0.00004	0.00003
97	Tenday Creek 1	46°27'33.20"N	121°18'10.31"W	0.030	3.58	0.00011	0.00010
Total				3.721		0.01507	0.01382

Appendix C. Eastern Cascades Ice Glaciers. From Sitts et al. (2010), Carisio (2012), and Heard (2012).

	Name	Latitude	Longitude	Year	Area (km ²)	Ice Volume (km ³)	Water (km ³)
1		48.50899	-120.787	2006	0.06	0.000626	0.000574
2	Wythe	48.49575	-120.941	2006	0.81	0.021412	0.019635
3		48.49294	-120.93	2006	0.05	0.000489	0.000448
4		48.51113	-120.946	2006	0.09	0.001086	0.000996
5		48.52333	-120.949	2006	0.13	0.001788	0.00164
6		48.52669	-120.819	2006	0.17	0.002574	0.00236
7		48.49224	-120.819	2006	0.05	0.000489	0.000448
8		48.50494	-120.791	2006	0.03	0.000245	0.000224
9		48.50916	-120.48	2006	0.06	0.000626	0.000574
10		48.509	-120.485	2006	0.11	0.001426	0.001307
11		48.54995	-120.574	2006	0.05	0.000489	0.000448
12		48.55047	-120.581	2006	0.12	0.001604	0.001471
13		48.55139	-120.587	2006	0.17	0.002574	0.00236
14		48.55543	-120.591	2006	0.02	0.000141	0.000129
15		48.56386	-120.594	2006	0.01	5.51E-05	5.05E-05
16		48.58813	-120.698	2006	0.02	0.000141	0.000129
17		48.58911	-120.702	2006	0.04	0.000361	0.000331
18		48.59286	-120.709	2006	0.02	0.000141	0.000129
19		48.60623	-120.735	2006	0.02	0.000141	0.000129
20		48.60326	-120.73	2006	0.01	5.51E-05	5.05E-05
21		48.72728	-120.569	2006	0.04	0.000361	0.000331
22		48.73699	-120.616	2006	0.01	5.51E-05	5.05E-05
23		48.98117	-120.855	2006	0.04	0.000361	0.000331
24		48.9841	-120.858	2006	0.03	0.000245	0.000224
25	Goode	48.48735	-120.905	2006	0.45	0.009644	0.008843
26		48.4892	-120.917	2006	0.18	0.002781	0.00255
27		48.49745	-120.925	2006	0.07	0.000772	0.000708
28		48.49601	-120.916	2006	0.04	0.000361	0.000331
29		48.47817	-120.89	2006	0.02	0.000141	0.000129
30		48.48155	-120.892	2006	0.07	0.000772	0.000708
31		48.25385	-120.425	2006	0.16	0.00237	0.002174
32		47.47784	-121.311	2006	0.11	0.001426	0.001307
33		47.48829	-121.299	2006	0.16	0.00237	0.002174
34		47.49652	-121.29	2006	0.06	0.000626	0.000574
35		47.49462	-121.296	2006	0.2	0.003209	0.002942
36		47.50455	-121.286	2006	0.29	0.005313	0.004872

Appendix C Continued. Eastern Cascades Ice Glaciers.

	Name	Latitude	Longitude	Year	Area (km ²)	Ice Volume (km ³)	Water (km ³)
37		47.50951	-121.28	2006	0.14	0.001978	0.001813
38		47.5116	-121.288	2006	0.21	0.003428	0.003144
39		47.51554	-121.274	2006	0.07	0.000772	0.000708
40		47.53096	-121.253	2006	0.08	0.000925	0.000849
41		47.56256	-121.168	2006	0.08	0.000925	0.000849
42		47.5664	-121.171	2006	0.53	0.012042	0.011042
43		47.55879	-121.162	2006	0.14	0.001978	0.001813
44		47.5851	-121.17	2006	0.05	0.000489	0.000448
45		47.55925	-121.169	2006	0.08	0.000925	0.000849
46		47.47212	-120.785	2006	0.05	0.000489	0.000448
47		47.48658	-120.811	2006	0.08	0.000925	0.000849
48	Snow Creek 1	47.46921	-120.806	2006	0.01	5.51E-05	5.05E-05
49	Snow Creek 2	47.47197	-120.815	2006	0.13	0.001788	0.00164
50	Snow Creek 3	47.47488	-120.821	2006	0.1	0.001253	0.001149
51	Snow Creek 4	47.47517	-120.826	2006	0.02	0.000141	0.000129
52	Snow Creek 5	47.47843	-120.828	2006	0.14	0.001978	0.001813
53	Snow Creek 6	47.47917	-120.838	2006	0.08	0.000925	0.000849
54	Snow Creek 7	47.47994	-120.841	2006	0.06	0.000626	0.000574
55		47.47319	-120.86	2006	0.07	0.000772	0.000708
56		47.47482	-120.89	2006	0.1	0.001253	0.001149
57		47.4761	-120.896	2006	0.07	0.000772	0.000708
58		47.47955	-120.902	2006	0.14	0.001978	0.001813
59		47.48047	-120.908	2006	0.07	0.000772	0.000708
60		47.70007	-120.93	2006	0.11	0.001426	0.001307
61		47.9404	-121.059	2006	0.02	0.000141	0.000129
62		47.96488	-120.991	2006	0.08	0.000925	0.000849
63		47.96421	-120.999	2006	0.04	0.000361	0.000331
64		47.95739	-121.016	2006	0.03	0.000245	0.000224
65		47.9496	-121.033	2006	0.05	0.000489	0.000448
66		48.01016	-121.087	2006	0.04	0.000361	0.000331
67		48.0096	-121.096	2006	0.05	0.000489	0.000448
68		48.0089	-121.103	2006	0.17	0.002574	0.00236

Appendix C Continued. Eastern Cascades Ice Glaciers.

	Name	Latitude	Longitude	Year	Area (km ²)	Ice Volume (km ³)	Water (km ³)
69		48.00911	-121.111	2006	0.04	0.000361	0.000331
70	White River	48.05853	-121.095	2006	1	0.0285	0.026135
71		48.05399	-121.087	2006	0.13	0.001788	0.00164
72		48.06199	-121.077	2006	0.2	0.003209	0.002942
73	Clark	48.0484	-120.951	2006	0.99	0.028114	0.02578
74		48.05502	-120.954	2006	0.09	0.001086	0.000996
75	Richardson	48.0552	-120.969	2006	1.24	0.038161	0.034994
76		48.06294	-120.97	2006	0.04	0.000361	0.000331
77		48.06338	-120.974	2006	0.05	0.000489	0.000448
78	Pilz	48.06557	-120.981	2006	0.63	0.015225	0.013961
79	Butterfly	48.06947	-120.998	2006	1.29	0.040264	0.036922
80		48.075	-121.011	2006	0.21	0.003428	0.003144
81		48.09067	-120.915	2006	0.12	0.001604	0.001471
82		48.09805	-120.916	2006	0.08	0.000925	0.000849
83		48.06479	-120.902	2006	0.15	0.002172	0.001991
84		48.09275	-120.906	2006	0.2	0.003209	0.002942
85		48.07123	-120.91	2006	0.36	0.007124	0.006533
86		48.1659	-120.881	2006	0.07	0.000772	0.000708
87		48.1273	-120.805	2006	0.09	0.001086	0.000996
88		48.09834	-120.768	2006	0.04	0.000361	0.000331
89		48.09839	-120.771	2006	0.05	0.000489	0.000448
90		48.10313	-120.778	2006	0.06	0.000626	0.000574
91		48.10437	-120.791	2006	0.06	0.000626	0.000574
92		48.11537	-120.797	2006	0.05	0.000489	0.000448
93	Entiat 1	48.13991	-120.786	2006	0.03	0.000245	0.000224
94	Entiat 2	48.13994	-120.793	2006	0.24	0.00411	0.003768
95	Entiat 5	48.15676	-120.807	2006	0.1	0.001253	0.001149
96	Entiat 3	48.14199	-120.801	2006	0.21	0.003428	0.003144
97	Entiat 4	48.14849	-120.803	2006	0.23	0.003879	0.003557
98		48.13262	-120.655	2006	0.02	0.000141	0.000129
99		48.10135	-120.605	2006	0.09	0.001086	0.000996

Appendix C Continued. Eastern Cascades Ice Glaciers.

	Name	Latitude	Longitude	Year	Area (km ²)	Ice Volume (km ³)	Water (km ³)
100		48.08929	-120.57	2006	0.02	0.000141	0.000129
101		48.16414	-120.798	2006	0.14	0.001978	0.001813
102		48.17177	-120.796	2006	0.12	0.001604	0.001471
103		48.18289	-120.799	2006	0.04	0.000361	0.000331
104		48.16659	-120.808	2006	0.09	0.001086	0.000996
105		48.15415	-120.821	2006	0.16	0.00237	0.002174
106		48.18194	-120.844	2006	0.03	0.000245	0.000224
107		48.18652	-120.848	2006	0.14	0.001978	0.001813
108		48.19381	-120.839	2006	0.04	0.000361	0.000331
109		48.19203	-120.845	2006	0.08	0.000925	0.000849
110		48.18145	-120.861	2006	0.04	0.000361	0.000331
111		48.17096	-120.887	2006	0.1	0.001253	0.001149
112	Lyman	48.17104	-120.896	2006	0.27	0.004822	0.004422
113		48.16867	-120.905	2006	0.26	0.004581	0.004201
114		48.22172	-120.898	2006	0.1	0.001253	0.001149
115	Hanging	48.17904	-120.911	2006	0.09	0.001086	0.000996
116	Isella	48.23396	-120.869	2006	0.37	0.007394	0.006781
117	Mary Green	48.23704	-120.855	2006	0.74	0.018941	0.017368
118		48.24348	-120.853	2006	0.08	0.000925	0.000849
119		48.2467	-120.852	2006	0.03	0.000245	0.000224
120	Company	48.24667	-120.87	2006	1	0.0285	0.026135
121		48.24026	-120.811	2006	0.19	0.002993	0.002745
122		48.27864	-120.763	2006	0.07	0.000772	0.000708
123		48.29391	-120.856	2006	0.05	0.000489	0.000448
124	Dark	48.25902	-120.886	2006	0.59	0.013928	0.012772
125	Grant	48.22605	-120.899	2006	0.26	0.004581	0.004201
126		48.21319	-120.914	2006	0.01	5.51E-05	5.05E-05
127		48.26398	-120.961	2006	0.03	0.000245	0.000224
128		48.25725	-120.983	2006	0.32	0.006072	0.005568
129		48.24738	-120.974	2006	0.08	0.000925	0.000849
130		48.29631	-120.999	2006	0.25	0.004344	0.003983
131		48.31332	-120.958	2006	0.08	0.000925	0.000849
132		48.31197	-120.979	2006	0.03	0.000245	0.000224
133	Blue	48.30787	-120.991	2006	0.27	0.004822	0.004422
134		48.31735	-120.998	2006	0.01	5.51E-05	5.05E-05
135		48.31104	-120.998	2006	0.1	0.001253	0.001149

Appendix C Continued. Eastern Cascades Ice Glaciers.

	Name	Latitude	Longitude	Year	Area (km ²)	Ice Volume (km ³)	Water (km ³)
136		48.30771	-120.997	2006	0.04	0.000361	0.000331
137	Chickamin	48.31011	-121.016	2006	4.27	0.204332	0.187372
138	Dana	48.3163	-121.047	2006	1.45	0.047187	0.04327
139		48.32062	-121.063	2006	0.79	0.020698	0.01898
140		48.35135	-121.039	2006	0.07	0.000772	0.000708
141		48.35453	-121.03	2006	0.09	0.001086	0.000996
142		48.35715	-121.026	2006	0.1	0.001253	0.001149
143		48.36305	-121.024	2006	0.25	0.004344	0.003983
144		48.373	-121.011	2006	0.01	5.51E-05	5.05E-05
145		48.36922	-121.021	2006	0.02	0.000141	0.000129
146		48.36713	-121.026	2006	0.12	0.001604	0.001471
147	Le Conte	48.36363	-121.037	2006	1.57	0.052563	0.0482
148		48.37907	-121.056	2006	0.21	0.003428	0.003144
149		48.40654	-121.031	2006	0.19	0.002993	0.002745
150		48.40783	-121.017	2006	0.05	0.000489	0.000448
151		48.41173	-121.019	2006	0.09	0.001086	0.000996
152		48.41203	-121.026	2006	0.21	0.003428	0.003144
153	Spider	48.41465	-121.037	2006	0.3	0.005563	0.005101
154		48.42038	-121.035	2006	0.1	0.001253	0.001149
155		48.42038	-121.025	2006	0.1	0.001253	0.001149
156		48.41909	-121.008	2006	0.04	0.000361	0.000331
157		48.42974	-121.041	2006	0.01	5.51E-05	5.05E-05
158		48.43079	-121.029	2006	0.02	0.000141	0.000129
159		48.43254	-121.026	2006	0.1	0.001253	0.001149
160		48.43429	-120.981	2006	0.1	0.001253	0.001149
161	S	48.43438	-121.033	2006	0.26	0.004581	0.004201
162		48.44083	-121.026	2006	0.16	0.00237	0.002174
163		48.44807	-121.024	2006	0.07	0.000772	0.000708
164		48.44661	-121.033	2006	0.03	0.000245	0.000224
165		48.44422	-121.035	2006	0.08	0.000925	0.000849
166	Yawning	48.45049	-121.039	2006	0.22	0.003652	0.003349
167		48.4501	-121.048	2006	0.09	0.001086	0.000996
168		48.45401	-121.055	2006	0.31	0.005816	0.005333
169	Davenport	48.49154	-121.029	2006	0.44	0.009354	0.008578
170		48.48266	-121	2006	0.03	0.000245	0.000224
171		48.47838	-120.992	2006	0.12	0.001604	0.001471

Appendix C Continued. Eastern Cascades Ice Glaciers.

	Name	Latitude	Longitude	Year	Area (km ²)	Ice Volume (km ³)	Water (km ³)
172		48.4736	-120.991	2006	0.06	0.000626	0.000574
173		48.47153	-120.976	2006	0.03	0.000245	0.000224
174		48.46948	-120.966	2006	0.05	0.000489	0.000448
175		48.47391	-120.968	2006	0.04	0.000361	0.000331
176		48.48116	-120.981	2006	0.06	0.000626	0.000574
177		48.48408	-120.978	2006	0.03	0.000245	0.000224
178		48.48357	-120.99	2006	0.26	0.004581	0.004201
179	Buckner 1	48.48996	-120.996	2006	0.29	0.005313	0.004872
180	Buckner 2	48.49544	-120.99	2006	0.26	0.004581	0.004201
181		48.48803	-120.937	2006	0.02	0.000141	0.000129
182		48.48365	-120.919	2006	0.05	0.000489	0.000448
183		48.48116	-120.915	2006	0.04	0.000361	0.000331
184		48.49713	-120.755	2006	0.01	5.51E-05	5.05E-05
185		48.49047	-120.755	2006	0.02	0.000141	0.000129
186	Lyll	48.48804	-120.746	2006	0.07	0.000772	0.000708
187		48.4879	-120.734	2006	0.02	0.000141	0.000129
188	Sandalee 5	48.40547	-120.761	2006	0.01	5.51E-05	5.05E-05
189	Sandalee 4	48.4055	-120.767	2006	0.02	0.000141	0.000129
190	Sandalee 3	48.40664	-120.775	2006	0.11	0.001426	0.001307
191	Sandalee 2	48.4088	-120.784	2006	0.11	0.001426	0.001307
192	Sandalee 1	48.40919	-120.791	2006	0.24	0.00411	0.003768
193		48.41023	-120.798	2006	0.16	0.00237	0.002174
194		48.40955	-120.805	2006	0.02	0.000141	0.000129
195		48.52826	-120.811	2006	0.02	0.000141	0.000129
196		48.10766	-120.97	2006	0.04	0.000361	0.000331
197		48.3316	-121.068	2006	0.05	0.000489	0.000448
198		48.33562	-121.067	2006	0.06	0.000626	0.000574
199		48.34165	-121.062	2006	0.03	0.000245	0.000224
200		48.34235	-121.05	2006	0.04	0.000361	0.000331
201		48.41792	-121.044	2006	0.03	0.000245	0.000224
202		48.42086	-121.043	2006	0.05	0.000489	0.000448
203	Sahale	48.48734	-121.042	2006	0.22	0.003652	0.003349
204	McCall -A	46.51674	-121.449	2009	0.3	0.005563	0.005101
205	McCall-B	46.5105	-121.45	2009	0.06	0.000626	0.000574
206	McCall-C	46.50536	-121.443	2009	0.32	0.006072	0.005568
207	Glissade	46.50003	-121.433	2009	0.05	0.000489	0.000448

Appendix C Continued. Eastern Cascades Ice Glaciers.

	Name	Northing	Easting	Year	Area (km²)	Ice Volume (km³)	Water (km³)
208	Tieton	46.49511	-121.421	2009	0.33	0.006331	0.005805
209	Conrad	46.49329	-121.406	2009	0.3	0.005563	0.005101
210	Meade	46.48534	-121.403	2009	0.21	0.003428	0.003144
211	Klickitat	46.18917	-121.466	2006	2.93	0.12257	0.112397
212	W. Salmon	46.1997	-121.504	2006	0.51	0.011429	0.010481
213	Mazama	46.18086	-121.47	2006	1.4	0.044993	0.041258
214	Avalanche	46.18549	-121.509	2006	0.86	0.023225	0.021297
215	Rusk	46.20407	-121.473	2006	1.47	0.048072	0.044082
216	Wilson	46.21278	-121.469	2006	1.03	0.029666	0.027204
217	Gotchen	46.1649	-121.475	2006	0.17	0.002574	0.00236
218	Crescent	46.1684	-121.487	2006	0.44	0.009354	0.008578
Total					46.51	1.171	1.074